I. Microphysics of Frost Metamorphism: Applications to Triton and Mars

II. A Global Analysis of the Ozone Deficit in the Upper Stratosphere and Lower Mesosphere

III. The Diabatic Circulation in the Stratosphere as Diagnosed from Microwave Limb Sounder Data

Thesis by

Janusz Eluszkiewicz

In Partial Fulfillment of the Requirements for the Degree of

Doctor of Philosophy

California Institute of Technology

Pasadena, California

1993

(submitted 25 January 1993)

To my parents

Moim Rodzicom

ACKNOWLEDGMENTS

My adventure with planetary science began in Poland, where Jacek Leliwa-Kopystynski advised me to study the porous structure of Mimas. That work continued in Oxford, where Andrew Fowler and Mike Ashby gave me invaluable help leading to the paper "Compaction and Internal Structure of Mimas" (*Icarus, 84,* 215-225, 1990). This paper, whose final stages were completed at Caltech, became the bridge between the European and North American chapters of my graduate career. I owe much to Dave Stevenson for nurturing my interest in planetary science, an interest which led to the paper on the microphysical state of Triton's surface. When I decided to leave the outer solar system and come down to study the Earth's atmosphere it was not for lack of interesting problems regarding icy satellites; rather, the quite mundane concern about being able to make a living prompted that decision. I would like to thank Yuk Yung and Mark Allen, who taught me that studying our planet can be not only practical, but also quite rewarding. The reward more often than not requires hard work in obtaining accuracy at the 10% level, as in the ozone deficit paper. Given my penchant for swimming, the lessons I learned while working with Mark were perhaps providential in securing for myself a scientific career. It was on Mark's recommendation that I became involved with the Upper Atmosphere Research Satellite; I sometimes wonder whether Rich Zurek would have taken me on, had not Yuk and Mark taught me the value and rewards of team work. The UARS project is very much a team effort and it is with great pleasure that I thank Rich Zurek, Dave Crisp, Joe Waters, Lee Elson, Evan Fishbein, and Lucien Froidevaux for giving me the opportunity to participate in this mission to our planet and their cheerful enduring of my endless requests. I hope to continue our collaboration in future (and yes, finish and publish both the UARS and the Crisp et al. radiation paper). Andy Ingersoll is thanked for his patent advice I have asked from him on all sorts of problems, ranging from my GRE exam through my visa status (back in 1988) to the proper balance condition for the diabatic heating. Tom Ahrens, with his cheer and sound judgment, made our collaboration on my only experimental paper ("Angular Momentum Transfer in Low Velocity Oblique Impacts: Implications for Asteroids," *Icarus, 94,* 272-282, 1991) very enjoyable. Masahisa Yanagisawa provided invaluable help in carrying out the experiments. To Peter Goldreich this thesis should be a demonstration what a desperate effort to catch up

with capitalism can accomplish. By completing my graduate studies in 4 years and 7 months I hope to have made up for at least some of the time "wasted" in the socialist system. Bruce Murray and Dewey Muhleman provided quite a few valuable insights during my stay at Caltech, especially with regard to Mars, Titan, politics, and history.

At Caltech, many other people have extended their hospitality and friendliness to me. "Mom" Kay Campbell has truly made me feel like home, all the way from my first request for a free airplane ticket from London to the last ticket request (to Boston). Kay, Irma Betters, and Mike Black are also thanked for lending their attentive ears to the many stories I stopped by to tell. I owe it to Annette McCusker, who endured way too many drafts of my Triton and ozone papers, that this thesis could be assembled on a very short notice. Stuart McMuldroch and Stuart Stevens have cheerfully put up with me and I am sure their reward will be great on Earth: patience is a great virtue. I will miss you very much. A little farther down the hall, Steve Leroy, Rich Dissly, and Jim Lyons have too become very special buddies of mine. Less frequent, but no less instructing, were my conversations with Laszlo Keszthelyi and Brian Butler. Michelle Santee is thanked not only for the streamfunction code, but also for the many thoughtful conversations we had. It has been both pleasure and great help to work with Mimi Gerstell. I hope that she will continue her unwavering support with problems I am likely to encounter with either the rtmod code or the cloud climatology (yes, I will use the latter some day). I will back up to a tape and take with me all her e-mail messages. All other students have also in various way enriched my Caltech experience and they are summarily thanked for that. Finally, Fr. Brian Wilson and Ken Klewicki are thanked for their companionship.

SUMMARY

The present thesis reflects work I have done as a graduate student at Caltech. It is devoted to two broad subjects, planetary frost metamorphism and the terrestrial middle atmosphere, and consists of three papers.

Paper I considers frost metamorphism on the surfaces of Triton and Mars. Based on an analysis of the microphysical processes involved in pressureless sintering, it is concluded that fine-grained nitrogen and carbon dioxide frosts can undergo seasonal metamorphism into semitransparent layers on the surface of Triton and in the martian seasonal polar caps, respectively. The presence of such layers explains a host of facts about Triton's surface and about the martian seasonal caps. The Triton portion of the paper has been published in the *Journal of Geophysical Research*, while the Mars portion has been submitted to *Icarus*.

Paper II is devoted to elucidating a long-standing issue in the terrestrial middle atmosphere chemistry, the so-called "ozone deficit problem." Based on an analysis of data acquired by the Limb Infrared Monitor of the Stratosphere (LIMS) instrument between October 1978 and May 1979, it is concluded that current photochemical models systematically underestimate observed ozone abundances in the upper stratosphere and lower mesosphere. Three modifications to the accepted photochemical scheme, capable of providing a global solution to this problem, are proposed and discussed. This paper is in press by the *Journal of Geophysical Research.*

Paper III differs from the other two in that it reports on results from an ongoing research effort. It considers the diabatic circulation in the stratosphere and lower mesosphere, using ozone and temperature measurements acquired by the Microwave Limb Sounder (MLS) instrument onboard the Upper Atmosphere Research Satellite (UARS). The present study extends past analyses of the diabatic circulation by considering a full annual cycle November 1991 - November 1992 and by taking advantage of the high vertical resolution of MLS data. In the tropical upper stratosphere and lower mesosphere, a semiannual oscillation (SAO) is observed in the computed circulation, with the region of downwelling reaching maximum spatial extent ~1 month before the equinox. The projected lifetime of UARS should enable the present analysis to be extended to several SAO cycles.

TABLE OF CONTENTS

LIST OF FIGURES

PAPER III:

PAPER I

Microphysics of Frost Metamorphism:

Applications to Triton and Mars

Janusz Eluszkiewicz

Division of Geological and Planetary Sciences,

California Institute of Technology, Pasadena, CA 91125

the Triton portion published in modified form in *J. Geophys. Res.*, *96*, 19,217-19,229, 1991

the Mars portion submitted to *Icarus*

ABSTRACT

On the basis of an analysis of the microphysical processes involved in pressureless sintering of particulate materials and an examination of the physical conditions likely to prevail on Triton, it is argued that a well-annealed transparent nitrogen layer can form on Triton at 37 K on a seasonal time scale (~100 Earth years), provided the initial grain diameter is less than 1 μm. Slightly larger grains (in the 1-10 μm range) are allowed if grain growth does not hinder densification, but grains larger than 100 μm will certainly not achieve seasonal densification. If densification is to occur simultaneously with deposition, an initial grain diameter of <0.3 μm is required. The proposed layer is polycrystalline, the final grain diameter being 10-30 μm. In the north this layer is currently forming, whereas in the south it is the remnant of the layer formed during the last winter. The following observations can be explained by the presence of this layer: (1) the 2.16-μm absorption feature, provided that in analogy to the visible absorptivity of water ice, grain boundaries do not reduce the absorptivity of flawless nitrogen ice; (2) the smoothness of the surface at the <100-μm scale, indicated by the absence of the opposition effect and a low thermal emissivity inferred from the analysis of Voyager ultraviolet, infrared, and imaging data; (3) the dark and bright appearance of the northern and southern hemisphere, respectively, despite the fact that frost should be currently condensing in the north and subliming in the south; if nitrogen forms a transparent layer upon condensation, Voyager may have seen a dark substrate in the north and a permanent nitrogen cap in the south; and (4) the plumes; a well-annealed nitrogen layer would provide the "seal" required by the solid-state greenhouse model. In addition to explaining these observations, two conclusions can be reached from the analysis presented in this paper. First, if the equatorial collar is the site of a recent snowfall, its fresh, bright and blue appearance can be understood if the characteristic size of the snowflakes is ~100 μm, as calculated in a recent model. For such large grains the annealing time scale exceeds 10^4 Earth years. A recent appearance of this collar on a dark frost-free surface would help to explain the decrease in the degree of reddening observed between 1977 and 1989. Second, the dust devils are unlikely to work on Triton if micron-sized nitrogen grains are intermixed with the dust: the rapid sintering of such grains would provide the cohesive forces whose absence is essential in that model.

In the appendix to this paper, a similar analysis is carried out for carbon dioxide in the martian seasonal polar caps. It is concluded that seasonal metamorphism into annealed polycrystalline layers is possible there, provided freshly condensed grains are smaller than a few microns. The presence of low porosity CO_2 deposits over large areas could lead to millimeter- to centimeter-sized path lengths required to explain several weak absorption features observed in the 1.5 and 2.3 μm spectral regions. In addition, a nearly transparent layer should allow the albedo dichotomy between the northern and southern caps to be associated with the underlying substrate and thus be permanent; this would explain the exposure of the northern residual H_2O cap even during years when no great dust storms occur. On the other hand, the formation of an annealed layer is not expected in places where snowfalls occur, if the characteristic size of the snowflakes is greater than a few tens of microns. The upcoming observations by the Mars Observer Camera may distinguish sites where fine-grained frost is forming on the ground from areas covered by coarse-grained CO_2 snow.

1. INTRODUCTION

The surface of Triton is a very intriguing place. *Cruikshank et al.* [1984] observed a weak absorption feature at 2.16 μm, which they attributed to the first overtone of the density-induced band of molecular nitrogen (the fundamental band at 4.24 μm is unobservable from the ground because of the complete absorption by telluric carbon dioxide). Since nitrogen is a nonpolar molecule, this band could only be observed in a path length of ~1 m, and this led Cruikshank et al. to propose that liquid nitrogen is present on the surface of Triton. *Goguen et al.* [1989] performed photometric studies of Triton and discovered that unlike most other satellites, Triton has virtually no opposition surge. The opposition surge is defined as an enhancement in the logarithmic brightness of an object when observed at very small phase angles, in excess of that predicted by a linear extrapolation from larger phase angles. It is usually attributed to the fluffiness of the optically active layer and is explained either by the disappearance of mutual shadowing at small phase angles [*Hapke*, 1981] or by the phenomenon called coherent backscatter [*Hapke*, 1990; *Muinonen*, 1990]. The latter mechanism may be particularly relevant to a surface composed of transparent grains. The absence of an opposition surge is consistent with a smooth surface, which led Goguen et al. to propose the possibility of surficial liquid nitrogen. However, *Lunine and Stevenson* [1985] argued on thermodynamical grounds that liquid nitrogen is very unlikely to exist on the surface of Triton. The Voyager flyby proved them right by determining the surface temperature. The direct measurement by the infrared interferometer spectrometer was rather uncertain (simply because Triton is a very cold object and does not emit much infrared radiation in excess of instrument noise), but the best fit to the data yielded a surface temperature of 38 K [*Conrath et al.*, 1989], well below the melting temperature of nitrogen (63 K). Thus the issue of liquid nitrogen on the surface of Triton was definitely put to rest, only to be replaced by a host of new intriguing findings. The tenuous atmosphere discovered by Voyager has a pressure of ~16 μbar [*Tyler et al.*, 1989; *Broadfoot et al.*, 1989], which happens to coincide with the equilibrium vapor pressure of nitrogen at 37 K. This coincidence and the above mentioned (albeit not fully understood) 2.16-μm absorption feature have been taken as evidence that the surface of Triton is covered by nitrogen frost, in equilibrium with the atmosphere. However, if nitrogen is present as frost, how can it produce the meter-sized path lengths

required to explain the 2.16-μm absorption? Another puzzle concerning the surface of Triton is its smoothness, as suggested by the ground-based photometry (I discuss the alternative explanation for the absence of an opposition surge, the high visual albedo of Triton, in section 5). A surface smooth on the 100-μm scale may also be responsible for the low thermal emissivity inferred from a simultaneous analysis of data from Voyager ultraviolet, infrared, and imaging instruments [*Nelson et al.*, 1990]. Can nitrogen frost become that smooth at 37 K on a seasonal time scale (~100 Earth years)? The list of outstanding questions is longer. Voyager observed Triton during a period when nitrogen frost should be condensing in the northern hemisphere [*Spencer*, 1990; *Stansberry et al.*, 1990]. Yet the northern hemisphere is darker than the south, something one would not expect (at least on the basis of terrestrial experience) from a region covered by freshly deposited frost. Can it be that nitrogen condenses as a transparent layer and what we see in the north is the dark substrate underlying the seasonal frost [*Moore and Spencer*, 1990]? If it can, what happened in the equatorial region, which has been proposed as the site of a recent snowfall [*Pollack et al.*, 1990] and which is brighter and bluer than the surrounding regions [*McEwen*, 1990]? Why would nitrogen not form a transparent layer there? And then there are the plumes [*Soderblom et al.*, 1990]. Are they geysers powered by a solid-state greenhouse effect produced in a transparent layer of solid nitrogen [*Brown et al.*, 1990]? Or are they dust devils, composed of micron-sized cohesionless grains [*Ingersoll and Tryka*, 1990]? Is the assumption of very low cohesion plausible for Triton?

In this paper I want to provide a unified answer to the above questions by examining the microphysical processes involved in the metamorphism of nitrogen frost. I will attempt to show that nitrogen frost can metamorphose into a well-densified, transparent layer at 37 K over a seasonal time scale, provided the initial grain size is smaller than ~1 μm. If this layer is to form simultaneously with frost deposition, then the required initial grain diameter is <0.3 μm. The proposed layer is polycrystalline (the final grain diameter being ~10-30 μm), and there is no need to invoke rapid grain growth to explain the 2.16-μm absorption. The only requirement is that nitrogen is bubble- and contaminant-free, a condition which may well be satisfied on Triton, where an inert atmosphere is absent and impurities are expected at a very low level (10 ppm for methane and 100 ppb for higher hydrocarbons [*Broadfoot et al.*, 1989]). I pose it as a challenge to the experimentalist to test my hypothesis that grain boundaries do not reduce the

absorptivity of flawless nitrogen ice, in analogy to flawless polycrystalline water ice, which shows essentially the same absorptivity in the visible as distilled liquid water [*Lyons and Stoiber*, 1959]. In addition to the 2.16-μm absorption, the presence of a well-annealed layer would explain the weakness of the opposition surge and the smoothness required by the low thermal emissivity. In the north this layer is currently forming, whereas in the south it is the remnant of the layer formed during the last winter. The dark northern and the bright southern hemisphere can be understood if the transparent nitrogen layer forming in the north is underlain by a dark organic substrate whereas in the south it lies on top of a permanent nitrogen cap [*Moore and Spencer*, 1990]. If the latter is fractured on the scale of millimeters or larger, microphysics indicates that the cracks would not anneal even on a geologic time scale, and this would produce a unity optical depth for scattering (required to explain the bright appearance) in addition to the unity optical depth for the 2.16-μm absorption produced in the overlying remnant of the seasonal well-annealed layer. The blue and bright (fresh?) appearance of the equatorial collar can be understood if the snowflakes have sizes in the 100-μm range, as calculated in a recent model [*Yelle et al.*, 1991]. According to my calculations, for such large grains the annealing time scale exceeds 10^4 Earth years, and thus the transparent layer has not had enough time to form there. Finally, since the transparent layer would provide the seal required by the solid-state greenhouse model for the plumes whereas the alternative dust devil model is based on the (in my opinion) implausible assumption of grains with extremely low cohesiveness, I will cast my vote in favor of the former model.

The organization of this paper is as follows. In section 2, the previous work on frost metamorphism as it applies to Triton is critically reviewed. That work has focused mainly on the issue of grain growth in systems with negligible porosity and invariably leads to the conclusion that meter-sized grains (seemingly required by the 2.16-μm absorption feature) cannot form on Triton on a seasonal time scale. This conclusion still holds when a full examination of the microphysical processes involved in isothermal frost metamorphism is presented in section 3. The limiting grain size is found to be 10-30 μm, regardless of the mode of growth (by grain boundary migration in fully dense systems or by sintering in porous systems). In section 4, it is shown that whereas large grains cannot grow on Triton, a well-annealed polycrystalline layer may form by pressureless densification on a seasonal time scale, provided grains do

not grow to sizes larger than ~10 μm. This requires that the grains are smaller than ~1 μm initially. Slightly larger grains (initial grain diameter in the 1-10 μm range) are allowed if grain growth does not hinder densification, but grains larger than 100 μm will certainly not achieve seasonal densification. A more stringent condition for the initial grain diameter <0.3 μm may apply if densification is to occur simultaneously with deposition (something akin to epitaxial growth albeit the resulting layer is polycrystalline). In section 4, densification by creep at depth (followed by uncovering during sublimation) and frost metamorphism in a thermal gradient (akin to depth hoar formation on Earth) are also discussed. On the basis of simple estimates, it is concluded that both are unlikely to be important on Triton. In section 5, I present arguments that a transparent layer is all that is required to explain most of what we see on the surface of Triton. Additional implications of the kinetic constraints on frost metamorphism in nitrogen are also discussed there. Also in that section a speculative, but rather intriguing observational test of the annealed-layer hypothesis is proposed. The paper proper concludes with a summary in section 6. In the appendix to this paper, the metamorphic behavior of CO_2 frost in the martian seasonal polar caps is analyzed. It is concluded that there too the formation of a nearly transparent layer is possible for frost which is sufficiently fine-grained.

Throughout this paper, an effort has been made to define the symbols where they first appear in the text. In addition, a complete list of symbols is included following section 6.

2. Previous Work on Frost Metamorphism

"Metamorphism" is defined here to include both densification (if the frost is porous) and recrystallization. Recrystallization involves changes in the shape and/or the size of the grains. However, throughout this paper, spherical grains will be assumed, and thus recrystallization will be considered only with regard to the change in the mean grain diameter. This definition of metamorphism is the same as the one applied to transformation of terrestrial snow into ice [*Gow*, 1969]. The issue of the initial texture of freshly condensed frost is relevant in the studies of metamorphism for the following reason. If the initial condensate is fluffy, densification will accompany metamorphism. In this case, grain growth is limited by

sintering (the growth of necks between grains) and not by grain boundary migration. The latter only becomes the rate-limiting process in fully dense systems. The two modes of grain growth are shown in Figure 1 (the transition from the left to the right panel of that figure corresponds to what I call "densification"). None of the existing models of frost metamorphism on planetary surfaces [*Clark et al.*, 1983; *Kirk*, 1990] address the issue of densification; they only consider recrystallization (which is equivalent to grain growth if grains are assumed to be spherical). In application to Triton, *Zent et al.* [1989] following the work of *Clark et al.* [1983] proposed a grain growth law of the form

$$a^2 - a_o^2 = Ate^{-B/T} \tag{1}$$

where a is the grain diameter at time t, a_o is the original grain diameter, T is temperature in kelvins, $A = 1.5 \times 10^8$ mm^2 yr^{-1}, and $B = H/R$, where H is the enthalpy of sublimation and R is the gas constant. With $H = 6.8$ kJ mol^{-1} [*Frels et al.*, 1974], nitrogen grains ~2 mm in diameter are predicted by this model to form over a Triton season (~100 Earth years) at the ambient temperature of $T = 37$ K. It is not clear whether Zent et al. apply their grain growth law to porous or fully dense systems. Equation (1) was established empirically by *Gow* [1969], who studied the size of crystals in the Antarctic firn. However, no physical mechanism has been offered to explain equation (1), and so the use of this relationship to materials and conditions very different from those studied by Gow seems unwarranted. Some of the pitfalls associated with a direct application of equation (1) have been pointed out by *Kirk* [1990]. It is beyond the scope of the present paper to analyze the physical basis for equation (1), and so I will limit myself to two comments. First, grain metamorphism at depths studied by Gow (up to 49 m) may have been affected by dislocation creep, which is unlikely to affect the uppermost few meters on the surface of Triton (see section 4.3). If not corrected for this effect, the growth constant A adopted by *Zent et al.* [1989] and *Clark et al.* [1983] may not be applicable to any other planetary object. Second, sintering of ice in the terrestrial firn is dominated by transport through the air [*Hobbs*, 1974, p. 405], in contrast to Triton, where sintering of nitrogen grains occurs in the absence of significant amounts of an inert gas and volume diffusion is the dominant metamorphic process (for large grains). Accordingly, the choice of H as the relevant activation energy may not be correct. See section 3 for a further discussion of these points.

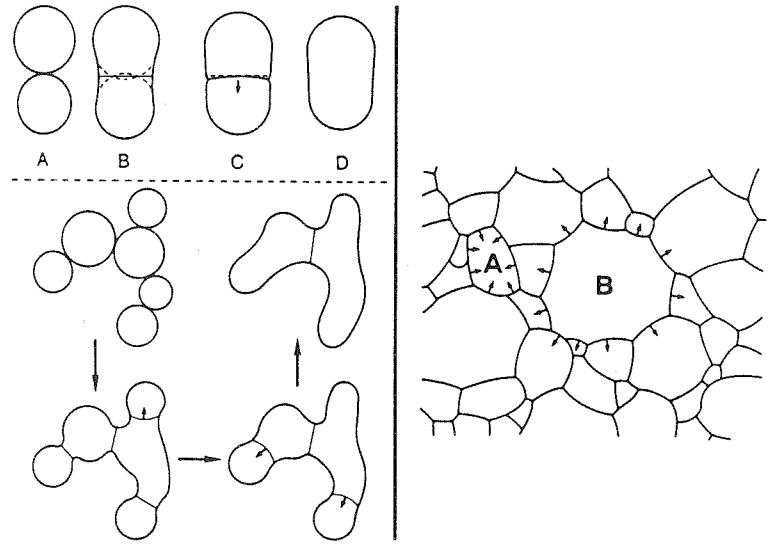

Fig. 1. The modes of grain growth. The small arrows illustrate the movement of grain boundaries. (Left, lower panel) General view of grain growth in porous systems. (Left, upper panel) Stages of grain growth in porous systems: (A) contact of grains of slightly different sizes, (B) growth of a neck between grains, (C) boundary migration through the smaller grain, and (D) formation of a new grain. Stage B is usually the rate-limiting step, and therefore the size of grains at time t is that for which the sintering time (the time to reach $2x = a$, where x is the neck size and a is the grain diameter) is equal to t. Whether a grain grows or shrinks depends only on the size of its neighbors. Figure adapted from *Greskovich and Lay* [1972]. (Right) Grain growth in low-porosity systems is limited by grain boundary migration. On average, grains with larger than a critical radius r_c (such as grain B) grow, whereas grains with radii smaller than r_c shrink (grain A). The microstructure shown in this figure corresponds to a nickel-zinc-ferrite sample (porosity $<1\%$) in the work by *Kurtz and Carpay* [1980].

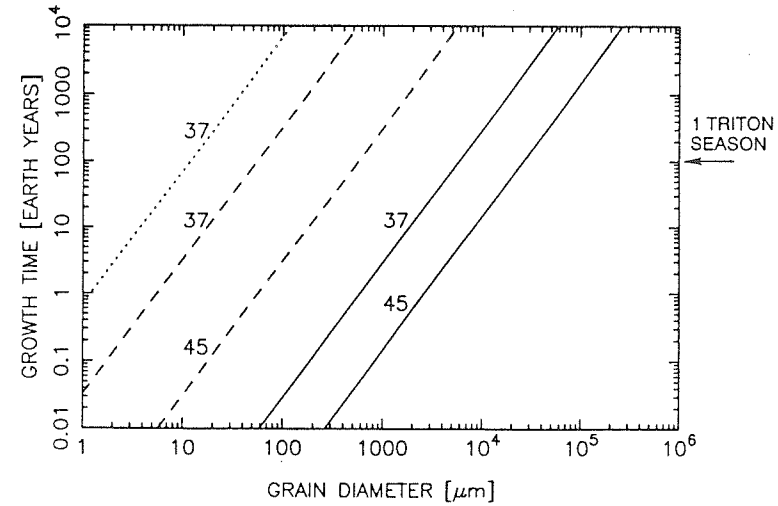

Fig. 2. Growth time versus grain diameter in nonporous solid nitrogen. The dashed and solid lines were obtained from equation (2) with D_b' equal to D_v and D_b, respectively (see text for details). The dotted line corresponds to the model of *Kirk* [1990] as best as I could reproduce it. The curves are labeled by the value of temperature in kelvins.

A physical model of grain growth has been offered by *Kirk* [1990], who used the equation

$$a^m - a_o^m = Kt \quad , \quad m = 2 \tag{2}$$

where $K = 2(16/81)\gamma M_i$, γ is the surface tension, M_i is the intrinsic grain boundary mobility equal to $D_b'\Omega/2\delta_b'kT$, D_b' is the rate of diffusion across the boundary, Ω is the molecular volume, δ_b' is the grain boundary width (assumed equal to $2\Omega^{1/3}$), and k is the Boltzmann constant. Equation (2) was originally derived by *Hillert* [1965]. Hillert's theory only applies to systems with negligible porosity (Figure 1, right panel). In such systems, grain growth is limited by grain boundary migration, which in turn depends on the radii of curvature. An essential concept in this theory is the critical radius r_c. At any time t, grains with radii smaller than $r_c(t)$ shrink, while grains greater than $r_c(t)$ grow. In this manner a "normal" grain growth is achieved, i.e., one in which the distribution of grain diameters normalized to the mean grain diameter changes little with time. Normal grain growth with a lognormal distribution of grain sizes (i.e., a Gaussian distribution of log$a$) is frequently observed in metallurgy.

The largest uncertainty in the above model is associated with the appropriate choice of D_b' and m. Kirk assumed $D_b' = D_v$ where D_v is the volume (lattice) diffusivity. However, his estimate of D_v was on the low side of the experimentally determined value (material parameters are listed in Table 1). In addition, Kirk may have underestimated the value of the "surface tension," although the only estimate of γ for solid nitrogen which I have been able to find in the literature refers to the surface tension between solid and vapor and may be higher than the "grain boundary" surface energy pertinent to Kirk's model. Kirk's original estimate is shown as the dotted line in Figure 2. The dashed lines in that figure correspond to the values of D_v and γ from Table 1. According to these estimates, no nitrogen grains larger than 50 μm can grow on Triton at $T = 37$ K on a seasonal time scale by this mechanism if $D_b' = D_v$. Even at $T = 45$ K, no grains larger than ~500 μm can grow. The situation is more favorable for grain growth if $D_b' = D_b$, where $D_b = D_{ob} \exp(-E_B/RT)$ is the rate of diffusion along the boundary. It is sometimes assumed [*Ashby and Verall*, 1978] that $D_b = D_{ov} \exp(-2/3E_v/RT)$, where D_{ov} and E_v are the preexponential factor and the activation energy, respectively, for volume diffusion. If this scaling holds for solid nitrogen, then the resulting growth lines correspond to the solid lines in Figure 2. In this "optimistic" scenario, centimeter-

sized grains can form on Triton at the elevated temperatures on a seasonal time scale. The time scale for growth of meter-sized grains exceeds 10^5 years.

The optimistic scenario discussed above may not apply, for several reasons. First, the $D_b = D_{ov} \exp(-2/3E_v/RT)$ scaling probably overestimates the grain boundary diffusivity, as volume diffusion usually dominates at high enough temperatures. This means that $D_{ob} << D_{ov}$. Second, the assumption of $D_b' = D_b$ probably overestimates the rate of diffusion across the boundary. In their studies of grain growth in polar ice, *Alley et al.* [1986*b*] found that D_b', while being 2 orders of magnitude greater than D_v, was 2 orders of magnitude lower than D_b. Third, in metallurgical practice the exponent on the left-hand side of equation (2) is usually found to be appreciably greater than 2 [*Hillert*, 1965], which is sometimes attributed to the pinning of grain boundaries by second-phase particles (in particular, trace porosity). This causes a slower grain growth. Fourth, Kirk's model may not be applicable if the frost on Triton is initially very porous. The following argument can be made to illustrate the last point.

As mentioned above, the theory of Hillert, and the grain growth models of *Alley et al.* [1986*a*] and *Kirk* [1990] based on that theory, only apply to materials of very low porosity (less than a few percent). As pointed out by *Alley et al.* [1986*b*], grain growth in highly porous systems may be limited by the rate of neck growth between grains rather than by grain boundary migration. This was demonstrated experimentally for alumina by *Greskovich and Lay* [1972]. They distinguished four steps in the grain growth occurring in their experiments (Figure 1, upper left panel): (A) contact of grains of slightly different sizes, (B) growth of the neck between contacting grains, (C) migration of the grain boundary away from the contact plane leading to (D) emergence of a new larger grain. The neck growth was the rate-limiting step; i.e., grain boundary migration was much faster than neck growth. Whether a grain grows or not depends in this case only on the size of its neighbors, not on a critical radius. As the grain geometry approached the "soap foam" structure (Figure 1, right), conventional grain growth as discussed by *Hillert* [1965] began to operate.

The above argument serves to illustrate the relevance of neck growth (sintering) in frost metamorphism on planetary surfaces. The initial state of the frost, in particular the degree of its fluffiness affects the rate of grain growth. The physical processes driving sintering are discussed in the next section.

TABLE 1. MATERIAL DATA FOR CRYOICES

Parameter	Nitrogen	Methane
Molecular volume Ω, m^3	4.7×10^{-29}	5.1×10^{-29}
Burgers vector b, m	3.6×10^{-10}	3.7×10^{-10}
Melting temperature T_m, K	63.148	90.67
Density Δ_o, kg m^{-3}	995	515
Shear modulus μ, Pa	10^{9a}	10^{9b}
Surface energy at T = 37 K γ, J m^{-2}	2×10^{-2} [c]	2×10^{-2} [d]
Dislocation density N, m^{-2}	10^{16}	10^{16}
Preexponential factor, volume diffusion D_{ov}, m^2 s^{-1}	1.6×10^{-7} [e]	10^{-3} [f]
Activation energy, volume diffusion E_v, kJ mol^{-1}	8.6 [e]	15.9 [f]
Preexponential factor, boundary diffusion $\delta_b D_{ob}$, m^3 s^{-1}	1.2×10^{-16} [g]	7.4×10^{-13} [g]
Activation energy, boundary diffusion E_b, kJ mol^{-1}	5.7 [h]	10.6 [h]
Preexponential factor, surface diffusion $\delta_s D_{os}$, m^3 s^{-1}	1.2×10^{-16} [g]	7.4×10^{-13} [g]
Activation energy, surface diffusion E_s, kJ mol^{-1}	8.6 [i]	15.9 [i]
Preexponential factor, vapor pressure P_o, Pa	5.5×10^9 [j]	. . . [k]
Heat of sublimation H, kJ mol^{-1}	6.8[j]	. . . [k]
Creep exponent, n [l]	3[m]	3 [n]
Preexponential factor, creep A_2, MPa^{-n} [l]	10^m	10 [p]
Activation energy, creep Q, kJ mol^{-1} [l]	5.8 [o]	8.4 [n]

NOTES TO TABLE 1

[a] *Scott* [1976].

[b] *Bezuglyi et al.* [1966].

[c] Estimated from the formula γ [mJ m^{-2}] = 13 - 0.32 (T [K] - 63), fitted to the data of *Gladkikh and Khotkevich* [1969].

[d] Assumed equal to the value for nitrogen.

[e] *Esteve and Sullivan* [1981].

[f] *Chezeau and Strange* [1979].

[g] Assumed equal to $2\Omega^{1/3}D_{ov}$.

[h] Assumed equal to 2/3 E_v.

[i] Assumed equal to E_v.

[j] *Frels et al.* [1974].

[k] Vapor pressure calculated from the formula $\log_{10}P_v$ [mm Hg] = 7.69540 – 532.20/(T [K] + 1.842) [*Ziegler,* 1959].

[l] Equation (6).

[m] Assumed equal to the value for methane.

[n] *Bolshutkin et al.* [1968].

[o] Calculated from the scaling Q/T_m = const and the value of Q for methane.

[p] Estimated from *Bolshutkin et al.* [1968].

3. PHYSICS OF SINTERING

Sintering refers to the growth of the neck between two grains driven by the differences in curvatures and surface tension. Under isothermal conditions it is the driving process in both grain growth and densification (the effect of a thermal gradient is discussed in section 4.4). Sintering of two equal spheres was studied in great detail by *Ashby* [1974] and *Swinkels and Ashby* [1981]. In the absence of external stresses, six microscopic mechanisms have been identified to contribute to sintering (Figure 3*a*). The rate of neck growth can be calculated from the equation

$$2\pi x\rho\theta\dot{x} = \sum_{i=1}^{6} \dot{V}_i \qquad (3a)$$

where x is the neck size (radius of disc of contact between the two particles), ρ is the radius of curvature of the neck, and $\dot{V}_i$ is the volume flowing per unit time into the neck region due to the ith mechanism. The angle θ is defined in Figure 3*b*. The six mechanisms and their rate equations are as follows [*Swinkels and Ashby*, 1981]:

3.1. *Surface Diffusion from a Surface Source*

$$\dot{V}_1 = \frac{3\pi x D_s \delta_s \gamma \Omega (K_3 - K_2)}{d_2 kT} \qquad (3b)$$

In this mechanism, surface diffusion delivers matter from region C to region B (see Figure 3*b*) because the curvature K_3 (= $2/a$) at C is less negative than the curvature K_2 at B (curvatures are negative when the center of curvature lies outside the material). $D_s = D_{os} \exp(-E_s/RT)$ is the surface diffusivity, E_s is the activation energy, δ_s is the effective surface thickness assumed equal to $2\Omega^{1/3}$, and d_2 is the diffusion distance defined in Figure 3*b*.

3.2. *Lattice Diffusion from a Surface Source*

$$\dot{V}_2 = \frac{3\pi x D_v \gamma \Omega (K_3 - K_m)}{kT} \qquad (3c)$$

Matter flows from C to A through the bulk of the material because K_3 is less negative than K_m (= $1/\rho$), the mean curvature of the neck. $D_v = D_{ov} \exp(-E_v/RT)$ is the volume (lattice) diffusivity.

3.3. *Vapor Transport from a Surface Source*

$$\dot{V}_3 = 2\pi x \rho \theta P_v \frac{\gamma \Omega}{kT} \sqrt{\frac{\Omega}{2\pi \Delta_o kT}} \left(K_3 - K_m \right) \tag{3d}$$

Matter evaporates at C and is deposited at A because of the difference in curvatures. P_v is the vapor pressure and Δ_o is the theoretical density. This rate equation refers to vapor transport in the absence of an inert gas. For the sintering of methane occurring in the presence of nitrogen a different equation may apply if vapor transport is limited by gaseous diffusion. The latter would occur if $\lambda < \rho$, where λ is the mean free path (~500 μm on the surface of Triton). This complication is neglected here.

3.4. *Grain Boundary Diffusion from a Boundary Source*

$$\dot{V}_4 = \frac{16\pi D_b \delta_b \gamma_b \Omega}{xkT} \left(1 - \frac{K_1 x}{2} \right) \tag{3e}$$

Grain boundary diffusion delivers matter from the boundary to the neck, which is then redistributed by surface diffusion (see *Swinkels and Ashby* [1981] for details). K_1 is the curvature at A, $\delta_b = 2\Omega^{1/3}$ is the effective thickness of the grain boundary, and γ_b is the grain boundary energy. In general, γ_b may be different from the solid-vapor surface tension γ, which enters equations (3*b*)-(3*d*); γ_b is a function of crystal misorientation: if the crystal structures in the neighboring grains were perfectly aligned, γ_b and the grain boundary itself would vanish. In the following, $\gamma_b = \gamma$ will be adopted. Also, δ_b may in general be different from δ_b' in equation (2) [*Ricoult and Kohlstedt*, 1983].

3.5. *Lattice Diffusion from a Boundary Source*

$$\dot{V}_5 = \frac{32\pi \rho \theta D_v \gamma_b \Omega}{xkT} \left(1 - \frac{K_m x}{2} \right) \tag{3f}$$

Matter is delivered from the boundary to the neck by diffusion through the lattice.

3.6. *Lattice Diffusion from Dislocation Sources*

$$\dot{V}_6 = \frac{8\pi x^2 \rho \theta N D_v \gamma_b \Omega}{9kT} \left(-K_m - \frac{3\mu x}{\gamma a} \right) \tag{3g}$$

N is the dislocation density and μ is the shear modulus. This process, the transient creep, is to be distinguished from the steady state creep discussed below. In transient creep, dislocations in the neck region

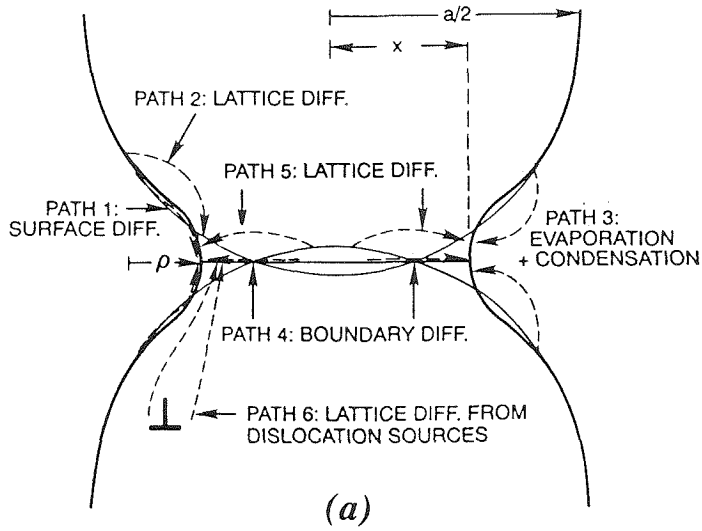

(a)

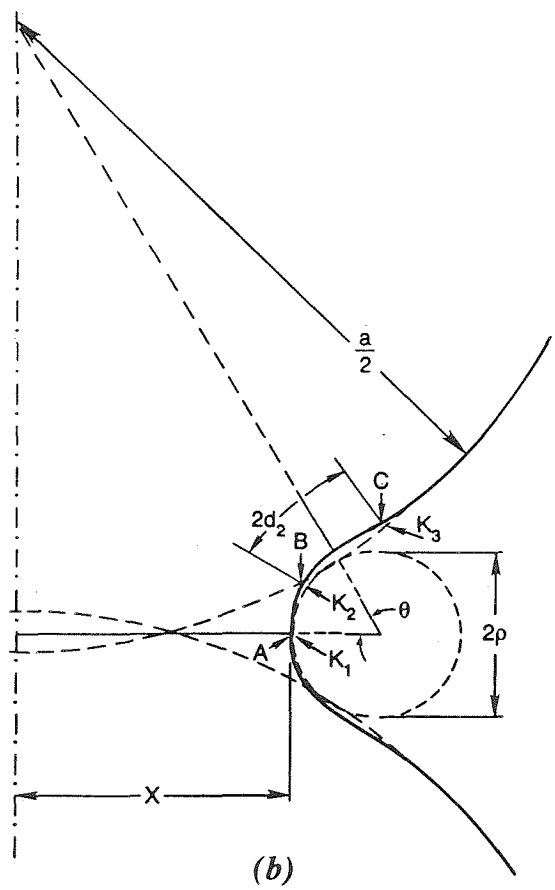

(b)

Fig. 3. (*a*) The mechanisms of sintering, where a is the grain diameter, x is the radius of the neck, and ρ is the radius of curvature of the neck. (*b*) The geometry involved in sintering. See text for details. Figure adapted from *Swinkels and Ashby* [1981].

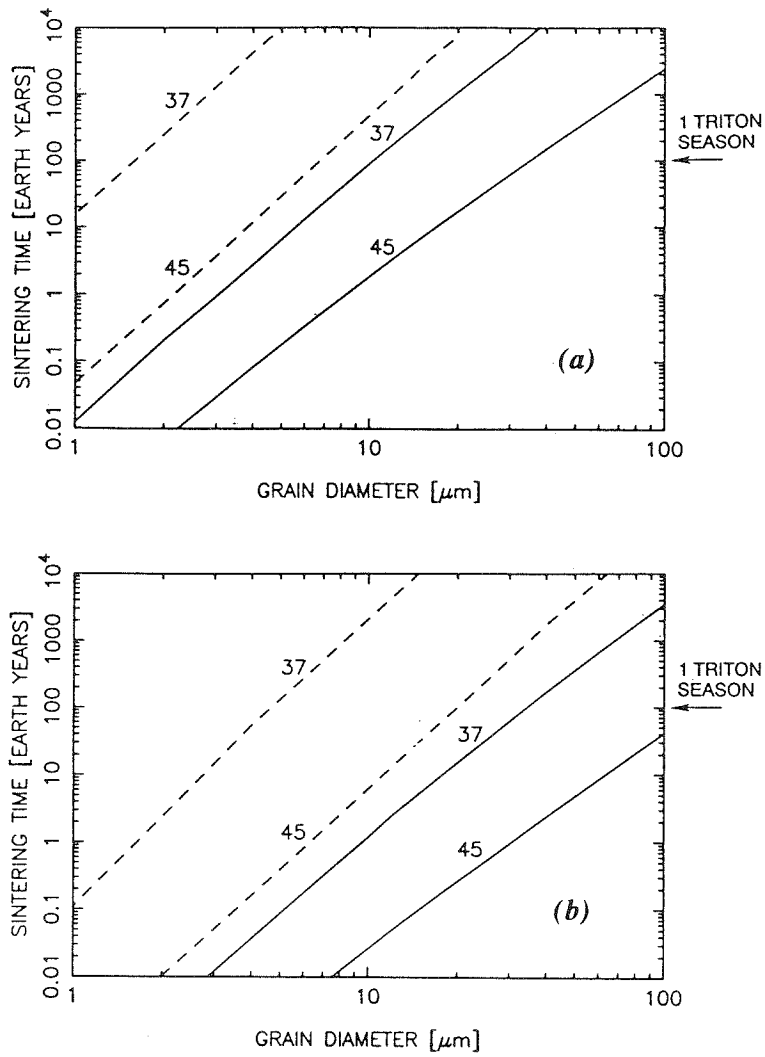

Fig. 4. Sintering times $\tau_{1,2}$ as functions of grain diameter a for nitrogen (solid lines) and methane (dashed lines): (*a*) τ_1 calculated as the time to reach $2x = a$, and (*b*) τ_2 calculated as the time to reach $2x = 0.45\ a$. The curves are labeled by the value of temperature in kelvins.

climb, becoming curved, until they reach static equilibrium. Matter is delivered to the neck. As discussed by *Ashby* [1974], in the absence of external stresses, the contribution from this mechanism is negligible for reasonable dislocation densities ($<10^{16}$ m^{-2}).

The values of material parameters for solid nitrogen and solid methane are given in Table 1. The measured activation energy for volume diffusion in solid nitrogen is appreciably lower than the value adopted by *Kirk* [1990]. It is clear that future experiments may lead to a revision of the values for the diffusivities assumed here. In fact, sintering measurements and the expressions for the rate coefficients given above can be used to determine $\delta_b D_b$ and $\delta_s D_s$ (the other method commonly employed to measure these quantities, namely tracer diffusion, is not applicable to nitrogen since nitrogen does not have an isotope with a convenient lifetime). The sintering calculations to be presented below are only as good (or as bad) as the material data entering the equations (to within a factor of ~2 [*Swinkels and Ashby*, 1981]).

In the absence of external stresses the above list of sintering mechanisms is believed to be exhaustive [*Ashby*, 1974]. However, additional mechanisms may operate if an external load σ is applied. The most important of them is steady state creep. For steady creep to be possible, dislocations must be multiplied, a process which requires $\sigma > \mu b/x$, where $b \sim \Omega^{1/3}$ is the Burgers vector of dislocations (assumed equal to the molecular diameter). Under lithostatic conditions $\sigma = \Delta g z$ at depth z, where Δ is the bulk density and g is the surface gravity (creep can affect sintering even under lithostatic conditions since the lithostatic pressure gives rise to deviatoric stresses at grain contacts). Dislocation multiplication is not possible in the absence of external stresses, as this would require $\gamma/x > \mu b/x$, a condition which is never satisfied. However, even at moderate stresses of 1 bar (which correspond to a depth of 10 m in the terrestrial firn) steady creep can be expected to be many orders of magnitude faster than any of the mechanisms listed above. Clearly, the grain sizes observed by *Gow* [1969] may have been affected by processes much faster than those relevant to frost metamorphism on the optical surfaces of planetary objects. This point is corroborated by the fact that the growth constant A in equation (1) adopted by *Clark et al.* [1983] and *Zent et al.* [1989] has very similar values for both water ice and metals. This calls the validity of their model into question as, other factors being equal, the rate equations given above suggest that A should be proportional to γ. However, surface tension of metals is 1 to 2 orders of magnitude higher than

for volatile ices. For this reason, the calculations by Zent et al. are not unlikely to overestimate the grain sizes on the surface of Triton by an order of magnitude. Note that on Triton to satisfy the condition $\sigma > \mu b/x$ at depths uncovered by seasonal sublimation ($z \sim 1$ m) requires $x > 1$ mm and thus $a > 1$ mm.

Starting with an initial neck size resulting from adhesion [*Ashby*, 1974], equation (3*a*) is integrated until $2x = a$ is reached. The expressions for d_2, ρ, θ, and the curvatures are taken from *Swinkels and Ashby* [1981]. The rate of sintering due to vapor transport is negligible in relation to the contributions from grain boundary and volume diffusion, the latter being the dominant process for large x and a. Since the activation energy for volume diffusion is usually greater than the enthalpy of sublimation (as is the case for nitrogen and methane), the use of the latter as the activation energy in grain metamorphism, as done by *Clark et al.* [1983] and *Zent et al.* [1989], may lead to an additional order of magnitude in the overestimate of the grain size. The resulting sintering time τ_1 is shown as a function of grain diameter in Figure 4*a*. In Figure 4*b*, another sintering time τ_2 is defined as the time to reach $\theta = 60°$, which corresponds to $2x = 0.45a$. This may be a more appropriate final condition when the spheres sinter in a closely packed assemblage [*Swinkels and Ashby*, 1981]. The two sintering times differ significantly. However, the resulting differences in grain sizes are much smaller owing to the strong dependence of the sintering times on the grain diameter ($\tau_{1,2} \propto a^4$). For example, at $T = 37$ K, $a = 10$ μm for $\tau_1 = 100$ years, whereas $a = 30$ μm for $\tau_2 = 100$ years. Similar estimates apply to methane. In particular, the sintering times for methane at $T = 45$ K are 5 times longer than sintering times for nitrogen at 37 K (the corresponding size estimates are very similar). Note that the sintering times for micron-sized nitrogen grains are very short, of the order of days or even hours. On the other hand, the sintering times for grains larger than 100 μm greatly exceed one Triton season at 37 K.

The sintering times shown in Figure 4 can be interpreted as the age at which grains reach a certain diameter. To see this, imagine a thin section in which the mean grain diameter is a. The fact that these grains are still recognizable means that the corresponding sintering times $\tau_{1,2} = \tau_{1,2}(a)$ are not much shorter than the age of the sample, otherwise the grains would have merged into larger grains. If the grains have already undergone some sintering, then the sintering times are also not much longer than the age of the grains. Clearly, this is only a very approximate solution to the problem of determining the growth law.

However, the approximation only comes from the neglect of geometrical complications (nonsphericity and interpenetrations of grains, size distribution, etc.), and given accurate material parameters it is unlikely that it introduces an error of more than an order of magnitude in the age estimate. Owing to $\tau_{1,2} \propto a^4$, the corresponding error in the estimate of a is much smaller (a factor of ~2). From this and Figure 4, I conclude that the limiting grain size in porous nitrogen frost at 37 K over 100 Earth years is 10-30 μm. Even at 45 K, no nitrogen grains larger than 100 μm would sinter on a seasonal time scale. As these estimates are not significantly different from *Kirk's* [1990] estimate for a fully dense system discussed in section 2, it seems that at 37 K, 10-30 μm may just be the characteristic size of grains on Triton, provided they grow from smaller sizes.

4. Formation of a Transparent Layer

4.1 *Densification*

On purely thermodynamical grounds, it is certain that given an infinite amount of time, a fluffy frost of pure nitrogen in vacuum would metamorphose into a single crystal: this is the state of minimum surface energy. The question to be addressed with regard to the formation of a transparent layer on Triton is therefore whether it will form at $T = 37$ K on the time scale of interest (one Triton season, ~100 Earth years) and whether there are no other factors which may hinder its formation. With regard to the latter question, I believe that Triton may indeed be the definite solar system test bed for the process of frost metamorphism: there is no inert gas present and therefore no "air bubbles" are expected, the winds are far too weak to lift grains as cohesive as nitrogen's, the level of impurities is on average low (~10 ppm and 100 ppb for methane and opaque impurities, respectively [*Broadfoot et al.*, 1989]), the frost temperature is constant on the diurnal time scale [*Spencer*, 1990] and changes very little over a season; the constancy of temperature may make thermal cracking insignificant (with the possible exception of the β-α transition; see section 5). Note that none of these conditions is satisfied in snow and ice on Earth. Until evidence to the contrary is presented, I will therefore assume that there are no external factors which would hinder the formation of a transparent layer on Triton. Thus, only the kinetic constraints remain to be investigated.

As discussed in section 2, I certainly do not expect the seasonal deposit of nitrogen (~1 m [*Ingersoll*, 1990]) to metamorphose into a single crystal on a seasonal time scale: the mobility of grain boundaries is far too low to achieve this under the most optimistic assumptions. I do believe, however, that densification into a very low porosity polycrystalline layer is possible. The sintering equations discussed in section 3 can be used to estimate the rate of change in the distance between the centers of the two spheres, and from this the rate of densification in a powdery sample can be inferred [*Swinkels and Ashby*, 1981; *Arzt et al.*, 1983]. This is only an approximate procedure, as it ignores grain growth which occurs simultaneously with densification. A complete model of metamorphism, including both densification and grain growth, is not yet forthcoming even in metallurgy [*Arzt et al.*, 1983], despite several decades of efforts and the accumulation of a vast literature related to either of the two components of the problem separately. In an assemblage of equal spheres whose radii r do not change with time the rate of densification is given by the following expression [*Ashby*, 1988]

$$-\dot{\varphi}_s = 72C(1-\varphi_o)\frac{D_v}{r^2}\frac{\gamma\Omega}{rkT} + 18C\frac{1-\varphi}{\varphi_o-\varphi}\frac{\delta_b D_b}{r^3}\frac{\gamma\Omega}{rkT} \qquad \text{for } \varphi > 0.1 \qquad (4a)$$

where φ is the porosity, φ_o is the initial porosity, $C = \varphi_o/(\varphi_o - \varphi)$, $r = a/2$, and the other symbols have the same meaning as before. The above expression only applies for $\varphi > 0.1$. In the final stages of densification when the pore space consists of isolated spherical pores the rate of densification is equal to

$$-\dot{\varphi}_s = 18\left(\frac{\varphi}{6}\right)^{1/3}\frac{D_v}{r^2}\left[\frac{2\gamma}{r}(6/\varphi)^{1/3} - p_i\right]\frac{\Omega}{kT} + 9\frac{\delta_b D_b}{r^3}\left[\frac{2\gamma}{r}(6/\varphi)^{1/3} - p_i\right]\frac{\Omega}{kT} \qquad \text{for } \varphi < 0.1 \qquad (4b)$$

where p_i is proportional to the pressure of the gas trapped in the pores. For nitrogen on Triton, where an inert atmosphere is absent, it seems reasonable to assume $p_i = 0$. The two terms on the right-hand side of equations (4) correspond to densification by volume and grain boundary diffusion, respectively. The only other sintering mechanism which leads to the approach of the centers of the grains and thus to densification is lattice diffusion from dislocation sources, but in the absence of external pressure its contribution is negligible. The time scale for densification $\tau_s = -\varphi/\dot{\varphi}_s$ at $T = 37$ K is plotted as a function of grain

diameter in Figure 5 (solid lines) for $\varphi_o = 0.36$ and $\varphi = 0.3$ (initial stage of densification) and $\varphi = 0.1$ (final stage of densification). Other choices of φ_o and φ would change the results only very slightly. It would seem from that figure that initial densification will occur in less than 100 Earth years for grains with diameters smaller than ~30 μm. The higher estimate of ~40 μm obtained previously by *Eluszkiewicz and Stevenson* [1990] resulted from an overestimate of the value for surface energy. Initial densification may be sufficient to achieve smoothness and impermeability of the surface. On the other hand, a complete elimination of the pores may be necessary to produce the long path lengths required by the 2.16-μm absorption. In this case, grains with diameters smaller than ~10 μm are called for. A question to be addressed by future research is whether a complete elimination of the pores can indeed by achieved. *Ashby*'s [1988] theory and equation (4*b*), based on this theory, may not be applicable in the limit $\varphi \rightarrow 0$. This limit is certainly never attained in metallurgical practice, toward which Ashby's theory is primarily geared, and may not be attainable even in the rather unique circumstances of nitrogen on Triton (no inert gas, very low levels of impurities) if the grain boundary energy leads to the formation of equilibrium "pockets" at grain contacts characterized by a dihedral angle not equal to 180°. Even if these pockets are strongly forward scattering, their sheer number (about 10^5 per meter for 10-μm-sized grains) would make unlikely the achievement of the required path length for the 2.16-μm absorption. At this moment I make the optimistic assumption that densification will indeed proceed to completion for grains smaller than 10 μm.

Note that the inclusion of grain boundary diffusion in the present calculation does not affect the estimate of the upper limit to the grain size for which densification is important, simply because for grains larger than ~10 μm, volume diffusion is the dominant mechanism of densification. In this regard, it is very fortunate that a direct measurement of the volume diffusivity D_v exists [*Esteve and Sullivan*, 1981].

In reality, however, 10 μm is only an upper bound on the initial grain size allowed to achieve densification. If the initial grain size were 10 μm, grains could grow to larger sizes as discussed in section 3. In the absence of a satisfactory theory of simultaneous grain growth and densification, I will assume that in initially porous frosts, porosity becomes smaller than 10% (at which point grain growth ceases to be important since the pores, whose size now determines the densification rate, cannot grow further) when the

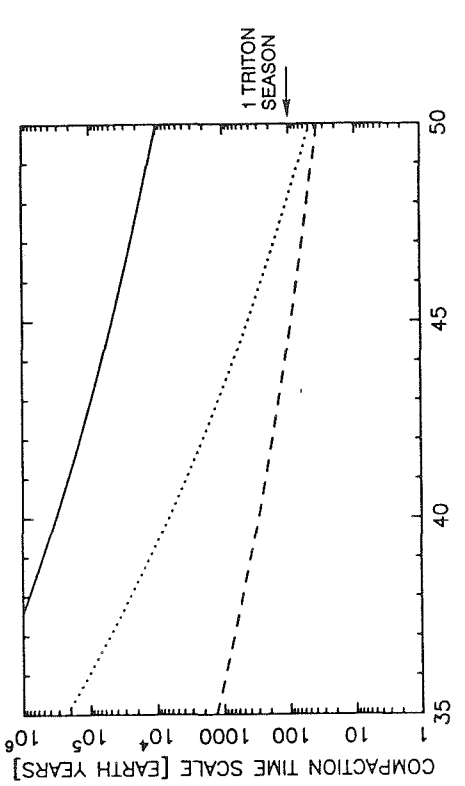

Fig. 6. Compaction time scale τ_c at depth z = 10 m on Triton as a function of temperature for different assumptions about the creep law in solid nitrogen: equation (5), dotted line; equation (6) with creep parameters from Table 1, solid line; and equation (6) with the activation energy 0.6 × value from Table 1, dashed line. The compaction time scale at z = 1 m is roughly 1000 times longer.

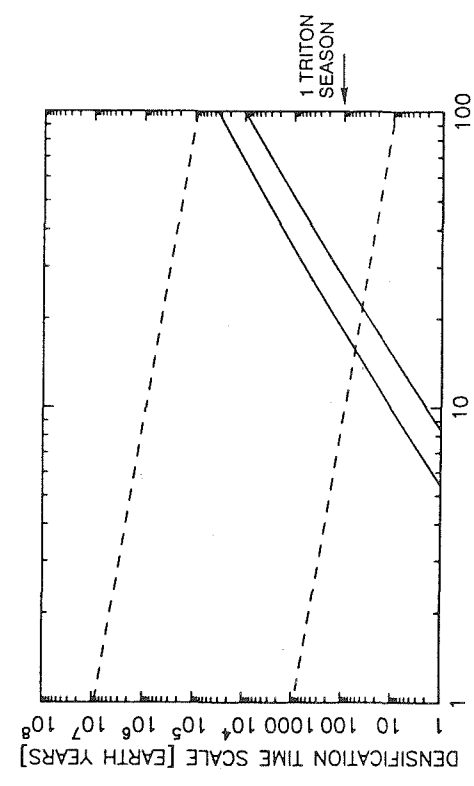

Fig. 5. (Solid lines) Densification time scale τ_s (due to pressureless isothermal sintering) as a function of grain diameter for solid nitrogen at 37 K in the initial and final stages of densification (lower and upper line, respectively). (Dashed lines) Time scale τ_i for the change of porosity due to pore migration in a thermal gradient at 37 K as a function of pore diameter. The thermal gradient is 10 K m^{-1} and 0.1 K m^{-1} (lower and upper line, respectively). The sign of the change of porosity in a thermal gradient is uncertain, but it may be positive (depth hoar formation).

growing grains become larger than ~10 times the initial grain diameter. This assumption is motivated by the behavior observed by *Greskovich and Lay* [1972] in their studies of grain growth in porous alumina. Note that simultaneous grain growth and densification is a geometrical, not a kinetic, problem and therefore the use of a different material as a guide to nitrogen seems warranted. Thus, as a conservative estimate I postulate that densification in nitrogen frost will be completed at 37 K on a seasonal time scale if the initial grain size is smaller than 1 μm. Grains in the 1-10 μm range may also achieve densification, but this is less certain. Grains larger than 100 μm will certainly not achieve it.

The above estimate of the initial grain size is based on the assumption that densification occurs on a seasonal time scale. However, smaller grains may be called for if densification is to occur simultaneously with deposition. This seems to be required for the northern hemisphere if frost deposition is currently occurring there and if one desires to explain the relative darkness of that hemisphere by the transparency of the forming deposit. In section 4.2 it is shown that grains smaller than 0.3 μm are necessary to achieve densification simultaneously with deposition. This process is similar to the process of epitaxial growth.

4.2 *Epitaxial Growth*

Epitaxial growth from the vapor phase has been mentioned as a mechanism to produce large nitrogen crystals [*Kirk*, 1990]. It refers to the situation where large single crystals are grown by deposition of atoms or molecules onto a substrate. It would seem that this is the most natural way of growing a transparent layer on Triton, where the rate of frost deposition is likely to be on average very low. However, recent experiments by *Volkmann and Knorr* [1991] indicate that a fundamental property of nitrogen makes this process impossible above 35.6 K, the transition temperature from the cubic α phase to the hexagonal β phase (β phase is the form which currently exists on Triton). In their experiments, Volkmann and Knorr attempted to build multilayers of nitrogen by sequential deposition of monolayers. What they found was that whereas it was possible to grow epitaxial, optically smooth layers of α-nitrogen this way, β-nitrogen always formed polycrystalline, strongly scattering layers under the conditions of vapor equilibrium. Volkmann and Knorr speculated that the anisotropy of surface tension in the β phase may be responsible for this behavior: [001] may not be the easy growth direction. The different behavior of the cubic and hexagonal forms of nitrogen has a prominent analogy: the formation of hexagonal graphite often spoils the

epitaxial growth of cubic diamond (G. R. Rossman has kindly pointed out this analogy to me). Certainly, this is a fascinating topic for an experimentally oriented reader, but for the moment I will assume that β-nitrogen cannot indeed form epitaxial (in the conventional sense of this word) layers on Triton. However, something akin to epitaxial growth may occur if the sintering time of the newly deposited grains is short in relation to the deposition time scale and grains simply merge with the substrate as they are deposited (very much as liquid droplets do). In this case, a fully dense transparent layer may be expected to form simultaneously with deposition, although it is polycrystalline rather than a single crystal. If, on the other hand, a new layer much thicker than the grain diameter a is deposited above the newly deposited grains before the latter can sinter with a characteristic time τ_1 (the longer sintering time in section 3), then the grains will be "buried," and the subsequent densification will occur as described in section 4.1. In this case, the forming layer may not be transparent at any given time. Thus, metamorphism can be expected to supersede "epitaxy" if $\varsigma = H_s/a >> 1$, where H_s is the thickness of the layer deposited over time τ_1. Assuming a constant deposition rate, H_s is equal to $\varepsilon\sigma_{SB}T^4\tau_1/L\Delta$ where ε is the thermal emissivity, σ_{SB} is the Stefan-Boltzmann constant, L is the latent heat of sublimation (~2.5×10^5 J kg^{-1} for solid N_2), and Δ is the bulk density of the layer. The emissivity can be less than 1 on Triton [*Nelson et al.*, 1990], while Δ can be expected to be less than the theoretical density Δ_o due to porosity, but in the following calculation, $\varepsilon = 1$ and $\Delta = \Delta_o$ will be assumed. At 37 K, $\varsigma \sim 0.1(a/0.1\ \mu m)^3$, and thus grains with diameters larger than 0.3 μm will be buried ($\varsigma > 1$) before they can sinter. Epitaxy will be efficient for grains smaller than 0.3 μm. In this context it is interesting to note that laboratory observations of condensing nitrogen frost are somewhat conflicting. *Vegard* [1932, p. 471] reported that condensing β-nitrogen tends to form a white grainy substance, whereas α-nitrogen forms transparent layers, in the original German text: "Wenn die α-Form sich auf die gekuehlte Flaeche niederschlaegt, bildet sich eine eisartige und durchsichtige Schicht; — die β-Form dagegen schlaegt sich nur in der Form einer koernigen weissen Masse nieder." This is similar to the behavior observed by *Volkmann and Knorr* [1991]. However, *Cook and Davey* [1976, p. 366] report the opposite: "All layers [of solid nitrogen] condensed at temperatures below 35 K had an even white appearance, the polycrystalline layer being made up of very small crystals. The one layer condensed at 50 K was completely transparent and no crystal boundaries were visible." In their experiments the fluffiness

of the frost increases as the condensation rate decreases. Certainly, future experiments can shed more light on this issue. Until such experiments are performed, I will simply assume that a well-annealed layer can form on Triton simultaneously with deposition for grains smaller than 0.3 μm. This is a special case of the densification discussed in section 4.1 (where somewhat larger grains were allowed since densification was assumed to proceed on a seasonal time scale). As noted above, densification concurrent with deposition may be required to explain the transparency of the layer in the north if frost is continuously being deposited there.

For the sake of completeness, in the remainder of this section I discuss two other processes which may contribute to frost metamorphism on Triton and conclude that they are both unlikely to be important. The reader who is not interested in technical details may proceed directly to the next section.

4.3. *Power-Law Creep*

As mentioned in section 3, power law creep may affect frost metamorphism under lithostatic pressure. This opens the interesting possibility that nitrogen is densified at depth and is then uncovered by sublimation. Since no creep data for nitrogen exist, two methods will be used to estimate the creep law. If creep is diffusion controlled, then the rate of creep is given by the expression [*Ashby and Verall*, 1978]

$$\dot{\varepsilon} = A_1 \frac{D\mu b}{kT} \left(\frac{\sigma}{\mu}\right)^n \tag{5}$$

where $\dot{\varepsilon}$ is the strain rate, σ is the deviatoric stress, $A_1 \sim 21$, $n = 3$, and D is a diffusion constant (usually assumed equal to the lattice diffusivity). In the second method a standard form of creep law will be assumed:

$$\dot{\varepsilon} = A_2 \sigma^n \exp(-Q/RT) \tag{6}$$

with the values of A_2, n, and Q given in Table 1.

The rate of compaction $\dot{\varphi}_c$ at depth z (which corresponds to pressure $p = \Delta gz$) is calculated from equations (5) and (6) for 10% porosity [*Eluszkiewicz*, 1990]. The corresponding compaction time scale $\tau_c = -\varphi/\dot{\varphi}_c$ is shown in Figure 6. It seems that unless rheology of nitrogen is very different from that of methane, power law creep is unlikely to contribute to seasonal frost metamorphism in the upper few meters

on the surface of Triton.

4.4. *Metamorphism in a Thermal Gradient*

The metamorphic processes considered thus far are isothermal. On Triton the assumption of isothermality is very good in the uppermost layers, where the frost temperature is kept constant by vapor equilibrium with the atmosphere. However, the temperature may rise at depth, owing to either the geothermal gradient or absorption of sunlight. In a thermal gradient, material evaporates at the warm end and condenses at the cold one, the net effect being a transport of material down gradient. At face value, this would imply densification of the colder layers. In reality the picture may be more complicated than that, as the condensing material may form a complicated texture. Such is the case on Earth, where the presence of a thermal gradient in a layer of snow leads to the formation of depth hoar [*Hobbs*, 1974], which consists of rather large crystals forming a loosely packed structure (this is the cause of avalanches). The evolution of porosity in a thermal gradient can be estimated using expressions presented by *Smoluchowski et al.* [1984]:

$$\frac{\partial \varphi}{\partial t} = - \varphi \frac{dv}{dT} \frac{dT}{dz} + v \frac{\partial \varphi}{\partial z} \tag{7}$$

where z is the vertical coordinate and the velocity of the pores is given by

$$v = \alpha r \sqrt{\frac{\Omega}{2\pi \Delta_o kT}} \frac{dP_v}{dT} \frac{dT}{dz} \tag{8}$$

In equation (8), α is the condensation coefficient [*Hobbs*, 1974], and r is the radius of the pores. Equation (7) can be rewritten to express the rate of change of porosity of a moving mass element:

$$-\varphi_t = - \left(\frac{\partial \varphi}{\partial t} - v \frac{\partial \varphi}{\partial z} \right) = \varphi \frac{dv}{dT} \frac{dT}{dz} \tag{9}$$

The "metamorphic" time scale $\tau_t = -\varphi/\varphi_t$ is plotted as a function of pore diameter (assumed equal to the grain diameter) in Figure 5 (dashed lines) for $\alpha = 1$ (an upper limit) and for two values of the thermal gradient: $dT/dz = 10$ and 0.1 K m^{-1}. The latter corresponds to the situation where the only source of heat is the geothermal flux from the interior (assumed equal to 6.6 mW m^{-2}, the higher value from the work by *Kirk and Brown* [1991]), whereas the former may be produced by a strong greenhouse effect [*Brown et al.*,

1990]. It seems that depth hoar formation can only be significant when the strong gradient is present (incidentally, a similar gradient is required for depth hoar formation on Earth [*Hobbs*, 1974]) and even then its influence only becomes important for pores (and grains) larger than 20 μm. Since I prefer smaller grains for the formation of the transparent layer and even the sign of the porosity change in a thermal gradient is rather uncertain, I will assume that thermal gradients would not change the conclusions of this paper with regard to the formation of the transparent layer. Strong thermal gradients (if they exist on Triton) may have to be considered for larger grains, such as the putative snowflakes in the equatorial collar (see section 5). However, if thermal gradients do not reduce porosity (as in depth hoar) and/or the frost is isothermal in the uppermost fluffy layers, the conclusion with regard to large grains (that they will not densify on a seasonal time scale) will not be affected.

5. IMPLICATIONS

In the preceding sections the microphysical processes involved in frost metamorphism have been reviewed and evaluated with application to solid nitrogen under conditions pertinent to Triton's surface. In sections 2 and 3 it was concluded that on a seasonal time scale (~100 Earth years) the limiting grain diameter is 10-30 μm, regardless of whether grain growth is limited by grain boundary migration (in fully dense systems) or by sintering (in porous systems). The formation of a well-annealed polycrystalline layer was shown in section 4 to be possible on a seasonal time scale, provided the initial grain size is smaller than 1 μm. Somewhat larger grain sizes (1-10 μm) are allowed if grain growth does not hinder densification, but because of the third-power dependence of the densification time scale on the grain diameter, grains larger than 100 μm will certainly not densify on a seasonal time scale. If a transparent layer is to form simultaneously with deposition, the required initial grain size is <0.3 μm. A transparent nitrogen layer provides a natural explanation for most of what is known about the surface of Triton:

1. The absorption feature at 2.16 μm can indeed be produced if grain boundaries do not reduce the absorptivity of nitrogen ice. Such is the case for flawless polycrystalline water ice, whose visible absorptivity is indistinguishable from that of distilled water [*Lyons and Stoiber*, 1959]. R. H. Brown

(personal communication, 1991) has recently observed similar behavior in polycrystalline nitrogen.

2. Smoothness at visible and infrared wavelengths, implied by ground-based photometry [*Goguen et al.*, 1989] and Voyager data [*Nelson et al.*, 1990], respectively, is compatible with the proposed layer. Although for an object as bright as Triton (albedo 0.8 and 0.6 in the south and north, respectively) the weakness of the opposition effect could also be due to multiple scattering, I prefer smoothness as an explanation, for several reasons. First, while a bright fluffy surface might also show no opposition surge, a fluffy surface would be difficult to reconcile with the 2.16-μm feature. Second, most bright airless objects do have an opposition surge, including Tethys (geometric albedo 0.8) [*Franz and Millis*, 1975] and Europa (geometric albedo 0.6) [*Domingue et al.*, 1991]. Finally, *Buratti et al.* [1991] conclude that the surface of Triton is unusually densified. They infer a porosity of ~ 40% for the optically active layer, but this result is highly model-dependent. It remains to be investigated whether a nonporous surface rough at the > 100-μm scale proposed in the present work is also consistent with the photometric data (I assume it is). At present the main point is that Triton's optical surface is more densified than on any other satellite.

3. The northern and southern hemisphere appear dark and bright, respectively, despite the fact that frost should be currently condensing in the north and subliming in the south. These observations can be explained if "frost" forms as a transparent layer and Voyager was looking through this layer at a dark substrate in the north and a permanent nitrogen cap in the south [*Moore and Spencer*, 1990]. The presence of a transparent veneer in the north has recently been confirmed by *Helfenstein et al.* [1992], who analyzed a set of specially processed Voyager images. The putative permanent cap in the south is bright if it is fractured on the length scale of millimeters or larger. Such fracturing may have occurred during the last southern winter, when surface nitrogen underwent the transition from the β to the α phase (around A.D. 1900 according to the history of atmospheric pressure presented by *Spencer* [1990]). This transition is known to be highly disruptive in the laboratory [*Scott*, 1976]. According to the results of sections 3 and 4, it takes more than 10^6 years for millimeter-sized fractures to heal. A problem with invoking the β-α transition to fracture the permanent cap is that in this case any seasonal deposit would have been fractured as well. According to *Spencer* [1990], in the southern hemisphere the seasonal deposit was at its thickest around A.D. 1900 and it is not clear whether enough deposition would have occurred there since the last

global shattering event to produce the transparent layer advocated in this paper. Two solutions to this problem can be proposed: either laboratory observations of shattering do not apply to Triton and the brightness of the permanent cap is due to other causes or indeed enough deposition has taken place. Can it be that nitrogen is only shattered when the phase transition is approached from the high temperatures (as in the reported laboratory experiments)? In this case, more time would have been available for the subsequent deposition as the β-α transition is likely to have occurred early in the last southern winter.

4. A well-annealed layer provides the seal required by the solid-state greenhouse model for the plumes [*Kirk et al.*, 1990]. In addition, the permeable reservoir required by that model is provided by the fractured permanent cap mentioned above.

5. The fresh, bright and blue appearance of the equatorial collar, where a recent snowfall may have occurred [*Pollack et al.*, 1990], results from the fact that the characteristic size of the snowflakes is >100 μm [*Yelle et al.*, 1991]. For such large grains the annealing time scale exceeds 10^4 years. The recent occurrence of the snowfall may help to explain the decrease in the degree of reddening observed between 1977 and 1989 [*Smith et al.*, 1989] and the apparent decrease in methane band strength since 1980 [*Cruikshank et al.*, 1988].

6. The dust in the dust devil model of the plumes [*Ingersoll and Tryka*, 1990] must be completely devoid of micron-sized nitrogen grains, as the very rapid sintering of the latter (of the order of days or even hours; see Figure 4) would provide the cohesion forces whose absence is essential to that model. Until it is shown that adequate quantities of completely frost-free dust (which Ingersoll and Tryka assume to be more than 1000 times less cohesive than the dust on Earth anyway) are indeed present southward of 50°S, I will therefore favor the greenhouse model for the plumes. Note that at those latitudes the seasonal nitrogen is still expected to be present, at least in a zonally averaged sense [*Spencer*, 1990; *Stansberry et al.*, 1990].

In the north the proposed transparent layer is currently forming, whereas in the south it is the remnant of the layer formed during (or since) the last winter. My current understanding of Triton's surface is reflected in Figure 7. A question to be addressed by future research is why nitrogen would condense as submicron grains in some places but form 100-μm-sized snowflakes in others. One possibility is that the

"standard" size of condensing grains is the same as the mean particle size in the clouds (believed to be sublimation clouds) observed by Voyager, namely <1 μm [*Pollack et al.*, 1990], whereas snowfalls are rare and/or preferentially occur in the equatorial region [*Yelle et al.*, 1991]. The other possibility is that *Yelle et al.* [1991] overestimated the size of snowflakes on Triton. In other words, the snowflakes are indeed ~1 μm, but the putative snowfall occurred just prior to the Voyager flyby, and the snow did not have enough time to densify. I consider this possibility to be unlikely, for two reasons. First, it puts a rather severe constraint on the timing of the snowfall and may not explain the decrease in the degree of reddening and/or the decrease in methane absorption. With regard to the timing of the snowfall, a question to be addressed by the dynamic meteorologist is how long the signature of a snowfall would persist in the atmosphere at altitudes studied by Pollack et al. Second, new microphysics would be required to reduce the particle size by 2 orders of magnitude. According to Yelle et al., $r \propto (S\alpha)^{1/2}$, where S is the supersaturation factor equal to $\rho_a/\rho_s - 1$, ρ_a and ρ_s are the atmospheric and the saturation vapor density, respectively, and α is the sticking coefficient (which may or may not be equal to the condensation coefficient introduced in section 4.4). Other parameters entering the calculation of r are rather well constrained. Yelle et al. calculated the value of S self-consistently for each value of α. They favor the case $\alpha = 10^{-3}$ and $S = 0.3$ in their studies of plume dynamics and apparently their estimate of $r = 85$ μm is based on this choice. Reducing r by 2 orders of magnitude would require the product $S\alpha$ to be reduced by 4 orders of magnitude, which seems to be hard to achieve, for the following reason. According to Yelle et al., $\alpha = 10^{-3}$ should give a lower limit to the value of the sticking coefficient. Thus the only way to reduce the product $S\alpha$ seems to be the reduction of S by at least 4 orders of magnitude. In fact, to obtain such low values of S, higher values of α are required, and thus the required reduction of S would have to be even greater than that. In effect, the atmosphere would have to be in vapor equilibrium, contrary to *Yelle et al.* [1991, p. 352], who claim that "the observed haze abundance in Triton's troposphere suggests that the heating due to N_2 condensation is too small to force the troposphere to vapor pressure equilibrium, implying that the troposphere is supersaturated." It is also doubtful whether snowfalls would occur in a not supersaturated atmosphere. Clearly, more studies are needed to gain a better understanding of these issues. At present, I simply take the $r = 85$ μm estimate at face value.

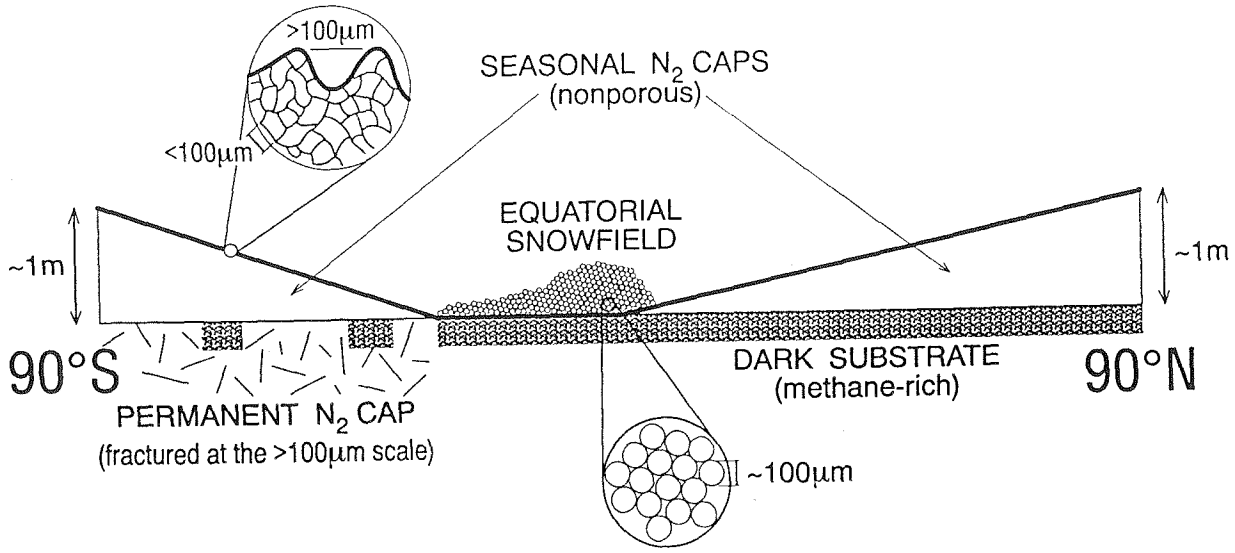

Fig. 7. A schematic representation of the model of Triton's surface (during 1980's) advocated in this paper. This figure is not to scale and is not intended to accurately represent either the latitudinal extent of various surface units or the albedo contrasts between them.

It must be noted that the search for specular reflection in Voyager high-resolution images of Triton yielded negative results [*Lee et al.*, 1991]. However, the annealed layer proposed here can be rough on the >100-μm scale, and this would greatly reduce the probability of detecting specular behavior, especially in a restricted data set with rather coarse spatial resolution (~3 to 7 km/line pair). With some luck, the hypothesis of a well-annealed layer on Triton may be testable during the current decade. According to the historical model of *Spencer* [1990], the atmospheric pressure on Triton will drop below 1 μbar before the year 2000. As the equilibrium vapor temperature is below 35.6 K at that pressure, it means that nitrogen will undergo the β-α transition during the current decade. This transition is likely to shatter the putative annealed layer severely [*Scott*, 1976]. If Nature is kind, the β-α transition may manifest itself in several ways: if the layer is indeed shattered, the appearance of the opposition effect and/or the disappearance of the 2.16-μm absorption feature are expected; if shattering somehow does not occur (for example, because the cooling rate is much lower than in laboratory experiments), the 2.16-μm absorption feature may become more pronounced, as α-nitrogen is apparently a stronger infrared absorber than the β phase. The infrared fundamental band has been observed in thin films of α-nitrogen [*Jodl et al.*, 1987]; no such observation has been reported for the β phase. The stronger absorption in the α phase may result if the crystal structure is $P2_13$ (see the remark by *Jordan et al.* [1964, p. 759]). More laboratory experiments and continuous telescopic observations of Triton are certainly called for.

6. SUMMARY

The presence of a well-annealed transparent nitrogen layer offers a natural explanation for most of what we see on the surface of Triton: the 2.16-μm absorption, the apparent smoothness at visible and infrared wavelengths, the albedo contrast between north and south, the plumes. On the basis of an analysis of microphysical processes involved in frost metamorphism it is concluded that such a layer may indeed form at 37 K on a seasonal time scale provided the initial grain size is <1 μm. This layer is polycrystalline, the mean grain diameter being 10-30 μm. In addition, the fresh appearance of the equatorial collar results from the grains' there being unusually large (~100 μm). For such large grains the metamorphic time scale

exceeds 10^4 Earth years. The presence of a transparent veneer in the northern hemisphere has recently been confirmed by *Helfenstein et al.* [1992]. Continuous observations of Triton may provide a further test of the "annealed-layer" hypothesis if photometric and/or spectrophotometric properties of Triton change when nitrogen undergoes the β-α transition. According to the model of *Spencer* [1990], this transition is expected to occur before A.D. 2000.

NOTATION

a, a_o current and initial mean grain diameter, respectively [m].

A growth constant, equation (1) [$m^2\ s^{-1}$].

A_1 creep constant, equation (5) [dimensionless].

A_2 creep constant, equation (6) [Pa^{-n}, where n is the creep exponent].

b Burgers vector of dislocations [m].

B growth constant, equation (1) [K].

C parameter in equation (4*a*), equal to $\varphi_o/(\varphi_o - \varphi)$, [dimensionless].

d_2 diffusion distance in Figure 3*b* [m].

D generic solid-state diffusion coefficient, equation (5) [$m^2\ s^{-1}$].

D_b' diffusivity across grain boundaries [$m^2\ s^{-1}$].

D_b diffusivity along grain boundaries, equal to $D_{ob}\exp(-E_b/RT)$ [$m^2\ s^{-1}$].

D_s surface diffusivity, equal to $D_{os}\exp(-E_s/RT)$ [$m^2\ s^{-1}$].

D_v volume (lattice) diffusivity, equal to $D_{ov}\exp(-E_v/RT)$ [$m^2\ s^{-1}$].

D_{ob}, D_{os}, D_{ov} preexponential factors for diffusivity along grain boundaries, surface diffusivity, and volume diffusivity, respectively [$m^2\ s^{-1}$].

E_b, E_s, E_v activation energies for diffusivity along grain boundaries, surface diffusivity, and volume diffusivity, respectively [$J\ mol^{-1}$].

g surface gravity [0.78 m s^{-2} on Triton].

H enthalpy of sublimation [$J\ mol^{-1}$].

H_s thickness of the layer deposited over sintering time (Section 4.2) [m].

k Boltzmann constant [$1.381 \times 10^{-23}\ J\ K^{-1}$].

K growth constant, equation (2) [$m^2\ s^{-1}$].

K_1, K_2, K_3, K_m curvatures in the sintering equations [m^{-1}].

L latent heat of sublimation [$J\ kg^{-1}$].

m growth exponent, equation (2) [dimensionless].

M_i grain boundary mobility [m^4 J^{-1} s^{-1}].

n creep exponent [dimensionless].

N dislocation density [m^{-2}].

p lithostatic pressure [Pa].

p_i a quantity proportional to the gas pressure in the pores in the final stages of densification, assumed zero for nitrogen on Triton [Pa].

P_v equilibrium vapor pressure, equal to $P_o \exp(-H/RT)$ [Pa].

Q activation energy for creep [J mol^{-1}].

r mean grain radius, equal to $a/2$ [m].

r_c critical grain radius in *Hillert's* [1965] theory of grain growth in nonporous systems [m].

R universal gas constant [8.314 J mol^{-1} K^{-1}].

S supersaturation, equal to $\rho_d/\rho_s - 1$ [dimensionless].

t time [s].

T temperature [K].

T_m melting temperature [K].

v velocity of pores migrating in a thermal gradient [m s^{-1}].

$\dot{V}_i$ volume flow rate into the neck due to the ith mechanism of sintering [m^3 s^{-1}].

x radius of the neck between two spherical grains [m].

$\dot{x}$ rate of neck growth [m s^{-1}].

z depth [m].

α condensation (sticking) coefficient [dimensionless].

δ_b', δ_b, δ_s grain boundary width for diffusion across the boundary, grain boundary width for diffusion along the boundary, and effective surface thickness, respectively [m].

Δ, Δ_o bulk and theoretical density of the material, respectively [kg m^{-3}].

$\dot{\varepsilon}$ strain rate [s^{-1}].

ε thermal emissivity [dimensionless].

φ, φ_o current and initial porosity, respectively [dimensionless].

$\dot{\varphi}_c$ rate of compaction due to power-law creep [s^{-1}].

$\dot{\varphi}_s$ rate of porosity change due to pressureless sintering [s^{-1}].

$\dot{\varphi}_t$ rate of porosity change due to a thermal gradient [s^{-1}].

γ, γ_b solid-vapor surface tension and specific grain boundary energy, respectively [J m^{-2}].

λ mean free path [m].

μ shear modulus [Pa].

θ angle in Figure 3*b* [rad].

ρ radius of curvature of the neck [m].

ρ_a atmospheric density [kg m^{-3}].

ρ_s density corresponding to the saturation vapor pressure [kg m^{-3}].

σ stress [Pa].

σ_{SB} Stefan-Boltzmann constant [5.67032×10^{-8} W m^{-2} K^4].

τ_1, τ_2 long and short sintering times [s].

τ_c compaction time scale due to power-law creep [s].

τ_s densification time scale due to isothermal pressureless sintering [s].

τ_t time scale for change of porosity in a thermal gradient [s].

Ω molecular volume [m^3].

ς parameter (Section 4.2), equal to H_s/a [dimensionless].

Acknowledgments. I wish to express my sincere thanks to R. H. Brown, B. J. Buratti, A. P. Ingersoll, B. Kamb, G. R. Rossman, D. J. Stevenson, and Y. L. Yung who lent me their helping hands as I went for a swim in the waters of this paper. The critical comments of an anonymous reviewer are also appreciated, despite our disagreement on several issues raised in my paper. I thank P. Lee and his coauthors for communicating to me the results of their paper prior to publication and A. W. Harris for drawing my attention to the work of K. Muinonen. This work was supported by NASA grants NAGW-185, NAGW-1538, and NAGW-2362. Contribution number 4960 from the Division of Geological and Planetary Sciences, California Institute of Technology, Pasadena.

REFERENCES

Alley, R. B., J. H. Perepezko, and C. R. Bentley, Grain growth in polar ice, I, Theory, *J. Glaciol.*, *32*, 415-424, 1986*a*.

Alley, R. B., J. H. Perepezko, and C. R. Bentley, Grain growth in polar ice, II, Application, *J. Glaciol.*, *32*, 425-433, 1986*b*.

Arzt, E., M. F. Ashby, and K. E. Easterling, Practical applications of hot-isostatic pressing diagrams: Four case studies, *Metall. Trans. A*, *14*, 211-221, 1983.

Ashby, M. F., A first report on sintering diagrams, *Acta Metall.*, *22*, 275-288, 1974.

Ashby, M. F., Background reading: Hot Isostatic Pressing and Sintering, report, Eng. Dep., Cambridge Univ., Cambridge, England, 1988.

Ashby, M. F., and R. A. Verall, Micromechanisms of flow and fracture, and their relevance to the rheology of the upper mantle, *Philos. Trans. R. Soc. London Ser. A*, *288*, 59-95, 1978.

Bezuglyi, P. A., N. G. Burma, and R. Kh. Minyafaev, Elastic constants of polycrystalline methane in the temperature range 14.4-77 K, *Sov. Phys. Solid State, Engl. Transl.*, *8*, 596-600, 1966.

Bolshutkin, D. N., L. I. Borisova, and A. V. Leonteva, Creep of crystalline methane, *Sov. Phys. Solid State, Engl. Transl.*, *10*, 1248-1249, 1968.

Broadfoot, A. L., et al., Ultraviolet spectrometer observations of Neptune and Triton, *Science*, *246*, 1459-1466, 1989.

Brown, R. H., R. L. Kirk, T. V. Johnson, and L. A. Soderblom, Energy sources for Triton's geyser-like plumes, *Science*, *250*, 431-435, 1990.

Buratti, B. J., A. L. Lane, J. Gibson, H. Burrows, R. M. Nelson, D. Bliss, W. Smythe, V. Garkanian, and B. Wallis, Triton's surface properties: A preliminary analysis from ground-based, Voyager photopolarimeter subsystem, and laboratory measurements, *J. Geophys. Res.*, *96*, 19,197-19,202, 1991.

Chezeau, J. M., and J. H. Strange, Diffusion in molecular crystals, *Phys. Rep.*, *53*, 1-92, 1979.

Clark, R. N., F. P. Fanale, and A. P. Zent, Frost grain metamorphism: Implications for remote sensing of

planetary surfaces, *Icarus*, *56*, 233-245, 1983.

Conrath, B., et al. Infrared observations of the Neptunian system, *Science*, *246*, 1454-1459, 1989.

Cook, T., and G. Davey, The density and thermal conductivity of solid nitrogen and carbon dioxide, *Cryogenics*, *16*, 363-369, 1976.

Cruikshank, D. P., R. H. Brown, and R. N. Clark, Nitrogen on Triton, *Icarus*, *58*, 293-305, 1984.

Cruikshank, D. P., R. H. Brown, A. T. Tokunaga, R. G. Smith, and J. R. Piscitelli, Volatiles on Triton: The infrared spectral evidence, 2.0-2.5 μm, *Icarus*, *74*, 413-423, 1988.

Domingue, D. L., B. W. Hapke, G. W. Lockwood, and D. T. Thompson, Europa's phase curve: Implications for surface structure, *Icarus*, *90*, 30-42, 1991.

Eluszkiewicz, J., Compaction and internal structure of Mimas, *Icarus*, *84*, 215-225, 1990.

Eluszkiewicz, J., and D. J. Stevenson, Rheology of solid methane and nitrogen: Applications to Triton, *Geophys. Res. Lett.*, *17*, 1753-1756, 1990.

Esteve, D., and N. S. Sullivan, NMR study of self-diffusion in solid N_2, *Solid State Commun.*, *39*, 969-971, 1981.

Franz, O. G., and R. L. Millis, Photometry of Dione, Tethys, and Enceladus, *Icarus*, 433-442, 1975.

Frels, W., D. R. Smith, and T. Ashworth, Vapor pressure of nitrogen below the triple point, *Cryogenics*, *14*, 3-7, 1974.

Gladkikh, N. T., and V. I. Khotkevich, Determination of the surface energy of nitrogen in the solid state (in Russian), *Ukr. Fiz. Zh., Russ. Ed.*, *14*, 1917-1919, 1969.

Goguen, J. D., H. B. Hammel, and R. H. Brown, V photometry of Titania, Oberon, and Triton, *Icarus*, *77*, 239-247, 1989.

Gow, A. J., On the rates of growth of grains and crystals in south polar firn, *J. Glaciol.*, *8*, 241-252, 1969.

Greskovich, C., and K. W. Lay, Grain growth in very porous Al_2O_3 compacts, *J. Am. Ceram. Soc.*, *55*, 142-146, 1972.

Hapke, B., Bidirectional reflectance spectroscopy, 1, Theory, *J. Geophys. Res.*, *86*, 3039-3054, 1981.

Hapke, B., Coherent backscatter and the radar characteristics of outer planet satellites, *Icarus*, *88*, 407-417,

1990.

Helfenstein, P., J. Veverka, D. McCarthy, P. Lee, and J. Hillier, Large quasi-circular features beneath frost on Triton, *Science*, 255, 824-826, 1992.

Hillert, M., On the theory of normal and abnormal grain growth, *Acta Metall.*, *13*, 227-238, 1965.

Hobbs, P. V., *Ice Physics*, Oxford at the Clarendon Press, London, 1974.

Ingersoll, A. P., Dynamics of Triton's atmosphere, *Nature*, *344*, 315-316, 1990.

Ingersoll, A. P., and K. A. Tryka, Triton's plumes: The dust devil hypothesis, *Science*, *250*, 435-437, 1990.

Jodl, H. J., W. Loewen, and D. Griffith, FTIR-spectra of solid O_2, N_2 and CO, *Solid State Commun.*, *61*, 503-506, 1987.

Jordan, T. H., H. W. Smith, W. E. Streib, and W. N. Lipscomb, Single-crystal X-ray diffraction studies of α-N_2 and β-N_2, *J. Chem. Phys.*, *41*, 756-759, 1964.

Kirk, R. L., Diffusion kinetics of solid methane and nitrogen: Implications for Triton (abstract), *Lunar Planet. Sci. Conf.*, *21*, 631-632, 1990.

Kirk, R. L., and R. H. Brown, The role of nonuniform internal heating in Triton's energy budget (abstract), *Lunar Planet. Sci. Conf.*, *22*, 721-722, 1991.

Kirk, R. L., R. H. Brown, and L. A. Soderblom, Subsurface energy storage and transport for solar-powered geysers on Triton, *Science*, *250*, 424-429, 1990.

Kurtz, S. K., and F. M. A. Carpay, Microstructure and normal grain growth in metals and ceramics, II, Experiment, *J. Appl. Phys.*, *51*, 5745-5754, 1980.

Lee, P., P. Helfenstein, and J. Veverka, Search for glazed surfaces on Triton, *J. Geophys Res.*, *96*, 19,231-19,239, 1991.

Lunine, J. I., and D. J. Stevenson, Physical state of volatiles on the surface of Triton, *Nature*, *317*, 238-240, 1985.

Lyons, J. B., and R. E. Stoiber, The absorptivity of ice: A critical review, *Sci. Rep. 3*, Dartmouth Coll., Hanover, N. H., 1959.

McEwen, A. S., Global color and albedo variations on Triton, *Geophys. Res. Lett.*, *17*, 1765-1768, 1990.

Moore, J. M., and J. R. Spencer, Koyaanismuuyaw: The hypothesis of a perennially dichotomous Triton,

Geophys. Res. Lett., 17, 1757-1760, 1990.

Muinonen, K., Scattering of light by solar system dust: The coherent backscatter phenomenon, *Proc. Finn. Astron. Soc.*, 12-15, 1990.

Nelson, R. M., W. D. Smythe, B. D. Wallis, L. J. Horn, A. L. Lane, and M. J. Mayo, Temperature and thermal emissivity of the surface of Neptune's satellite Triton, *Science, 250*, 429-431, 1990.

Pollack, J. B., J. M. Schwartz, and K. Rages, Scatterers in Triton's atmosphere: Implications for the seasonal volatile cycle, *Science, 250*, 440-443, 1990.

Ricoult, D. L., and D. L. Kohlstedt, Structural width of low-angle grain boundaries in olivine, *Phys. Chem. Miner., 9*, 133-138, 1983.

Scott, T. A., Solid and liquid nitrogen, *Phys. Rep., 3*, 89-157, 1976.

Smith, B. A., et al., Voyager 2 at Neptune: Imaging science results, *Science, 246*, 1422-1449, 1989.

Smoluchowski, R., M. Marie, and A. McWilliam, Evolution of density in solar system ices, *Earth, Moon, Planets, 30*, 281-288, 1984.

Soderblom, L. A., S. W. Kieffer, T. L. Becker, R. H. Brown, A. F. Cook II, C. J. Hansen, T. V. Johnson, R. L. Kirk, and E. M. Shoemaker, Triton's geyser-like plumes: Discovery and basic characterization, *Science, 250*, 410-415, 1990.

Spencer, J. R., Nitrogen frost migration on Triton: A historical model, *Geophys. Res. Lett., 17*, 1769-1772, 1990.

Stansberry, J. A., J. I. Lunine, C. C. Porco, and A. S. McEven, Zonally averaged thermal balance and stability models for nitrogen polar caps on Triton, *Geophys. Res. Lett., 17*, 1773-1776, 1990.

Swinkels, F. B., and M. F. Ashby, A second report on sintering diagrams, *Acta Metall., 29*, 259-281, 1981.

Tyler, G. L., et al., Voyager radio science observations of Neptune and Triton, *Science, 246*, 1466-1473, 1989.

Vegard, L., Die Struktur von β-Stickstoff und die verschiedene Phosphoreszenzfaehigkeit der beiden Formen des festen Stickstoffs, *Z. Phys., 79*, 471-491, 1932.

Volkmann, U. G., and K. Knorr, Multilayer growth and wetting behavior of nitrogen physisorbed on

graphite, *Phys. Rev. Lett.*, *66*, 473-476, 1991.

Yelle, R. V., J. I. Lunine, and D. M. Hunten, Energy balance and plume dynamics in Triton's lower atmosphere, *Icarus*, *89*, 347-358, 1991.

Zent, A. P., C. P. McKay, J. B. Pollack, and D. P. Cruikshank, Grain metamorphism in polar nitrogen ice on Triton, *Geophys. Res. Lett.*, *16*, 965-968, 1989.

Ziegler, W. T., The vapor pressures of some hydrocarbons in the liquid and solid state at low temperatures, *NBS Report U.S.*, *6038*, 1959.

APPENDIX: MARTIAN SEASONAL POLAR CAPS

There are several pieces of evidence that the "grain size" or "textural scale" in the martian polar caps could be quite large. From an analysis of the northern cap spectra taken by *Moroz* [1964], *Kieffer* [1970] came to the conclusion that the strength of an absorption feature at 1.5 μm, if it be due to a weak transition in CO_2 ice, would require a textural scale on the order of 10 cm. Such large path lengths seemed out of question for a frosty surface and this led Kieffer to suggest a different explanation involving H_2O frost. H_2O ice was also invoked by *Clark and McCord* [1982] to explain absorption features in the northern cap spectra both in the 1.5 and 2.0 μm spectral regions. However, since solid CO_2 also absorbs in these spectral regions, its presence at the time and location of the Clark and McCord observations cannot be ruled out (albeit only for large grain sizes), especially because Clark and McCord also saw indications of an absorption feature at 2.3 μm, where solid CO_2 absorbs, but water ice does not. Solid CO_2 has indeed been identified in high resolution spectra of the southern cap taken by *Larson and Fink* [1972], who were able to resolve the individual absorption features around 1.5 μm and who identified additional CO_2 features in the 1.2 μm spectral region. More recently, in an analysis of Mariner 7 spectra of the southern polar cap, *Calvin* [1990] inferred a grain size on the order of millimeters to centimeters from the strength of the absorption in the 2.3 μm spectral region, which he interpreted as being due to forbidden transitions in solid CO_2. All of the above spectra were obtained during winter or spring in the respective hemispheres, when the seasonal CO_2 caps should have been present at the observed locations.

It seems that in analogy to Triton, the long path lengths may be produced in a clear polycrystalline layer even if the grains are small, provided the layer is sufficiently flawless, i.e., devoid of pores, cracks, impurities etc. The conditions which make the formation of a clear layer possible on Triton are also to a large extent satisfied in the seasonal caps on Mars. Carbon dioxide condenses in the near absence of an inert gas and thus no "air-bubbles" are expected. By virtue of the vapor pressure equilibrium, the temperature of the seasonal caps changes very little over diurnal and seasonal time scales; this should make thermal cracking insignificant and eliminate thermal gradients. The abundances of impurities is probably

higher on Mars than it is on Triton, the most abundant of them being dust; however, the average dust abundance in the residual caps is probably on the order of 0.1% [*Kieffer*, 1990] and it is unlikely to be higher in the seasonal deposits (otherwise the latter would be darker); this should not hinder the annealing of the putative CO_2 layers. Stirring of the CO_2 condensate by the stronger martian winds is another potential complication, but if CO_2 grains indeed sinter as fast as I will argue they do, then they are too cohesive to be lifted. Note that not all or none of these conditions are likely to be satisfied in a martian H_2O cap. In particular, frost metamorphism in a martian H_2O cap is likely to be dominated by diffusion in the ambient atmosphere [*Kieffer*, 1990], a process which leads to grain growth but not to densification. In the absence of an inert atmosphere, the contribution of vapor transport is negligible compared with other metamorphic processes. Also, the contribution of thermal gradients that are important for the martian H_2O cap [*Clow*, 1987] should be negligible in the CO_2 caps which are nearly isothermal (at least before they densify).

The rate of densification can again be estimated from equations (4). A complicating factor is the fact that neither the diffusivities nor the surface tension have been measured for solid CO_2, and so recourse must be had to "educated guesses." The surface tension can with a good degree of confidence be assumed to have a value between 0.02 and 0.1 J m^{-2}, the values for solid nitrogen and water ice, respectively. As a conservative estimate, $\gamma = 0.02$ J m^{-2} will be assumed. The activation energy for lattice diffusion may be estimated from the Van Liempt relation $E_v = 16.1\ RT_m$, where T_m is the melting temperature (217 K for CO_2). This relation is obeyed by a wide range of molecular crystals [*Chezeau and Strange*, 1979], including solid nitrogen [*Esteve and Sullivan*, 1981]. The preexponential factor is more difficult to estimate, as it could be in the wide range $10^{-5} < D_{ov} < 10^4$ m^2 s^{-1} covered by other plastic crystals [*Esteve and Sullivan*, 1981]. I will assume $D_{ov} = 10^{-5}$ m^2 s^{-1}, which I expect to be a conservative estimate. Larger values of D_{ov} would strengthen my conclusions by increasing densification rates. The grain boundary diffusivity will be calculated from the scaling $E_b = 2/3\ E_v$, $D_{ob} = D_{ov}$. Larger values of D_b would again strengthen my conclusions, whereas smaller values would not affect them significantly since with the assumed scaling, the contribution to densification from grain boundary diffusion at 148 K becomes smaller

than the contribution from volume diffusion for grains larger than 10 μm. Clearly, there are many uncertainties associated with an application of equations (4) to solid carbon dioxide and they should be addressed in future experiments. In view of the preceeding discussion it seems, however, that these uncertainties are unlikely to significantly alter my conclusions with regard to the grain size required to achieve seasonal densification. This robustness stems primarily from the very strong size dependence on the right-hand side of equations (4).

The densification time scale $\tau = -\varphi/\dot{\varphi}$ at 148 K, calculated from equation (4*b*) for $\varphi = 0.1$ (final stage of densification), is shorter than 100 Mars days for grains smaller than 20 μm. Other choices of φ or a different definition of the "relevant" time scale (say 10 instead of 100 Mars days) would change this result only slightly. As discussed in section 4.1, this condition requires that the grains are smaller initially, perhaps by a factor of 10, but given the uncertainties in material parameters, there is a good chance that densification will be achieved for grains with initial diameters in the few to a few tens of microns range. *Pollack et al.* [1990] conclude that the latter should be the upper limit to the size of particles formed in the atmosphere, based on their atmospheric fallout times. A similar conclusion was reached by *Kieffer* [1990], who inferred rapid fallout for 10-μm particles. The formation of larger grains upon condensation on the surface is not likely, as this would amount to epitaxial growth, a process that requires very special circumstances and one which does not occur for solid nitrogen on Triton (see section 4.2). Thus it seems that for plausible initial grain sizes, densification into a low porosity polycrystalline layer is likely or at least possible in the martian seasonal caps. The average grain size in this layer would be less than 100 μm (for reasons analogous to those pertaining to the annealed nitrogen layer on Triton), but this should not prevent the formation of centimeter-sized path lengths for absorption in the weak CO_2 bands. The latter conclusion is based on the observation, made both for nonporous polycrystalline water ice and nonporous polycrystalline nitrogen, that grain boundaries are inefficient light scatterers (see section 5). Note that the thickness of the proposed layer would not be unrealistic for the layer to be nearly transparent at visible wavelengths: with the classical estimate of *Leighton and Murray* [1966] of 80 g cm^{-2} average annual CO_2 deposition, the layer may be expected to be ~0.5 m thick in the fully dense state (density 1.67 g cm^{-3}).

If the martian seasonal polar caps are indeed nonporous or nearly so over large areas, the implications could be quite profound. The presence of the weak infrared absorption features in the 1.5 and 2.3 μm spectral regions would be explained. An annealed layer smooth at the 20-μm length scale could also be responsible for the low thermal emissivity inferred from Viking measurements [*Kieffer et al.*, 1976], in a similar way as a nitrogen deposit smooth at the 80-μm scale may explain the low thermal emissivity of Triton's surface inferred from Voyager observations. The albedo dichotomy invoked by *Paige and Ingersoll* [1985] to explain the asymmetry between the northern and southern caps could reside in the underlying residual caps and thus be permanent, again in analogy to Triton. In addition, the penetration of sunlight through a clear layer should help to stabilize the asymmetry [*Lindner*, 1992]. Paige and Ingersoll associated the albedo dichotomy with the seasonal deposits and suggested preferrential dust deposition during great dust storms as a possible mechanism to darken the northern cap. They noted that the northern residual H_2O cap would not be exposed during storm-free years. On the other hand, with nearly transparent seasonal caps and a permanent albedo dichotomy, the exposure should occur every year. Great dust storms would still be an attractive darkening agent, but they would not need to operate every year (and in fact they do not); their darkening effect could accumulate over longer time scales.

The hypothesis of a low porosity CO_2 layer is amenable to ground-based observational tests, mainly in the 1.5 μm spectral region. I wish to emphasize that the identification of the 1.5 and 1.9 μm absorption features by *Kieffer* [1970] and *Clark and McCord* [1982] as being due to water ice cannot be dismissed. Note, however, that neither can an annealed CO_2 layer on top of a H_2O ice cap be ruled out based on these features: solid CO_2 also absorbs in these spectral regions. In fact, such a configuration has been suggested by *Pimentel et al.* [1974], who detected the 3.1-μm water ice absorption feature in the Mariner 7 infrared spectra of selected locations in the southern polar cap. Moreover, as pointed out by *Jakosky* [1982], the seasonal CO_2 cap should have been present at the time and location of the Clark and McCord observations. In addition, the wing of an absorption feature at 2.3 μm in the Clark and McCord spectra could be due to annealed CO_2 ice, but not water ice.

Additional tests of the annealed layer hypothesis should be possible during the upcoming Mars

Observer mission. An image analysis similar to that performed for Triton by *Helfenstein et al.* [1992] could directly reveal the presence of a nearly transparent layer. Time series of thermal emissivity obtained from measurements by the Thermal Emission Spectrometer may indicate the metamorphic time scale. If such time series were obtained for a site of known frost deposition and the initial grain size were obtained (e.g., from observations of CO_2 condensate clouds), then a test of equations (4) could become possible, provided the material parameters are known. The latter could be obtained from sintering experiments. I also note that if the albedo dichotomy does indeed reside in the residual caps, the exposure of the northern residual cap would not be expected during years with extensive snowfalls over the northern cap, if the snow grains are sufficiently large, > 20 μm say; the estimated densification time scale for such large grains is longer than a season. This hypothesis might also be testable by Mars Observer.

REFERENCES

Calvin, W. M., Additions and corrections to the absorption coefficients of CO_2 ice: Applications to the martian south polar cap, *J. Geophys. Res., 95,* 14,743-14,750, 1990.

Chezeau, J. M., and J. H. Strange, Diffusion in molecular crystals, *Phys. Rep., 53,* 1-92, 1979.

Clark, R. N., and T. B. McCord, Mars residual polar cap: Earth-based spectroscopic confirmation of water ice as a major constituent and evidence for hydrated minerals, *J. Geophys. Res., 87,* 367-370, 1982.

Clow, G. D., Generation of liquid water on Mars through the melting of a dusty snowpack, *Icarus, 72,* 95-127, 1987.

Esteve, D., and N. S. Sullivan, NMR study of self diffusion in solid N_2, *Solid State Commun., 39,* 969-971, 1981.

Helfenstein, P., J. Veverka, D. McCarthy, P. Lee, and J. Hillier, Large quasi-circular features beneath frost on Triton, *Science,* 255, 824-826, 1992.

Jakosky, B. M., Comment on "Mars residual north polar cap: Earth-based spectroscopic confirmation of water ice as a major constituent and evidence for hydrated minerals" by Roger N. Clark and Thomas B. McCord, *J. Geophys. Res., 88,* 4329-4330, 1983.

Kieffer, H., Interpretation of the Martian polar cap spectra, *J. Geophys. Res., 75,* 510-514, 1970.

Kieffer, H. H., Water grain size and the amount of dust in Mars' residual polar cap, *J. Geophys. Res., 95,* 1481-1493, 1990.

Kieffer, H. H., P. R. Christensen, T. Z. Martin, E. D. Miner, and F. D. Palluconi, Temperatures of the martian surface and atmosphere: Viking observations of diurnal and geometric variations, *Science, 194,* 1346-1351, 1976.

Larson, H. P., and U. Fink, Identification of carbon dioxide frost on the martian polar caps, *Astrophys. J. Lett., 171,* 91-95, 1972.

Leighton, R. B., and B. C. Murray, Behavior of carbon dioxide and other volatiles on Mars, *Science, 153,* 136-144, 1966.

Lindner, B. L., Sunlight penetration through the martian polar caps: Effects on the thermal and frost budgets, *Geophys. Res. Lett., 19,* 1675-1678, 1992.

Moroz, V. I., The infrared spectrum of Mars (λ1.1-4.1μ), *Sov. Astron., AJ, 8,* 273-281, 1964.

Pimentel, G. C., P. B. Forney, and K. C. Herr, Evidence about hydrate and solid water in the martian surface from the 1969 Mariner Infrared Spectrometer, *J. Geophys. Res., 79,* 1623-1634, 1974.

Paige, D. A., and A. P. Ingersoll, Annual heat balance of the martian polar caps: Viking observations, *Science, 228,* 1160-1168, 1985.

Pollack, J. B., R. M. Haberle, J. Schaeffer, and H. Lee, Simulations of the general circulation of the martian atmosphere. 1. Polar processes, *J. Geophys. Res., 95,* 1447-1474, 1990.

PAPER II

A Global Analysis of the Ozone Deficit in the Upper Stratosphere and Lower Mesosphere

Janusz Eluszkiewicz

Division of Geological and Planetary Sciences,

California Institute of Technology, Pasadena, CA 91125

and

Mark Allen

Earth and Space Sciences Division, Jet Propulsion Laboratory,

California Institute of Technology, Pasadena, CA 91109, and

Division of Geological and Planetary Sciences,

California Institute of Technology, Pasadena, CA 91125

to appear in: *J. Geophys. Res.*

ABSTRACT

The global measurements of temperature, ozone, water vapor, and nitrogen dioxide acquired by the Limb Infrared Monitor of the Stratosphere (LIMS), supplemented by a precomputed distribution of chlorine monoxide, are used to test the balance between odd oxygen production and loss in the upper stratosphere and the lower mesosphere. An efficient photochemical equilibrium model, whose validity is ascertained by comparison with the results from a fully time-dependent one-dimensional model at selected latitudes, is used in the calculations. The computed ozone abundances are systematically lower than observations for May 1-7, 1979, which suggests, contrary to the conclusions of other recent studies, a real problem in model simulations of stratospheric ozone. The "ozone deficit" at 30N is smaller than previous analyses of LIMS data have indicated. In the stratosphere, this reduction in the deficit is due to the fact that ClO abundances for the 1979 period utilized in this study are much lower than in earlier work, mainly as a result of lower Cl_y concentrations. In the mesosphere, a correlation of the ozone deficit with the distribution of water vapor is indicated. The ozone deficit in the stratosphere can be eliminated by modifying only one model reaction rate: either by decreasing the rate of odd oxygen loss (e.g., by decreasing the abundances of atomic oxygen through an increase in the rate of the reaction $O + O_2 + M \rightarrow O_3 + M$ within the recommended uncertainties) or by increasing the rate of odd oxygen production (by increasing the photodissociation rate of molecular oxygen primarily in the Herzberg continuum and/or invoking photolysis of vibrationally excited molecular oxygen). With the ozone abundances thus increased, a small residual deficit in the lower mesophere can be eliminated by reducing, within recommended kinetic uncertainties, the efficiency of odd-hydrogen-catalyzed odd oxygen loss. With the adjusted model, the calculated ozone abundances for the week January 1-7, 1979, outside of winter latitudes, also agree with the LIMS observations to within 10%.

1. INTRODUCTION

The concern about possible ozone depletion due to human activities has motivated most studies in middle atmosphere chemistry during the last two decades. The region of the atmosphere above ~ 35 km, comprising the upper stratosphere and the mesosphere, is particularly well suited for testing model simulations of atmospheric chemistry since ozone in this region is in photochemical steady-state during daylight hours and its abundance is directly controlled by a relatively small number of chemical reactions. However, despite simple chemistry, the factors controlling ozone abundances in this region are still not well understood. Perhaps the most dramatic manifestation of this imperfect understanding is the fact that current photochemical models systematically underestimate the observed ozone abundances [*World Meteorological Organization* (WMO), 1986]. This issue, which has become known as the "ozone deficit problem," is of great concern, since our inability to reproduce present ozone abundances questions our ability to predict future ozone trends.

It is customary to discuss the ozone abundance in terms of the abundance of odd oxygen [O_x] (brackets denote species concentrations in molecules cm^{-3}), defined as the sum of abundances of ozone and atomic oxygen, $[O_x] = [O_3] + [O]$. Given [O_x], [O_3] can be determined provided the ratio [O]/[O_3] is known. The latter is given by the expression

$$\frac{[O]}{[O_3]} = \frac{J_2 + J_3}{k_1[O_2][M]} \qquad (1)$$

where [M] is the atmospheric density and J_i and k_j are the photolysis and kinetic rate coefficients for reactions i and j, respectively (the reader is referred to Table 1 for a list of the photochemical reactions discussed in this paper). In the upper stratosphere and lower mesosphere, the only known source of odd oxygen is the photodissociation of molecular oxygen in the Schumann-Runge bands and Herzberg continuum, while the known sinks of odd oxygen include direct recombination of ozone and atomic oxygen as well as four catalytic cycles involving odd hydrogen ($[HO_x] = [H]+[OH]+[HO_2]$, odd chlorine ($[ClO_x]$

TABLE 1. KEY MODEL REACTIONS

Reaction	Rate Coefficient
$O_2 + h\nu \rightarrow 2O$	J_1
$O_3 + h\nu \rightarrow O_2 + O$	J_2
$O_3 + h\nu \rightarrow O_2 + O(^1D)$	J_3
$H_2O + h\nu \rightarrow OH + H$	J_4
$NO_2 + h\nu \rightarrow NO + O$	J_5
$O + O_2 + M \rightarrow O_3 + M$	k_1
$O + O_3 \rightarrow 2O_2$	k_2
$O + HO_2 \rightarrow OH + O_2$	k_3
$O_3 + H \rightarrow OH + O_2$	k_4
$O + ClO \rightarrow Cl + O_2$	k_5
$O + NO_2 \rightarrow NO + O_2$	k_6
$NO_2 + O_3 \rightarrow NO_3 + O_2$	k_7
$O + OH \rightarrow O_2 + H$	k_8
$OH + HO_2 \rightarrow H_2O + O_2$	k_9
$Cl + CH_4 \rightarrow HCl + CH_3$	k_{10}
$Cl + HO_2 \rightarrow HCl + O_2$	k_{11}
$HCl + OH \rightarrow H_2O + Cl$	k_{12}
$ClO + NO \rightarrow Cl + NO_2$	k_{13}
$Cl + O_3 \rightarrow ClO + O_2$	k_{14}

= [Cl]+[ClO]), and odd nitrogen ($[NO_x]$ = [NO]+$[NO_2]$) species. During daytime, a balance between production P and loss L of odd oxygen is expected, with the result

$$2J_1[O_2] = 2k_2[O][O_3] + 2k_3[O][HO_2] + 2k_4[O_3][H] + 2k_5[O][ClO] + 2k_6[O][NO_2] \quad . \qquad (2)$$

The photolysis of a O_2 molecule leads to the production of two odd oxygen species and in each catalytic cycle two odd oxygen species are destroyed. The balance expressed in equation (2) is often referred to as odd oxygen photochemical equilibrium.

Initial attempts to verify model descriptions of odd oxygen involved the analysis of individual ozone profiles. In both the upper stratosphere [*Natarajan et al.*, 1986, *Natarajan and Callis*, 1989; *Froidevaux et al.*, 1989; *McElroy and Salawitch*, 1989*a*, 1989*b*; *Allen and Delitsky*, 1991*a*] and the mesosphere [*Allen et al.*, 1984; *Froidevaux et al.*, 1989; *Clancy et al.*, 1987; *Allen and Delitsky*, 1991*a*] the calculated ozone abundances were systematically lower than the measurements (or equivalently, the calculated odd oxygen loss exceeded production). In addition, *Crutzen and Schmailzl* [1983] concluded that the globally averaged odd oxygen loss exceeds production above 35 km when the "low" molecular oxygen cross sections are adopted (such cross sections correspond to the currently accepted values). However, given sufficiently large measurement uncertainties, *Natarajan and Callis* [1989] argued that no "ozone deficit" exists in the upper stratosphere (a similar conclusion was reached by *McElroy and Salawitch* [1989*b*] for one of the two profiles they were analyzing). We will return to this issue of interpretation in section 4. The conclusions with regard to the ozone deficit based on individual profiles have been supported by *Jackman et al.* [1986] and *Rusch and Eckman* [1985], who studied two-dimensional zonally averaged ozone distributions in the stratosphere and mesosphere, respectively.

The calculations of daytime ozone abundances from equation (2) are straightforward, provided the radical abundances and the rate coefficients are known. At any given temperature, the latter can in principle be determined from laboratory measurements. However, not all of the above referenced studies had the benefit of analyzing measurements of O_3 obtained simultaneously with observations of the reactive species in equation (2) (or source/reservoir species that constrain the abundances of the reactive species). There

exist two comprehensive sets of such measurements, of which some of the previous studies did take advantage. From the measurements of thermal emission by the Limb Infrared Monitor of the Stratosphere (LIMS) instrument onboard the Nimbus 7 satellite, global distributions of temperature, ozone, water vapor, and nitrogen dioxide were obtained between October 25, 1978 and May 28, 1979 [*Gille and Russell*, 1984]. Since the abundances of O, H, and HO_2 can be determined from these measurements (e.g., *Froidevaux et al.* [1989]), LIMS provided the observational data required to test equation (2), except for the ClO abundances. If the latter could somehow be constrained, a test of the odd oxygen balance would become possible. This was the procedure adopted for a single zonally averaged LIMS profile by *Natarajan et al.* [1986] and *Froidevaux et al.* [1989] and for the two-dimensional fields by *Jackman et al.* [1986]. In addition to LIMS data, comprehensive measurements at two latitudes were acquired during the period April 30 - May 1, 1985 by the Atmospheric Trace Molecule Spectroscopy (ATMOS) experiment flown on Spacelab 3. ATMOS obtained nearly simultaneously vertical profiles of O_3, along with temperature, water vapor, odd nitrogen, and chlorine reservoir species; these data were used in the studies of *Natarajan and Callis* [1989], *McElroy and Salawitch* [1989*b*], and *Allen and Delitsky* [1991*a*]. As already noted, even with the availability of the necessary correlative measurements, the models did not reproduce the ozone observations.

In past studies, several suggestions were offered as to the possible errors in the photochemical models which may be responsible for the ozone deficit problem. However, while individual ozone profiles can be better reproduced when one or several model parameters are modified, the question remains how unique is the chosen solution. The global character of LIMS data offers a special opportunity to shed more light on this issue by providing a wider range of physical conditions under which the photochemical balance needs to be satisfied. In particular, in a given time period LIMS measurements at different latitudes sample a range of temperatures and solar zenith angles at a given pressure level. As a result, errors in temperature-dependent kinetic rate coefficients might be better disentangled from those in photochemical rate coefficients.

In this paper, we will use the global measurements from LIMS in order to reexamine the odd oxygen balance in both the upper stratosphere and the lower mesosphere. Our study complements that by *Jackman et al.* [1986] by extending the analysis into the lower mesosphere (which might help to identify

a common model deficiency at all altitudes) and by taking advantage of the most recent NASA compilation of recommended values for the kinetic rate coefficients and photodissociation cross sections [*DeMore et al.*, 1990]. Our study also complements that of *Rusch and Eckman* [1985], who examined the mesospheric ozone distribution obtained by the Solar Mesospheric Explorer (SME) satellite, but did not have simultaneous fields of temperature nor of any other radical species in equation (2).

The organization of this paper is as follows. In section 2, the photochemical steady state (also referred to as photochemical equilibrium) model used in the present study is described. In section 3, the latitude- and altitude-varying model parameters used in this study are described. In section 4, we present the results of our calculations for the first week of May 1979 which demonstrate the existence of a global ozone deficit problem based on LIMS data. Possible modifications to the photochemical model which might eliminate the deficit are considered in section 5. Also in section 5 the results for the week of January 1-7, 1979, are presented. The paper concludes with a summary in section 6.

2. PHOTOCHEMICAL MODEL

The photochemical equilibrium (PE) model used in the present study is based on the assumption of photochemical steady state for ozone and other reactive species, which enables us to use a small subset of the full photochemical reaction set in the calculations of odd oxygen balance. The PE model solves equation (2) for the daytime ozone concentration using LIMS measurements of temperature and mixing ratios of O_3, H_2O, and NO_2. The concentrations of O, H, and HO_2 are derived from the observed species abundances by means of the expressions discussed by *Froidevaux et al.* [1989]. Since LIMS acquired no measurements of chlorine species, an independently calculated daytime ClO distribution is adopted in the computations (see section 3.4). The greater computational efficiency of the PE model (relative to a fully time-dependent model) is essential for performing the multiple calculations necessary to explore various modifications to the adopted O_x chemistry. The present work extends the analysis of Froidevaux et al. to the global atmosphere between 6 and 0.4 mbar and 60°S and 70°N latitude. The upper boundary to the model has been dictated by the quality of ozone measurements (see section 3.1), whereas the lower

boundary and the latitudinal extent are determined by the assumption of photochemical equilibrium (or chemical control of the O_x family, *Garcia and Solomon* [1985]) and the availability of LIMS data, respectively. Our calculations differ from those of Froidevaux et al. in that we fix the photodissociation rate coefficients to values precomputed with the observed ozone concentrations, whereas Froidevaux et al. calculated the rate coefficients self-consistently with the computed model ozone. We feel that the new approach comes closer to the goal of calculating model ozone using observed atmospheric values whenever possible. In addition, we have updated the kinetic rate coefficients and photodissociation cross sections in accordance with the latest NASA recommended values [*DeMore et al.*, 1990].

To verify the altitude range for which the PE assumption is valid, we carried out diurnal runs with the Caltech/JPL one-dimensional (1D) time-dependent model for latitudes 30°N, 15°S, and 45°S and the subsolar latitude fixed as appropriate for May 1. This latitude range covers most solar illumination conditions to be found in the course of a year in non-polar regions. From "converged" time-dependent model results (ozone concentrations between 6 and 0.4 mbar differing by less than 1% at times separated by 24 hours), values of the relevant atmospheric quantities at the time of daytime LIMS observations (~ 1300 LT) were incorporated into the PE model. The differences in ozone concentrations between those obtained from the PE model and those obtained directly from the time-dependent model are shown in Figure 1. This figure shows that the PE assumption is valid to better than 5% above 3 mbar (to better than 10% above 4 mbar) at low and mid-latitudes; at high winter latitudes the PE region only extends above 2 mbar. The decrease in the pressure-altitude of the lower boundary for the PE region with increasing winter latitudes is in qualitative agreement with the behavior of the photochemical lifetime of odd oxygen discussed by *Garcia and Solomon* [1985]. Since the main conclusions of our work pertain to the region above 3 mbar, the PE model is sufficient for our purposes.

3. Adopted Model Parameters

The LIMS instrument was flown aboard the Nimbus 7 satellite, which orbited the Earth in a sun-synchronous orbit and, as a result, at each latitude measurements were performed twice during the course

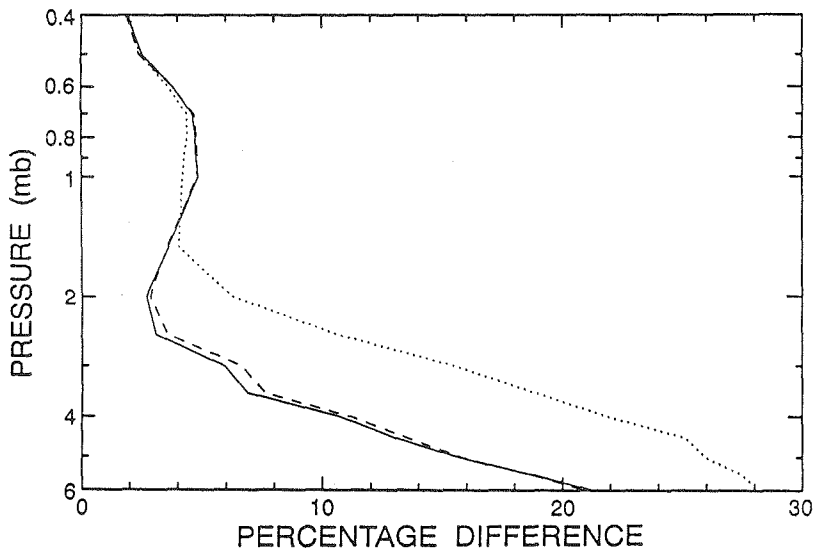

Fig. 1. Percentage differences between ozone abundances calculated by the photochemical equilibrium (PE) model using species distributions generated by the Caltech/JPL one-dimensional (1D) model and ozone abundances calculated by the one-dimensional model at 1300 LT, equal to (PE-1D)/1D x 100%. Solid line: 30°N, dashed line: 15°S, dotted line: 45°S (all curves correspond to calculations for May 1).

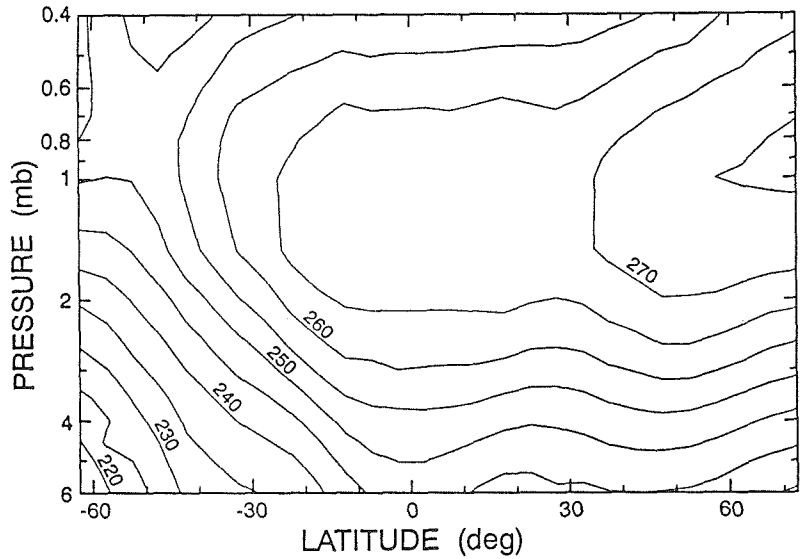

Fig. 2. Zonally averaged distributions of LIMS daytime temperature in degrees Kelvin for the week of May 1-7, 1979, used in the calculations of ozone abundances by the photochemical equilibrium model.

of a day. Over most of the latitude range, the times of the two measurements were ~1300 LT and ~2300 LT (the two sets of measurements are referred to as "daytime" and "nighttime," respectively). In this paper, we use zonally averaged distributions (in 5° latitude intervals) derived from individual profile measurements stored on the Inverted Profile Archival Tapes (IPATs). Since our objective is to study the photochemical balance between odd oxygen production and loss, we use daytime data whenever possible. However, for reasons discussed below, important exceptions to this rule have been made. We modeled data from several weeks selected from the LIMS operational period October 25, 1978 - May 28, 1979. Since most of our conclusions generally apply to all weeks analyzed, the discussion in this paper is restricted to the week May 1-7, 1979, unless otherwise stated.

3.1 Temperature and Ozone

Above 0.4 mbar, the daytime values of ozone measured by LIMS may be in error by more than 10% due to the nonlocal thermodynamic equilibrium (NLTE) [*Solomon et al.*, 1986]. Also, at these altitudes the systematic errors in the ozone measurements start to increase rapidly, reaching 26% and 40% at 0.3 and 0.1 mbar, respectively [*Remsberg et al.*, 1984]. Consequently, 0.4 mbar has been adopted as the upper boundary for the present model. The lower boundary has been set at 6 mbar (which corresponds to ~35 km), but in view of the discussion in section 2, we do not place much weight on the results below 3-4 mbar. The daytime temperature and ozone distributions adopted for our study are shown in Figures 2 and 3, respectively.

3.2 Water Vapor

The nighttime (rather than daytime) values for H_2O are used in the calculations, since the observed diurnal variation in H_2O is not physically plausible at the altitudes considered, with the daytime data spuriously high due to NLTE [*Russell et al.*, 1984; *Kerridge and Remsberg*, 1989]. As the nighttime values only extend to 0.8 mbar, extrapolation was required to obtain values up to 0.4 mbar. For most latitudes, the IPAT data show a decrease in the water vapor mixing ratio above 1 mbar. Since this decrease has not been reported in any other measurements and is most likely an instrumental artifact, we have discarded the data above 1 mbar and assumed the mixing ratio to be constant above 1 mbar, at least up to 0.4 mbar. This extrapolation is probably valid for two reasons. First, the radiance-averaged distribution for May shown

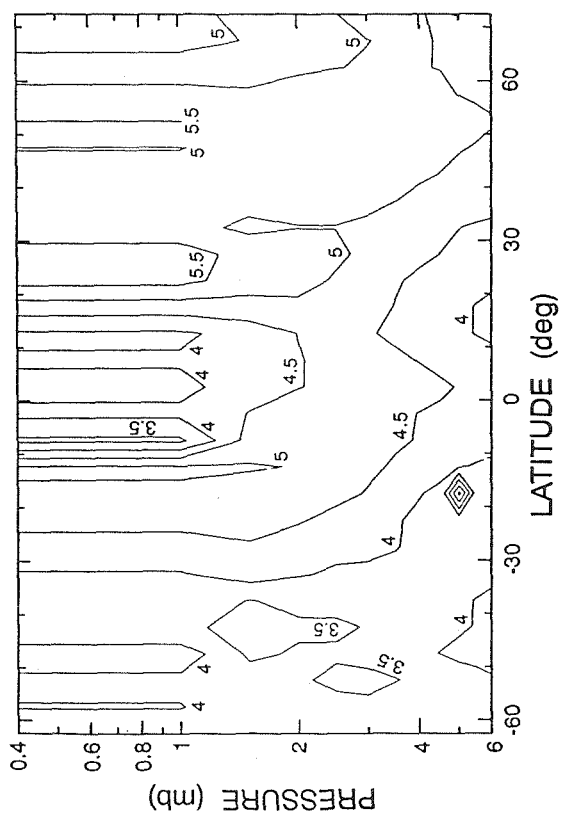

Fig. 4. The mixing ratio of LIMS nighttime water vapor (ppmv) for the week of May 1-7, 1979.

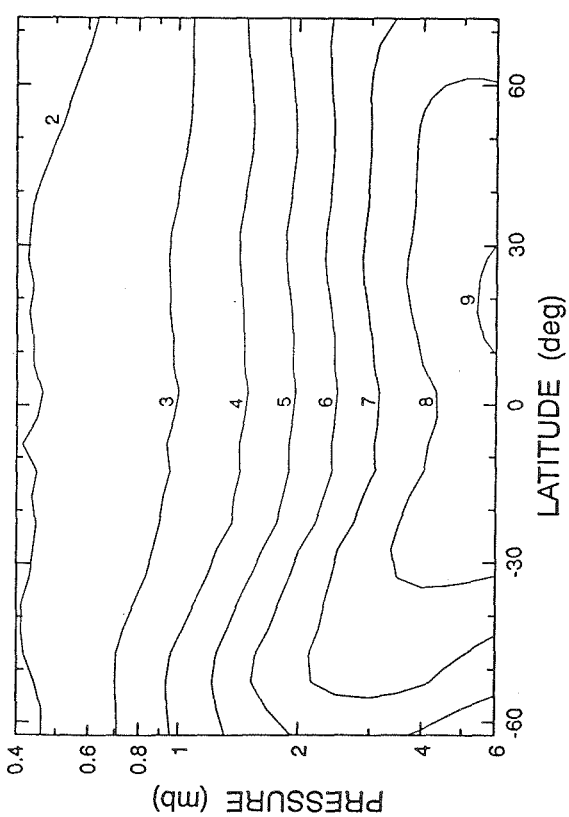

Fig. 3. The mixing ratio of LIMS daytime ozone in parts per million by volume (ppmv) for the week of May 1-7, 1979.

by *Kerridge and Remsberg* [1989] indicates that the water vapor mixing ratio increases above 1 mbar by ~ 10%. Adopting a constant value should therefore lead to an underestimate of the odd hydrogen-catalyzed ozone destruction and, if anything, a small underestimate of the ozone deficit (see section 5.1). Second, the O_3 concentration in the lower mesosphere is only weakly dependent on the water vapor mixing ratio [*Allen et al.*, 1984, Table 2]. Accordingly, any uncertainties in the adopted water vapor distribution should have a small effect on the calculated ozone. The water vapor distribution utilized in our calculations is shown in Figure 4.

3.3 Nitrogen Dioxide

The direct use of the LIMS daytime NO_2 data is not reliable at the high altitudes of interest due to a low signal-to-noise ratio [*Russell et al.*, 1984]. In addition, the inferred daytime values are probably also too high due to NLTE [*Kerridge and Remsberg*, 1989]. Since NO_2 exhibits significant diurnal variations, the daytime values of $[NO_2]$ required in the present study are not equal to the nighttime data. Instead, the daytime abundances have been inferred by means of an approximate procedure similar to that described by *Callis et al.* [1986].

First, the local sunset values of $[NO_2]$ are obtained from nighttime concentrations under the assumption that the conversion of NO_2 into N_2O_5 is the principal cause for the decline in the NO_2 concentration after sunset [*Solomon et al.*, 1986; *Webster et al.*, 1990]. The distribution of nighttime $[NO_2]$ measured by LIMS is shown in Figure 5*a*. The values of $[NO_2]$ at sunset can then be obtained from measurements of $[NO_2]$ later in the night by means of the following formula:

$$[NO_2]_{sunset} = [NO_2]_{measured} \exp[2.0\, k_7\, [O_3]\, (t_m - t_s)] \qquad (3)$$

where t_m is the local time of the nighttime measurement (~ 2300 LT for most latitudes), t_s is the local sunset time calculated by relating pressure to altitudes in the draft Committee on Space Research Standard Atmosphere [*Labitzke et al.*, 1985], and k_7 is the rate coefficient for the reaction $NO_2 + O_3 \rightarrow NO_3 + O_2$, the rate limiting step in the nighttime conversion of NO_2 into N_2O_5. Nighttime values of temperature and ozone are used in equation (3) (they differ by less than 3K and 13%, respectively, from their daytime

counterparts; the resulting differences in the computed ozone abundances are less than 1%). At 30°N, the sunset $[NO_2]$ values thus calculated are higher (by <21%) than the ATMOS 30°N values of $[NO_2]$ + [NO] below 3 mbar, agree with the latter (to within 3%) at 2.5 mbar, and are lower (by 44% at 1.5 mbar) above 2 mbar (the two profiles are expected to be equal on theoretical grounds; see equation (4) below). Very similar results were reported by *Russell et al.* [1988] who concluded that the discrepancies were within the error bars of the two data sets.

From the local sunset NO_2 abundances, the daytime values are obtained on the assumptions that the sum $[NO_2]$ + [NO] is conserved during the course of a day and NO is totally converted into NO_2 at sunset; that is,

$$\{[NO_2] + [NO]\}_{daytime} = [NO_2]_{sunset} \tag{4}$$

and using the calculated ratio $[NO_2]/[NO]$ at ~1300 LT. The latter is obtained from equation (A7) of *Froidevaux et al.* [1989] (note that $[O_2]$ should read $[HO_2]$ in that equation). The resulting daytime distribution of NO_2 is shown in Figure 5*b*. The inferred values are lower than the measured daytime values at the highest altitude for which LIMS daytime NO_2 data are available (1.5 mbar), but are higher by up to 3 ppbv at lower altitudes. Both of these findings are consistent with the results reported by *Callis et al.* [1986]. The measured daytime NO_2 concentrations at the highest altitudes are probably overestimates of the true abundances due to NLTE effects [*Kerridge and Remsberg,* 1989], which would help to explain the discrepancy between the inferred and measured daytime $[NO_2]$ values at pressures less than 2 mbar. On the other hand, the source of the discrepancy at lower altitudes remains unexplained. However, consistent with the inferred daytime NO_2 abundances being higher, and correctly so, than the observed daytime values are the findings of *Russell et al.* [1984] that the observed NO_2 night/day ratio below ~40 km is larger than theoretical values. In section 5.1 we discuss recent results that demonstrate the accuracy of our model simulations of the NO_2 diurnal variation.

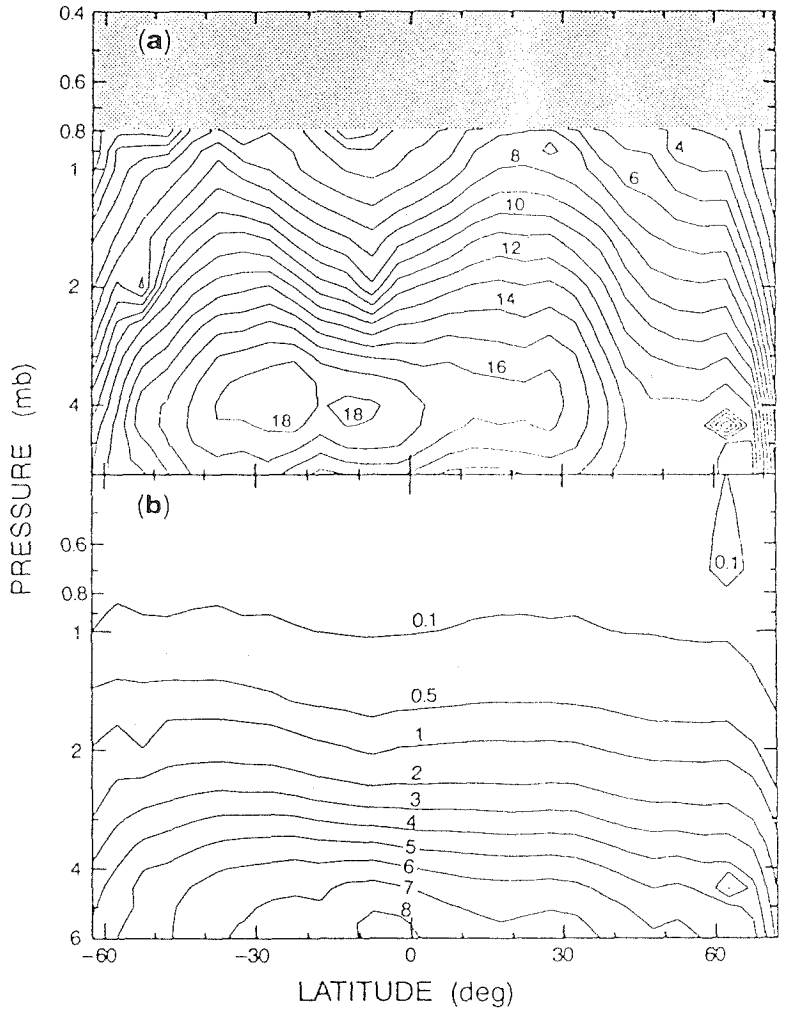

Fig. 5. The mixing ratios of *(a)* LIMS nighttime nitrogen dioxide (ppbv) (values above 0.8 mbar are either nonexistent or unreliable) and *(b)* daytime nitrogen dioxide (ppbv) inferred from nighttime measurements. Both distributions are for the week of May 1-7, 1979.

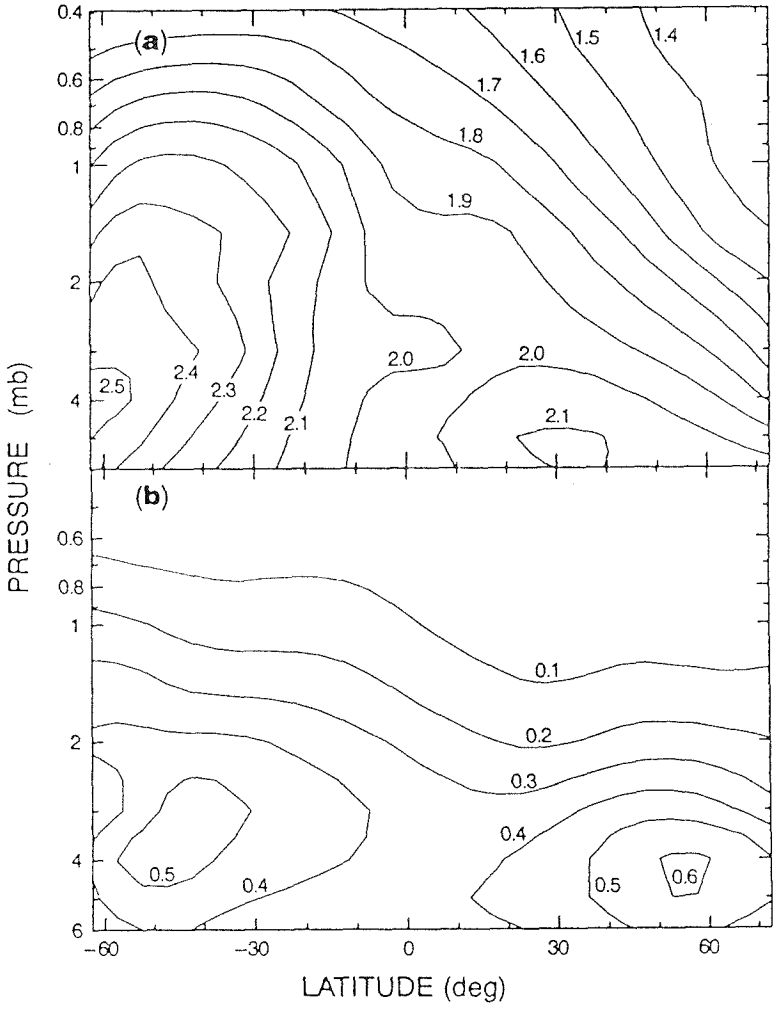

Fig. 6. The mixing ratios of *(a)* total odd chlorine (ppbv) from the model of *Yang et al.* [1991] and *(b)* daytime-average chlorine monoxide (ppbv), derived as described in section 3.4. Both distributions are monthly averages for May 1979.

3.4 Chlorine Monoxide

The LIMS experiment made no measurements that would constrain the ClO abundances. This is most unfortunate, since ~2-3 mbar is the pressure range at which the ClO_x cycle contributes most significantly to the loss of odd oxygen. In place of observations, an independently calculated distribution of daytime-averaged ClO corresponding to the period of LIMS measurements has been adopted for the present study. It has been kindly provided to us by K. K. Tung and is derived from the model described by *Yang et al.* [1991].

However, we believe that the ClO abundances calculated by Yang et al. are systematically too high. This is because the methane distribution also calculated by Yang et al. is up to a factor of 5 lower than the values measured by the Stratospheric and Mesospheric Sounder (SAMS) instrument onboard Nimbus 7 (cf. Yang et al.). Methane directly affects the partitioning between chlorine species in the stratosphere, as expressed in the formula [*Solomon and Garcia*, 1984; *Froidevaux et al.*, 1985]:

$$\frac{[HCl]}{[ClO]} = \frac{k_{10}[CH_4]+k_{11}[HO_2]}{k_{12}[OH]} \frac{k_5[O]+k_{13}[NO]}{k_{14}[O_3]} \quad . \tag{5}$$

Model results from the fully time-dependent Caltech/JPL one-dimensional model runs described in section 2 indicate that the term $k_{11}[HO_2]$ is smaller than $k_{10}[CH_4]$ and consequently it will be neglected here, with the result that the ratio [HCl]/[ClO] becomes directly proportional to $[CH_4]$. If the abundance of total reactive chlorine (Cl_y) is equal to the sum of [HCl] and [ClO], then any underestimate in the CH_4 abundances leads to a significant overestimate of the ClO distribution for 1979. In what is another manifestation of this effect, *Solomon and Garcia* [1984] noted that natural variations in stratospheric CH_4 abundances may cause [ClO] to vary by as much as a factor of 3.

We adjusted the [ClO] values received from Yang et al. as follows. We assumed that the distribution of $[Cl_y]$ calculated by Yang et al. is appropriate for the 1979 atmosphere. This distribution is shown in Figure 6*a*. It exhibits latitudinal and vertical variation, which may be related to the fact that a steady state has not been reached in the Yang et al. calculations, but we note the recent study by *Weisentein et al.* [1992], who showed that the steady state should not indeed be expected given the long term increase

in chlorofluorocarbon emissions. We also note that the global average Cl_y mixing ratio calculated by Yang et al. (1.9 ppbv at the stratopause) agrees with the 1979 value obtained by Weisenstein et al. (cf. their Figure 11*a*). Next we used the distributions of Cl_y and ClO from Yang et al. to derive the proportionality constant A such that

$$\frac{[HCl]_{Yang}}{[ClO]_{Yang}} = \frac{[Cl_y]_{Yang} - [ClO]_{Yang}}{[ClO]_{Yang}} = A\ [CH_4]_{Yang} \qquad (6)$$

where, by comparison with equation (5), A is a function of the abundances of O, O_3, NO, and OH. The first equality in equation (6) follows from our assumption $[Cl_y] = [HCl] + [ClO]$. We further assumed that the values of A are correctly calculated by Yang et al. The adjusted concentrations of ClO were then computed with the SAMS observations of $[CH_4]$ and the values of $[Cl_y]$ from Yang et al., i.e.,

$$[ClO]_{adj} = \frac{[Cl_y]_{Yang}}{1 + \left(\frac{[HCl]}{[ClO]}\right)_{adj}} = \frac{[Cl_y]_{Yang}}{1 + A[CH_4]_{SAMS}} \quad . \qquad (7)$$

While $[CH_4]$ rapidly decreases with altitude in the upper stratosphere, the values of $[Cl_y]$ show much less or no variation there (our Figure 6*a* and Figure 10 in *Raper et al.* [1987]). Therefore we believe that the assumptions in the Yang et al. treatment of dynamics (in particular the absence of cross-isentropic mixing) which led to the underestimate of $[CH_4]$ do not introduce similarly large errors in the calculated $[Cl_y]$ fields.

The revised May ClO distribution utilized in this paper is shown in Figure 6*b*. It is generally lower than the distribution presented by *Callis et al.* [1986], but we note that the latter used a higher boundary condition for the total chlorine reservoir (2.55 ppbv at the stratopause versus 1.9 ppbv global average in the Yang et al. study). More recently, *Natarajan and Callis* [1989] utilized a smaller value (2.0 ppbv) for total reactive chlorine at the stratopause in 1979. On the other hand, our revised values for the ratio $[ClO]/[Cl_y]$ are similar to the values obtained by Callis et al. who used the observed values of $[CH_4]$ to constrain the partitioning of reactive chlorine. In addition, our model value (~0.2) for this ratio at 30°N and 40 km is in excellent agreement with the ratio calculated from the ClO observations of *Waters et al.* [1988] and the Cl_y

measurements from ATMOS for the period April-May 1985 [*Raper et al.*, 1987]. We expect such agreement, since the factors defining this ratio (see equations (5) and (7)) should have changed only a little between 1979 and 1985. Similarly, in the recent analysis of ATMOS data by *Natarajan and Callis* [1991], the model $[ClO]/[Cl_y]$ ratios at 40 km at noon also well approximate the measurements (see their Figures 1 and 10), since these calculations use other ATMOS observations to constrain the abundances of CH_4 and of the other species. The values of $[ClO]/[Cl_y]$ in the present study are also close to values in the earlier models of *Froidevaux et al.* [1985] and *Jackman et al.* [1986], but the adopted values of $[Cl_y]$ are higher in those models (3.39 and 3.0 ppbv in 1979, respectively) than in either the present study or the atmosphere as characterized by ATMOS. Therefore their values of [ClO] are significantly larger than those shown in Figure 6*b*. Finally, while our model ClO abundances at 30°N are lower than the mean of the balloon ClO measurements (at a similar latitude and epoch) discussed in *WMO* [1986], the model values at 40 km are consistent with the results obtained by *Brune et al.* [1985] and Waters et al., given the expected long term increase in $[Cl_y]$.

The values of [ClO] at the local times of LIMS measurements have been assumed equal to the daytime averages. This procedure is based on the expectation that the concentration of ClO shows only little variation during the middle of the day after a rapid increase right after sunrise [*Froidevaux et al.*, 1985] and adopting it seems reasonable in view of the other uncertainties associated with the ClO distribution.

3.5 Photodissociation Rate Coefficients

The photodissociation rate coefficients were precomputed for the ozone calculations with the values of the relevant physical quantities corresponding to the LIMS measurements. The photodissociation rate coefficients are a product of molecular cross sections and solar flux penetrating to a given pressure level, integrated over wavelength. The values of the cross sections were taken from the *DeMore et al.* [1990] compilation. At a given latitude, the solar flux is a function of the solar zenith angle at the time of the daytime LIMS measurements. The weekly-averaged measurements span a range of zenith angles at any given latitude. The total actinic flux (the appropriate quantity for photodissociation calculations) is the sum of direct and diffuse terms [*Madronich*, 1987; *Michelangeli et al.*, 1992]. In the present study, the direct

flux has been calculated with solar irradiances reported in *WMO* [1986] and for atmospheric opacity corresponding to the observed ozone profile and pressure (which determines the overhead column of molecular oxygen) at each latitude. The diffuse flux at a given pressure level has been calculated by solving the radiative transfer equation for the global-mean ozone profile. The radiative transfer model described by *Michelangeli et al.* [1992], which accounts for multiple scattering, has been employed. A Lambertian surface with albedo 0.25 (the average reflection from clouds and the surface) has been assumed. We have explored the sensitivity of the computed photodissociation rate coefficients to the choice of the ozone profile (global-mean vs. values at any specified latitude) in the diffuse flux calculation and found that under the most extreme conditions the resulting uncertainty is less than 10%. Since this is much less than other uncertainties entering our calculations and since multiple solutions of the radiative transfer equation are a time-consuming task, adopting a diffuse flux term dependent on the zenith angle alone seems to be a reasonable procedure. The mean solar zenith angle for daytime LIMS measurements in each latitude interval and the associated precomputed values for four of the five photodissociation rate coefficients important in our model (Table 1) are plotted in Figures 7 and 8, respectively. The fifth important photodissocation rate coefficient, J_5, is almost independent of altitude and closely follows the zenith angle, with a peak value of ~1.42 (in units 10^{-2} s^{-1}) at the subsolar latitude of 17.5°N (which corresponds to a minimum zenith angle of 12°) and decreasing to 1.3 and 1.0 at the zenith angles of 55° and 75°, respectively.

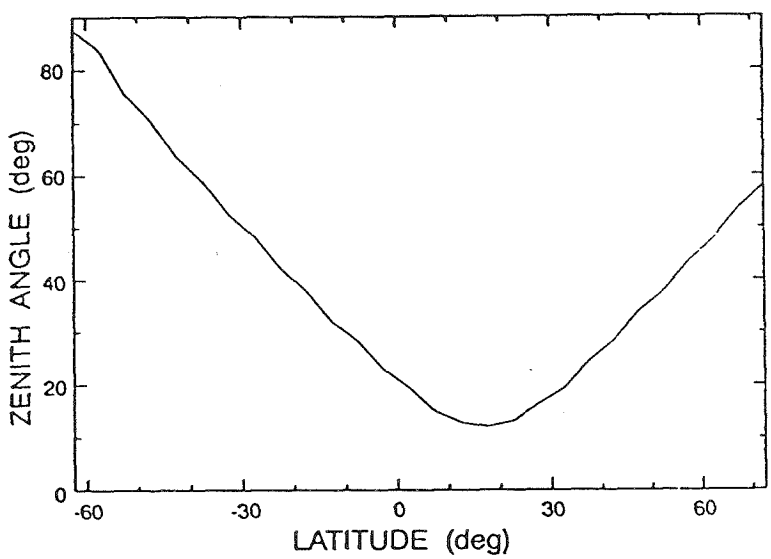

Fig. 7. The mean solar zenith angle at the times of LIMS daytime observations during May 1-7, 1979, as a function of latitude.

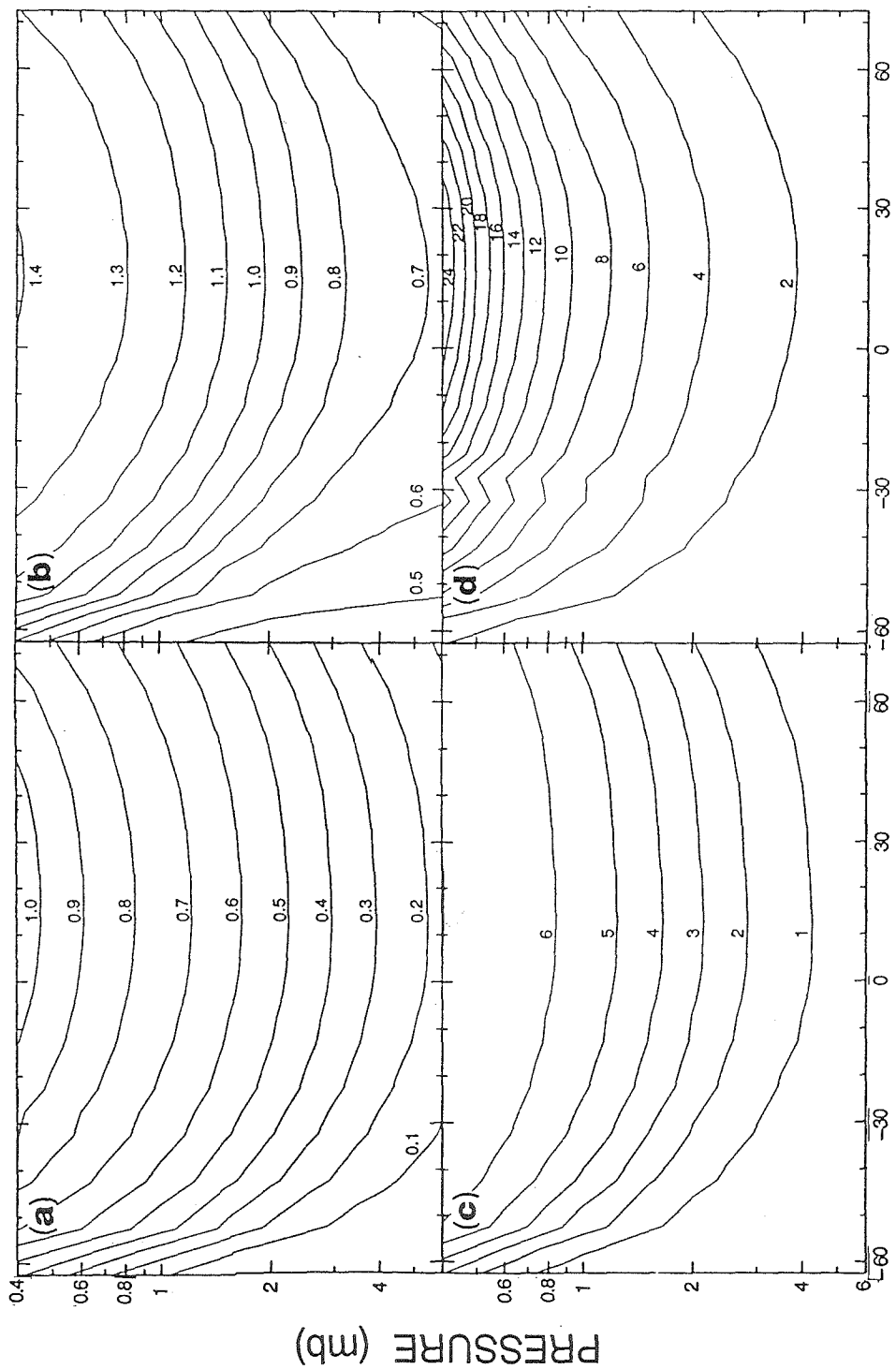

Fig. 8. Photodissociation rate coefficients calculated from LIMS measurements of ozone (units are given in brackets): *(a)* J_1 (10^{-9} s^{-1}), *(b)* J_2 (10^{-3} s^{-1}), *(c)* J_3 (10^{-3} s^{-1}), *(d)* J_4 (10^{-9} s^{-1}). See Table 1 for list of reactions.

4. Model Ozone Deficit

The ozone deficit D is defined as the difference between the PE-calculated ozone abundances $[O_3]_{PE}$ and the LIMS observations $[O_3]_o$; that is,

$$D = ([O_3]_{PE} - [O_3]_o)/[O_3]_o \times 100\% \quad (8)$$

The values of D for our simulation of the first week of May 1979 for latitudes between 60°S and 70°N and pressures between 6 and 0.4 mbar are shown in Figure 9*a*. The deficit at 30°N is significantly lower than the values calculated for the same week and latitude by *Froidevaux et al.* [1989] and those calculated by *Natarajan et al.* [1986] in their one-dimensional study of LIMS data for March 1979. Our deficit values are, however, similar to the results of *Natarajan and Callis* [1989], *McElroy and Salawitch* [1989b], and *Allen and Delitsky* [1991*a*] obtained from the analysis of ATMOS data, especially if one takes into account that ATMOS ozone measurements may be systematically too low by up to 10%. We understand the differences with the previous LIMS-based studies as resulting from overestimates of ClO abundances (as discussed in section 3.4) and the agreement with ATMOS-based studies to be the result of accurate and low ClO abundances used in both cases. This conclusion is corroborated by *Natarajan and Callis* [1989] in their reanalysis of LIMS data at 30°N in March. Using a smaller value for $[Cl_y]$, they were able to reduce the deficit at 40 km by 18% below the previous value calculated with higher $[Cl_y]$.

In the lower mesosphere, the distribution shown in Figure 9*a* is quite different from that reported for day 180 of 1983 by *Rusch and Eckman* [1985]; our values are lower than theirs. We have no explanation for this difference, although we note that simultaneous measurements of temperature and H_2O were not available to Rusch and Eckman.

Our model ozone abundances marginally agree with the LIMS measurements, which have systematic errors of 16 and 26% at 3 and 0.3 mbar, respectively [*Remsberg et al.*, 1984]. However, they are systematically lower than the measurements. We believe that this directly reflects deficiencies in the model calculations, rather than LIMS measurements errors, because model measurement comparisons using

ozone data sets from other instruments (e.g., ATMOS and SME) also show the same systematic discrepancy (see discussion in section 1).

Figure 9*a* shows that with altitude increasing into the mesosphere, the deficit increases (in this paper we mean by this that D becomes more negative and vice versa for decreasing deficit), a trend also reported by *Rusch and Eckman* [1985] and *Allen and Delitsky* [1991*a*]. At constant stratospheric pressure the deficit decreases by ~4% between the late-spring and late-fall hemisphere. The largest and smallest deficits at a given mesospheric pressure level correspond to the mid-latitude maxima and the equatorial minimum in the distribution of water vapor (see Figure 4). These deficit extrema in the lower mesosphere were not reported by Rusch and Eckman (see their Figure 6). Since the latitudinal gradients in the mesospheric H_2O seen in Figure 4 are present in the distribution published by *Kerridge and Remsberg* [1989], it is unlikely that the latitudinal gradients in the mesospheric deficit are an artifact of the procedure we adopted in the extrapolation of the water vapor profiles above 1 mbar. We also note that our mesospheric deficit decreases towards winter latitudes, a trend opposite to that reported by Rusch and Eckman. This may have some implications for the evaluation of an additional source of odd oxygen discussed in section 5.2.

There are two alternative ways to express the ozone deficit which will be useful in the subsequent discussion. One is the quantity P - L, where P and L are the left- and right-hand sides of equation (2), calculated using LIMS ozone abundances. This quantity (with negative sign) can be interpreted as the missing production term which must be added to the left-hand side of equation (2) to achieve a balance between odd oxygen production and loss. Equivalently, L - P is the amount by which the loss rate must be reduced to bring about a balance. The features seen in Figure 9*a* are even more pronounced in Figure 9*b*, which shows the distribution of P - L, and in Figure 9*c* which shows the distribution of (P-L)/L x 100%, the percentage change in L needed to balance odd-oxygen production and loss. The latter quantity can be compared with L/P, whose distribution was presented by *Jackman et al.* [1986]. In the Jackman et al. study, the diurnally averaged L/P in the upper stratosphere increases towards winter latitudes, a trend similar to that found in the present study (albeit we calculate values of L/P that are smaller than those of Jackman et al.; this is probably a result of the differences in model Cl_y abundances discussed in section 3.4).

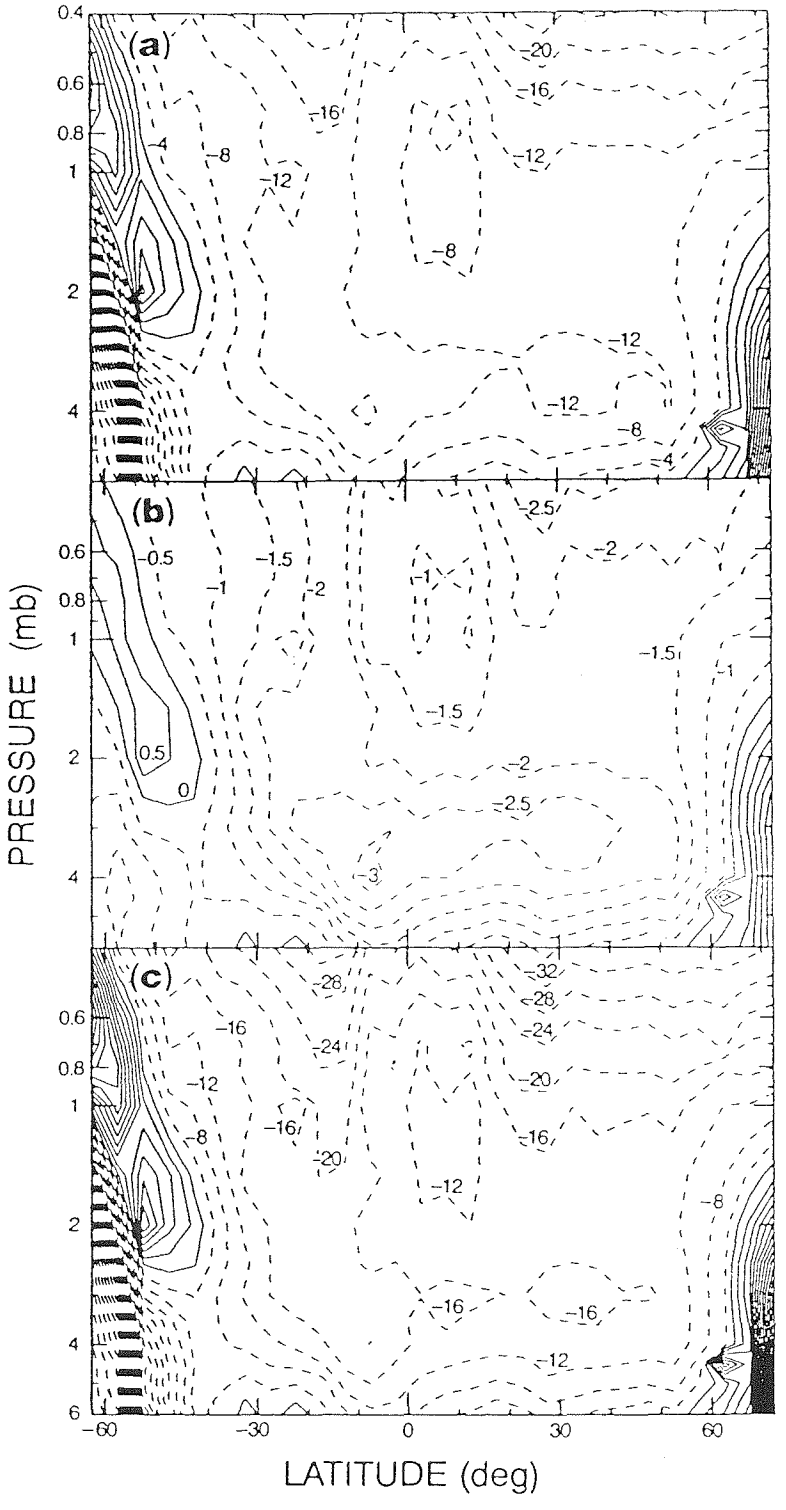

Fig. 9. *(a)* Percentage difference (cf. equation (8)) between the ozone abundances calculated by the PE model and the LIMS observations. *(b)* The difference (in 10^6 cm^{-3} s^{-1}) between the production and loss rates of odd oxygen (left- and right-hand sides of equation (2), respectively), calculated with the observed ozone abundances. *(c)* Same as Figure 9*b*, except the difference (in percent) is expressed as a fraction of the loss rate. All figures correspond to the LIMS week of May 1-7, 1979.

5. POSSIBLE MODEL DEFICIENCIES

Since the ozone deficit results from an imbalance between odd oxygen production and loss, it can be eliminated by either decreasing the latter or increasing the former. These two scenarios are discussed in this section.

5.1 Reduction in Odd Oxygen Loss

The odd oxygen loss rate can be decreased by reducing either the five kinetic rate coefficients or the radical abundances on the right-hand side of equation (2). The effect of any change in these quantities on the model ozone abundances is related to the fractional contributions of the five catalytic cycles to the total loss (cf. Figure 10). If any one of the five rate coefficients is reduced by the currently recommended uncertainties [*DeMore et al.*, 1990], model ozone abundances only increase by less than 5%; a simultaneous reduction in several rate coefficients would thus be required to eliminate the ozone deficit. This conclusion is generally consistent with *Froidevaux et al.* [1989, Table 1]. The smaller fractional increases in $[O_3]$ we obtain from decreasing the rate of the reaction $O + HO_2 \rightarrow OH + O_2$ are a result of a reduction in the rate coefficient uncertainty since the Froidevaux et al. study. A similar effect for the reaction $O + ClO \rightarrow Cl + O_2$ can be explained both by a reduction in the rate coefficient uncertainty and a decrease in the fractional contribution of the ClO_x cycle to the total odd oxygen loss rate (now less than 20% at 30°N) as a consequence of lower ClO abundances adopted in the present study.

More likely, the abundances of one of the key radicals have been overestimated. Of these, atomic oxygen is involved in all five catalytic cycles and thus a reduction in its concentration offers the most general means of decreasing L. We can most easily reduce the O abundances and remain consistent with the LIMS observations of O_3 by decreasing the $[O]/[O_3]$ ratio through increasing the rate coefficient k_1 for recombination to form O_3 (see equation (1)). The uncertainty in k_1 in the most recent NASA compilation [*DeMore et al.*, 1990] is 13% and 19% at 275 and 250 K, respectively (this is the range of temperatures in the PE region, see Figure 2), which translates into a similar uncertainty in L. Referring to Figure 9*c* we see that the increase in k_1 (to the values given by the formula $6.5 \times 10^{-34}\ (T/300)^{-2.8}$ cm^6 molecule^{-2} s^{-1}) can thus effectively eliminate the ozone deficit in the stratosphere and significantly reduce it in the lower

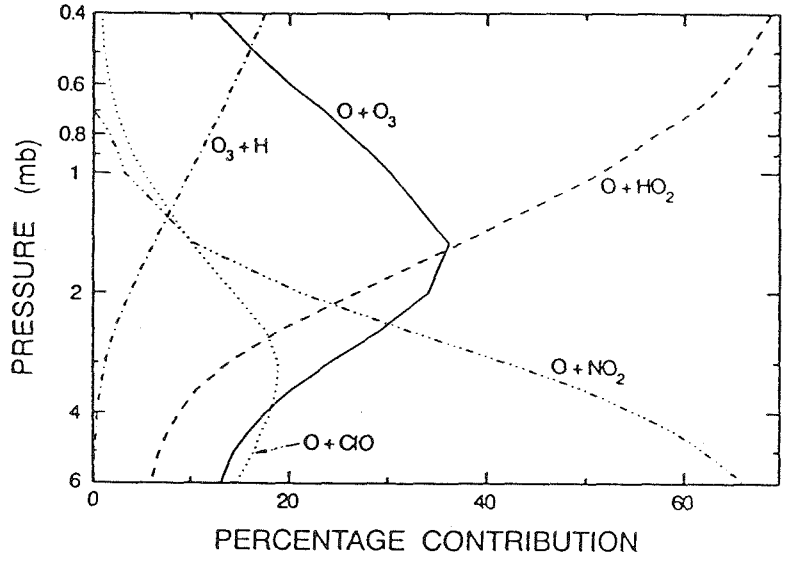

Fig. 10. Percentage contribution of the catalytic cycles to the total odd oxygen loss rate at 30°N in May evaluated with the standard model. The curves are labeled by the reactants in the rate limiting reaction in each cycle (cf. equation (2)).

mesosphere. The resulting ozone deficit is shown in Figure 11. The importance of k_1 in determining ozone abundances has previously been pointed out by *Jackman et al.* [1986] and *Froidevaux et al.* [1989].

Of the other radicals whose concentrations enter into equation (2), HO_2 is most important in the mesosphere, where the second term in equation (2) contributes 50-70% of the total odd oxygen loss (cf. Figure 10). Since L needs to be reduced by ~30% to bring about odd oxygen balance in the lower mesosphere (see Figure 9*c*), a reduction in $[HO_2]$ by a factor of ~2 would be required to eliminate the ozone deficit there. A similar conclusion has been reached by *Rusch and Eckman* [1985] and *Clancy et al.* [1987]. At present we are unaware of what could lead to such a large reduction. Uncertainties in the adopted distribution of water vapor are unlikely to achieve this, given the square-root dependence of $[HO_2]$ on $[H_2O]$ in the lower mesosphere [*Allen et al.*, 1984, equations (5) and (6)]. Reflecting this relationship, *Froidevaux et al.* [1989] estimate that, at 30°N in the lower mesosphere, the uncertainties in the adopted LIMS H_2O profile cause less than 10% uncertainty in the model ozone. Note that the abundances of H_2O above 1 mbar we adopted in this study are likely to be underestimates of the true abundances [*Kerridge and Remsberg*, 1989], whereas lower abundances are needed to reduce the ozone deficit. An alternative way to reduce $[HO_2]$ by a factor of 2 would be to decrease by a factor of 4 any of the kinetic rate coefficients entering the relationship between $[HO_2]$ and $[H_2O]$. This again is unlikely, since the recommended uncertainties for those reactions are less than 30% at mesospheric temperatures [*DeMore et al.*, 1990]. One exception is the rate coefficient k_9 for the reaction $OH + HO_2 \rightarrow H_2O + O_2$ whose recommended uncertainty is 38% and 48% at 275 and 250 K. Even if these uncertainties, at face value, are not sufficiently large to bring about the required reductions in $[HO_2]$, this reaction certainly deserves further study. In this context we note that increasing k_9 by the recommended uncertainty increases model ozone abundances in the lower mesosphere by up to 8%.

We believe that the ozone deficit is not a result of overestimates in the model abundances of either atomic H or ClO. The uncertainties in [H] are very unlikely to lead to large uncertainties in L, since the third term on the RHS of equation (2) contributes less than 20% to the total loss. Consequently, even a complete elimination of the $H + O_3$ cycle would not be enough to bring about an odd oxygen balance (cf. Figure 9*c*). Since we have already adopted a low distribution of [ClO] and, as a result, the ClO_x cycle

contributes less than 25% to the total odd-oxygen loss, reducing [ClO] further is also an unlikely solution to the ozone deficit problem. In fact, model [ClO] would have to be reduced by 80-100% to eliminate the deficit in the upper stratosphere, but even with such drastic change the deficit would not decrease in the mesosphere.

Finally, although it is difficult to estimate the uncertainties in our inferred distribution of $[NO_2]$, we believe that our model $[NO_2]$ has not been so overestimated as to be the sole cause of the deficit. This is because the contribution of the NO_x catalytic cycle to the total odd oxygen loss is less than 20% at pressures less than 2 mbar and thus even a 100% decrease in our model $[NO_2]$ would not solve the deficit problem there (cf. Figure 9*c*). However, uncertainties in $[NO_2]$ may be important at lower altitudes, where the NO_x contribution reaches 30 and 40% at 2.5 and 3 mbar, respectively. Since the loss rate is overestimated by ~16% in that region (cf. Figure 9*c*), a 40-50% reduction in the adopted $[NO_2]$ values could thus solve the deficit problem there.

Such a reduction might be consistent with the errors in the daytime $[NO_2]$ values we have inferred through the procedure described in section 3.3. These errors stem from three sources: (1) the systematic errors in the nighttime NO_2 concentrations, (2) errors involved in calculating the sunset values of $[NO_2]$ from the nighttime measurements, and (3) errors associated with the ratio $[NO]/[NO_2]$, which describes daytime partitioning of the total odd nitrogen reservoir between NO and NO_2. Of these, errors involved in calculating the sunset values are probably negligible, since *Allen and Delitsky* [1990] and *Tuomi et al.* [1991*a*] have shown that the nighttime conversion of NO_2 into N_2O_5 at ~38 km is very accurately simulated by equation (3) and its equivalents. *Russell et al.* [1984] estimate the systematic errors in the nighttime NO_2 concentrations to be less than 25% at pressures greater than 2 mbar. As for the errors associated with the $[NO]/[NO_2]$ ratio, *McElroy and Salawitch* [1989*a*], *Allen and Delitsky* [1990], and *Natarajan and Callis* [1991] agree that between 35 and 40-50 km the model $[NO]/[NO_2]$ ratio is within 20% of ATMOS measurements. In all three works, above some altitude between 40 and 50 km (depending on latitude and model), the calculated ratio becomes increasingly larger than the observed values.

The above estimates suggest that the total error in our model values of daytime $[NO_2]$ may be as much as 40-50% at pressures greater than ~2 mbar. At lower pressures the uncertainties may be even larger,

but if anything, the model [NO_2] values are probably underestimated there [*McElroy and Salawitch*, 1989*a*; *Natarajan and Callis*, 1991]. This suggests that the uncertainties in our adopted [NO_2] distribution may have led to an overestimate of the ozone deficit at altitudes below 2 mbar, but are very unlikely to provide a solution to the deficit problem above that level.

In conclusion, the rate of odd oxygen loss is best reduced by increasing the rate coefficient for the reaction $O + O_2 + M \rightarrow O_3 + M$ within the recommended uncertainties. With the ozone deficit eliminated in this way throughout the upper stratosphere and reduced significantly in the lower mesosphere, the residual mesospheric deficit can be eliminated by increasing the rate of the reaction $OH + HO_2 \rightarrow H_2O + O_2$ by the recommended uncertainty.

5.2 Enhancement in Odd Oxygen Production

In past studies of the ozone deficit, increased O_2 photolytic cross sections have been proposed as a way of increasing the rate of odd oxygen production. *Rusch and Eckman* [1985] and *Clancy et al.* [1987] considered increased O_2 production in both the Herzberg continuum and in the Schumann-Runge bands as a remedy in the mesosphere. *Froidevaux et al.* [1989] suggested that at 30°N in May 1979, the stratospheric and lower mesospheric deficit could be reduced most significantly by increasing molecular oxygen cross sections. Similar conclusions were obtained by *Allen and Delitsky* [1991*a*], who showed that the ozone deficit could be eliminated throughout the whole altitude range monitored by ATMOS upon increasing molecular oxygen cross sections in the Schumann-Runge bands and the Herzberg continuum by 40%.

In Figure 12 we show values of the deficit calculated when odd oxygen production is increased by enhancing the O_2 cross sections in the Herzberg continuum by 30% (such increases are in accord with uncertainties given by *DeMore et al.* [1990]). The stratospheric model ozone abundances agree with observations to within 5%, corroborating the findings of *Allen and Delitsky* [1991*a*]. A residual deficit of up to 16% remains in the mesosphere. Our calculations suggest that the additional 40% increase in the Schumann-Runge cross sections advocated by Allen and Delitsky for the middle and upper mesosphere (see also *Clancy et al.* [1987]) has only a minor effect on the model ozone abundances at pressures greater than 0.4 mbar, leading to increases of less than 5%.

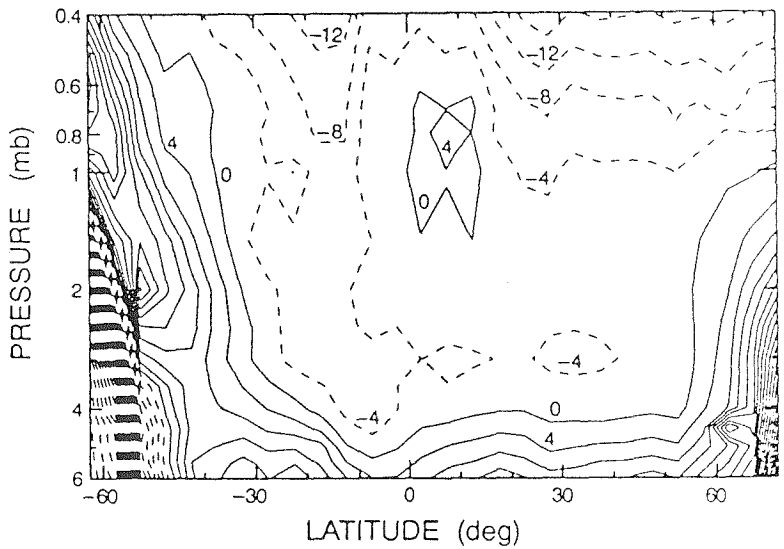

Fig. 11. Percentage difference between the ozone abundances calculated by the modified PE model and the observed LIMS abundances for May 1-7, 1979; the rate coefficient k_1 increased within the recommended uncertainties.

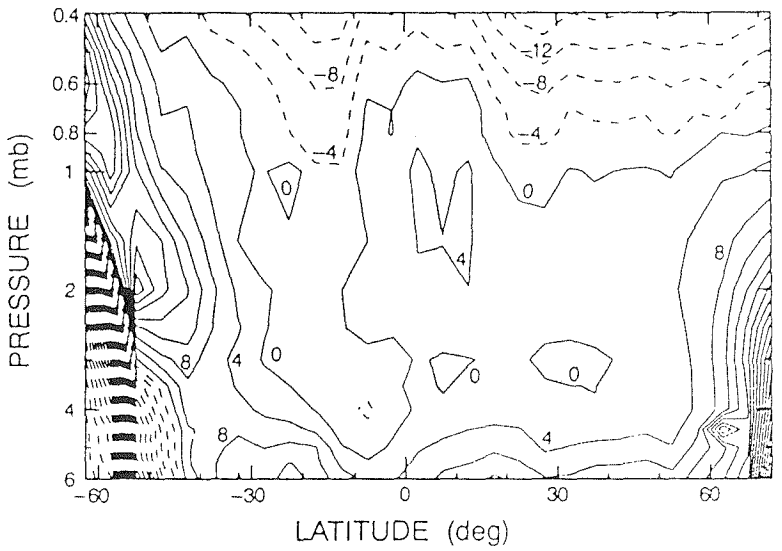

Fig. 12. Percentage difference between the ozone abundances calculated by the modified PE model and the observed LIMS abundances for May 1-7, 1979; the cross sections in the Herzberg continuum increased by 30% relative to the NASA recommendations [*DeMore et al.*, 1990].

A new source of odd oxygen has been proposed by *Slanger et al.* [1988], who reported on laboratory results which showed the autocatalytic production of ozone through photodissociation of vibrationally excited oxygen produced in the photolysis of ozone. *Tuomi et al.* [1991*b*] found that, at 30°N latitude in September, the inclusion of this mechanism for odd oxygen production in model calculations can increase the calculated ozone abundance in the upper stratosphere and lower mesosphere by ~30%, and thus largely solve the ozone deficit problem. We too will assess the viability of the Slanger et al. mechanism as a way to eliminate the calculated ozone deficit, this time on a global scale. Since many key parameters (discussed below) required to perform such an analysis have not been determined experimentally, we have followed the approximate approach of Tuomi et al. as closely as possible, for the sake of comparison with their work. Our results for 1300 LT at 45°N in May will be comparable to the Tuomi et al. calculations for noon at 30°N in September, since the zenith angles are similar in both cases.

The following photochemical scheme was proposed by Slanger et al. to account for their experimental measurements:

$$O_3 + h\nu \rightarrow O(^3P) + O_2^{\ddagger}(X^3\Sigma_g)$$

$$O_2^{\ddagger}(X^3\Sigma_g) + h\nu \rightarrow O_2(B^3\Sigma_u) \rightarrow 2O$$

$$\text{net: } O_3 \rightarrow 3O$$

where $O_2^{\ddagger}$ denotes vibrationally excited oxygen in the ground electronic state. In the above scheme, there is a net gain of two odd oxygen species (oxygen atoms). The photodissociation of highly vibrationally excited oxygen proceeds through the Schumann-Runge transitions to the strongly predissociated B state at longer wavelengths (up to 480 nm) than possible for absorption from the ground vibrational level. In the atmosphere, the excited vibrational levels of the ground electronic state are more efficient in producing odd oxygen than their populations relative to the ground vibrational level would predict, since at the longer wavelengths the local solar flux is more intense (atmospheric opacity is smaller and solar irradiances larger than at shorter wavelengths).

The rate at which odd oxygen is produced by this mechanism is equal to

$$P_s = 2 \sum_{v''=1}^{21} J_{v''}[O_2^{\ddagger}]_{v''} \tag{9}$$

where $J_{v''}$ and $[O_2^{\ddagger}]_{v''}$ are the photodissociation rate coefficient and concentration, respectively, of oxygen excited to vibrational level v″. The photodissociation rate coefficient is equal to

$$J_{v''} = \sum_{\lambda} \sum_{v'=0}^{13} \sigma(\lambda, v', v'')F(\lambda) \tag{10}$$

where $\sigma(\lambda, v', v'')$ is the cross section for the transition between level v″ and v′ at wavelength λ, $F(\lambda)$ is the actinic flux, and the summation extends over the wavelength range 176-480 nm. The cross sections were calculated by a procedure described by Slanger et al., whereas actinic fluxes were calculated using solar irradiances from *WMO* [1986] and the radiative transfer scheme of *Michelangeli et al.* [1992]. For v″ = 15, the photodissociation rates we calculated are ~20% higher than those reported by Tuomi et al. We will show below that this discrepancy is likely to have only a minor effect on our conclusions.

The concentration of $O_2^{\ddagger}$ at vibrational level v″ was calculated under the assumption that it is (1) produced by photolysis of ozone and by quenching from level v″+1 and (2) lost by quenching to level v″-1. As in the previous treatments of the Slanger et al. mechanism, we assumed that collisions with ground state oxygen molecules dominate quenching. These assumptions lead to the following steady-state expression

$$[O_2^{\ddagger}]_{v''} = \frac{\phi(v'')\, J\, [O_3] + k_{v''+1}[O_2][O_2^{\ddagger}]_{v''+1}}{k_{v''}[O_2] + J_{v''}} \tag{11}$$

where $\phi(v'')$ is the quantum efficiency for the production of level v″ by photolysis of ozone in the $O_3 \rightarrow O_2(X^3\Sigma_g) + O(^3P)$ channel (assumed equal to the distribution obtained by *Kinugawa et al.* [1990] at 226

nm), J is the photodissociation rate coefficient for ozone in this channel at wavelengths less than 300 nm, and $k_{v''}$ is the quenching rate coefficient for level v''. The latter was calculated from the expression

$$k_{v''} = P_{v''} (8\pi kT/\mu)^{1/2} \delta^2 \qquad (12)$$

where $P_{v''}$ is the quenching probability, μ is the reduced mass of two colliding oxygen molecules, and δ is the collisional diameter [*Gardiner*, 1972, p. 89]. We assume here that any activation energy which may be involved in quenching is included in $P_{v''}$. The probability is calculated from the theory of *Rapp and Englander-Golden* [1964] and *Rapp* [1965] in the way described by *Slanger et al.* [1988]. It is not clear, however, what is the appropriate value of δ to be used in this calculation. The gas kinetic values of δ for O_2 determined from viscosity and self-diffusion measurements can differ by 10% [*Hirschfelder et al.*, 1965, chapter 8]. In addition, Rapp and Englander-Golden suggested that the relevant value of δ^2 may be greater than the gas kinetic cross section due to oblique collisions. In this study, δ = 3.43 Å has been adopted. For v''=15, our peak computed value of $[O_2^{\ddagger}]$ is equal to that of Tuomi et al.

The rate of odd oxygen production due to the Slanger et al. mechanism evaluated in the above way is shown in Figure 13. Its peak value at 45°N is ~15% higher than the peak value obtained by Tuomi et. The rate is also higher than the "missing production" shown in Figure 9*b* and thus leads to an overproduction of ozone, as shown in Figure 14*a*. These results are fairly insensitive to the precise value of P_s; calculated ozone only decreases by ~4% when P_s is reduced by 20% accounting for a possible overestimate in our photodissociation rates of $O_2^{\ddagger}$ referred to above.

Clearly, in view of parameter uncertainties the above results must be regarded with caution. In particular, if the quenching rates were faster by a factor of 4, the resulting model ozone would be brought into a ~10% agreement with observations, as shown in Figure 14*b*. This increase, which obviously needs to be confirmed experimentally, could be due to the effect of oblique collisions referred to above. Also, there are indications (T. Slanger, personal communication, 1992) that molecular nitrogen may be at least as efficient as ground state molecular oxygen at quenching the very high levels of $O_2^{\ddagger}$. If this were the

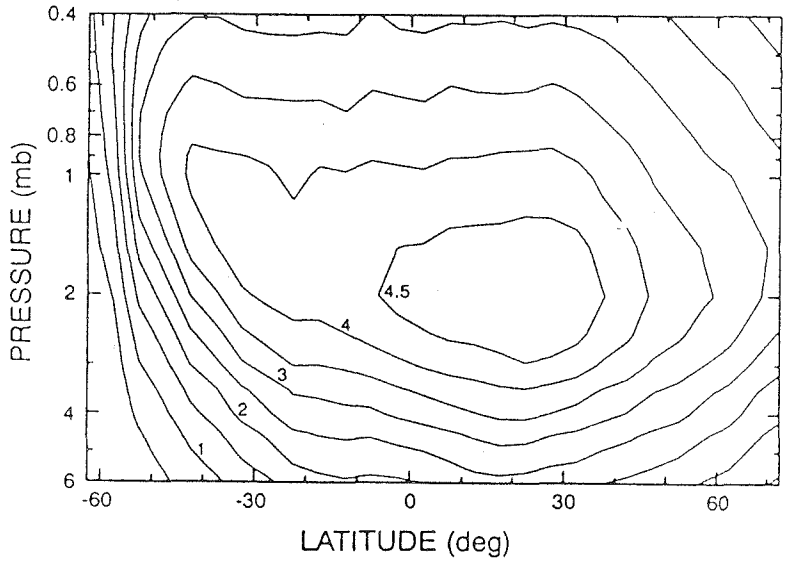

Fig. 13. Rate of odd oxygen production [10^6 molecules cm^{-3} s^{-1}] due to photolysis of vibrationally excited oxygen molecules. The collisional quenching rates for $O_2^{\ddagger}$ have been evaluated in the manner described by *Slanger et al.* [1988], and the adopted vibrational distribution of $O_2^{\ddagger}$ is from *Kinugawa et al.* [1990].

Fig. 14. *(a)* Ozone deficit (in percent) for May 1-7, 1979, calculated with the inclusion of the photolysis of vibrationally excited oxygen as described in the caption to Figure 13. *(b)* Same as Figure 14*a*, but the collisional quenching rates for $O_2^{\ddagger}$ increased by a factor of 4.

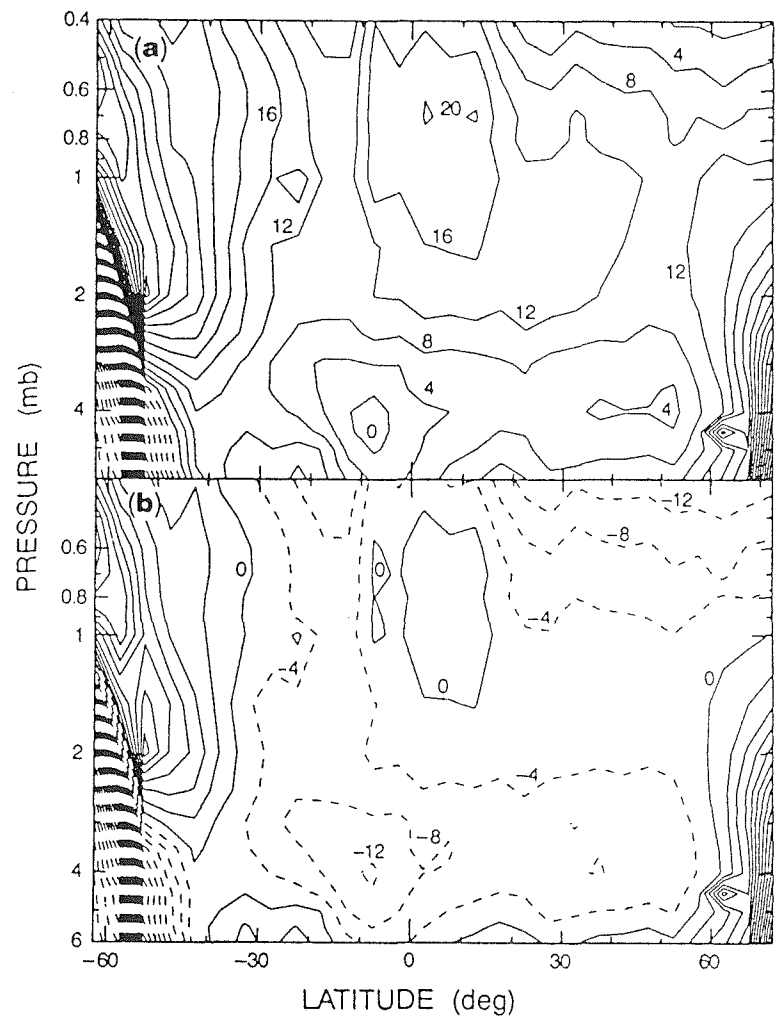

case, then a fourfold increase in the quenching rates for those levels might be related to the atmospheric $[N_2]/[O_2]$ ratio.

It must be noted that the overproduction of ozone is a strong function of the vibrational distribution $\phi(v'')$ in equation (11). Thus far, we have applied to all wavelengths the distribution at 226 nm which peaks around $v'' = 13$ [*Kinugawa et al.*, 1990]. However, the distribution at 248 nm may have a minimum at $v'' \sim 16$, with significant populations of levels $v'' > 16$ (T. Slanger, personal communication, 1991; see also *Park and Slanger* [1991]). If such a distribution is adopted at all wavelengths in the calculation of extra odd-oxygen production, then the excess ozone problem is much more severe, leading to ozone overabundances of up to 50% at the tropical stratopause. This is because levels with $v'' > 16$ are photolyzed at longer wavelengths where the opacity is smaller and the actinic flux larger. Moreover, with the vibrational-vibrational energy transfer assumed here, the high v'' levels are quenched much less efficiently than lower levels; a higher rate of odd oxygen production thus results. The degree of overproduction becomes larger towards high zenith angles in the winter mesosphere, a behavior which can be understood by a comparison between Figure 9*b* and Figure 13. At a constant mesospheric pressure level in Figure 9*b*, the missing production decreases rather sharply southwards of 20°S, with the O_x production actually exceeding loss at high southern latitudes. In constrast, in Figure 13 the term P_s, which is supposed to make up for the missing production, remains fairly constant at a given mesospheric pressure level up to at least 40°S and obviously never becomes negative. The relative insensitivity of P_s to increasing zenith angle at winter mid-latitudes is a consequence of the fact that the optical depths in the Schumann-Runge bands of vibrationally excited molecular oxygen are small, especially for high v''. The issue of optical thinness is likely to arise with any vibrational distribution which gives large populations of high vibrational levels. It needs to be examined in more detail in future studies, both experimental and observational, since, for example, it would probably not arise for a basic ozone deficit distribution like that of *Rusch and Eckman* [1985], which increases with increasing zenith angle in the lower mesosphere.

In conclusion, the rate of odd oxygen production can be increased so as to eliminate the ozone deficit in the upper stratosphere and reduce it in the lower mesosphere by either increasing the oxygen photodissociation cross sections in the Herzberg continuum by the recommended uncertainty of 30% or by

invoking the production of odd oxygen from photodissociation of vibrationally excited molecular oxygen. However, in the latter case the quenching rates for $O_2^{\ddagger}$ must be increased by a factor of 4 (or more for the alternative vibrational distribution) relative to the estimates by *Slanger et al.* [1988] in order to bring about an agreement between model ozone and LIMS observations. In both cases, the small (~10%) deficit residual in the mesosphere can be eliminated by reducing the efficiency of the HO_x catalytic cycle, most effectively by increasing the rate coefficient k_9 by the recommended uncertainty.

5.3 Results for the Week of January 1-7, 1979

Thus far we have considered the week of May 1-7, 1979, and concluded that an increased rate coefficient k_1, increased model values for oxygen cross sections in the Herzberg continuum (with a small contribution from increased cross sections in the Schumann-Runge bands), and the inclusion of the Slanger et al. mechanism (with the quenching rates increased by a factor of at least 4 over the "standard" values), may all provide a solution to the ozone deficit problem in the upper stratosphere. We will now examine how general are these solutions by considering another week, with physical conditions different from May, for which LIMS data are available. The global ozone deficit in the week of January 1-7, 1979, calculated with input parameters obtained in the manner described in section 3, is shown in Figure 15*a*. In the stratosphere, the calculated deficit is slightly larger than in May; it peaks at around 40 km near the subsolar point. As in May, the deficit increases with altitude into the mesosphere and exhibits a tropical minimum and mid-latitude maxima at a given pressure level in the lower mesosphere; these features again correlate with the mesospheric distribution of water vapor (not shown). The mesospheric deficit is ~4% smaller than in May. The overabundance of ozone at the extreme summer latitudes is probably an artifact of the average zenith angles adopted in this study; in a given latitude bin the zenith angles at the time of LIMS observations vary between 45° and 90° in the course of a week.

The three model modifications discussed for May solve the ozone problem at the 10% level in January as well, as shown in Figures (15*b*)-(15*d*). As in May, in all three cases the residual mesopheric deficit can be eliminated by reducing the efficiency of the HO_x cycle within the recommended uncertainties, most effectively by increasing the rate coefficient for the reaction $OH + HO_2 \rightarrow H_2O + O_2$.

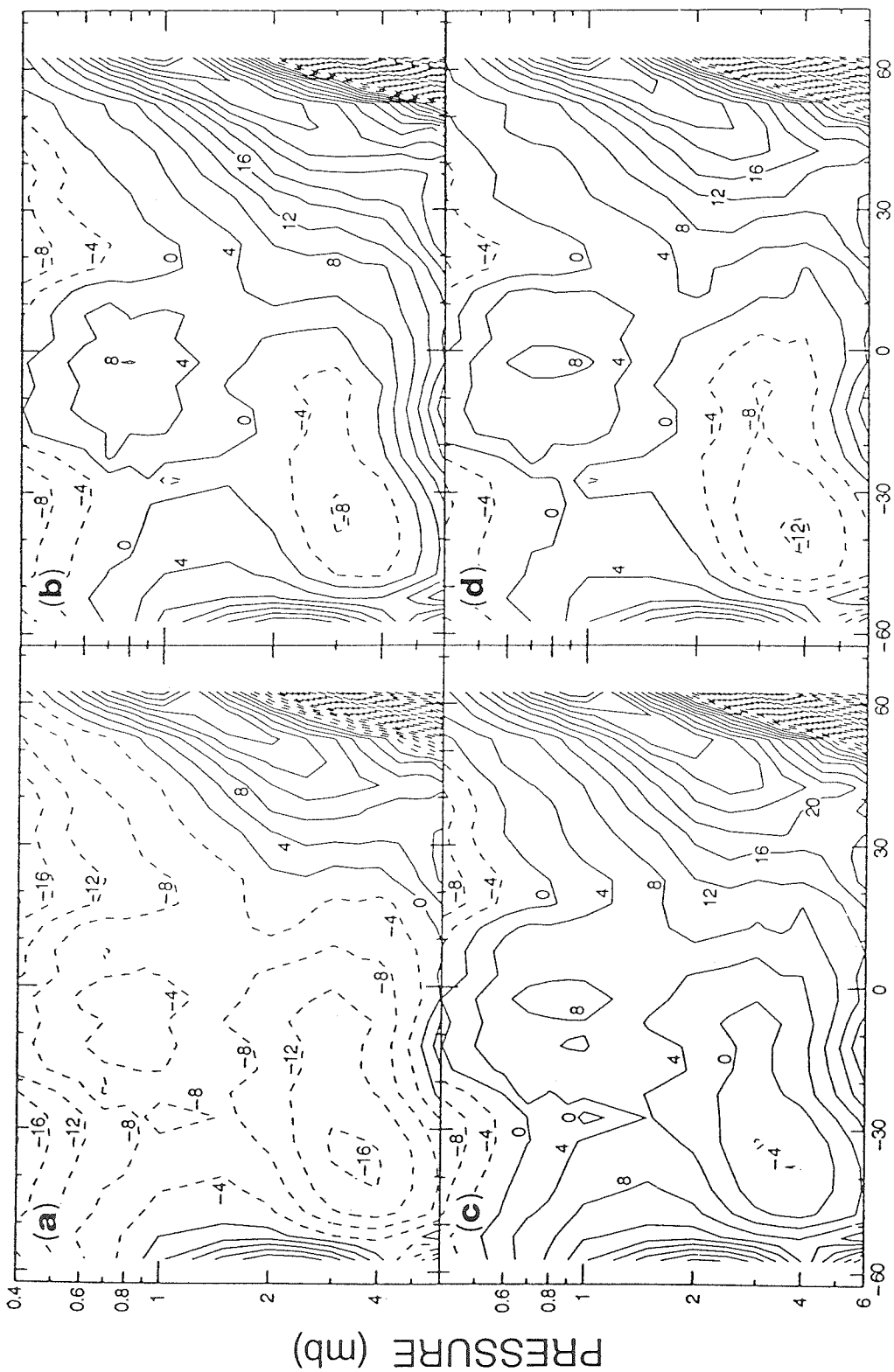

Fig. 15. Model results for the week of January 1-7, 1979. *(a)* Ozone deficit (in percent) computed with the standard model. *(b)-(d)* Ozone deficit computed with the rate coefficient k_1 increased, Herzberg continuum cross sections increased, and the Slanger et al. mechanism included with increased quenching rates, respectively (see the captions to Figures 11, 12, and 14*b*, respectively).

6. Discussion and Conclusions

In this paper, we have used the global measurements of temperature, ozone, water vapor, and nitrogen dioxide acquired by the Limb Infrared Monitor of the Stratosphere (LIMS), in conjunction with a precomputed distribution of chlorine monoxide, to test the balance between odd oxygen production and loss in the upper stratosphere and lower mesosphere. We report results from a photochemical equilibrium model which, by a comparison with the results from a fully time-dependent model, is shown to be valid at pressures less than 4 mbar at low and midlatitudes and at progressively lower pressures at higher winter latitudes.

Using the most recent NASA recommendations for the kinetic and photolytic input parameters, we find that the calculated ozone concentrations are systematically lower than observations, thus a global "ozone deficit." This suggests that there is a real problem in current model simulations of upper stratospheric ozone, contrary to the results of some other recent analyses. Mainly as a result of a low ClO distribution adopted in the present study, the ozone deficit is significantly smaller than previous LIMS-based studies have indicated, but is in agreement with the ATMOS-based studies (which had the benefit of both a direct measurement of the total reactive chlorine content and of observational constraints on the reactive chlorine partitioning). The deficit increases with altitude and, at a given pressure level in the lower mesophere, shows a tropical minimum and two mid-latitude maxima which correlate with the minimum and the maxima, respectively, in water vapor distribution. Other than these features and their apparent correlation with H_2O, the deficit exhibits little latitudinal variation at a given pressure level.

The ozone model-observations discrepancy has important implications beyond photochemistry, notably for calculations of the diabatic circulation in the middle atmosphere. For example, using the radiative transfer code developed by *Crisp* [1986, 1990] and the streamfunction code developed by *Santee* [1993], we find that reducing ozone abundances (relative to their climatological values) by amounts similar to those shown in Figure 9*a* leads to increases in the pole-to-pole meridional velocity by ~40% and decreases in the upward vertical velocity by ~20% in the late-spring upper stratosphere. This sensitivity of our diabatic circulation to a nonuniform reduction in the ozone abundances is in contrast to the results of *Rosenfield et*

al. [1987], who reported no significant effect from a uniform 20% reduction in $[O_3]$ between 40 and 55 km. Clearly, more studies are needed to gain a better understanding of the role an accurate representation of ozone photochemistry may play in models in which radiation, dynamics, and chemistry are coupled.

Since the deficit we calculate shows little latitudinal variation, it is not easy to disentangle the effects of the uncertainties in the kinetic rate coefficients from those in the photolytic rate coefficients in producing the discrepancy between the model and measurements. There are several processes, any one of which if modified within known uncertainties will eliminate the deficit over a large range of latitudes and altitudes. In particular, either a reduction in the odd oxygen loss as a result of a decreased $[O]/[O_3]$ ratio (brought about by increasing the rate coefficient for the reaction $O + O_2 + M \rightarrow O_3 + M$) or an increase in the odd-oxygen production due to increased photolysis of molecular oxygen (either in the ground- or vibrationally excited states) leads to the elimination of the deficit in the latitude pressure domain of this study. With our model adjusted in any of these ways, the calculated ozone distribution agrees with stratospheric LIMS observations to within 10%, except at high winter latitudes where photochemical equilibrium breaks down. A residual deficit in the lower mesosphere can be eliminated by reducing the efficiency of the HO_x catalytic cycle within the recommended kinetic uncertainties (with the greatest contribution from an increase in the rate coefficient for the reaction $OH + HO_2 \rightarrow H_2O + O_2$). In addition, any of these solutions are valid for both May 1-7 and January 1-7, 1979 periods, which indicates their general value.

An increase in the rate coefficient for atomic oxygen recombination (k_1) and the resulting decrease in [O] would decrease the rate of odd oxygen chemical loss throughout the middle atmosphere. However, its effect on the partitioning between odd hydrogen, odd nitrogen, and odd chlorine species in the middle and lower stratosphere is minimal (for the partitioning expressions, see e.g., *Allen and Delitsky* [1991*b*, equation (17)], *Allen and Delitsky,* [1990, equation (6)], and *Froidevaux et al.* [1985, equation (3)], respectively). This is because, for those altitudes in the equations just cited, the terms involving [O] are much smaller than some other term. Changes in [O] are important for the odd hydrogen and odd nitrogen partitioning in the altitude range studied in the present work and this effect is accounted for in our PE calculations.

The 30% uncertainty in the Herzberg continuum cross sections quoted by *DeMore et al.* [1990] reflects the discrepancies between laboratory measurements performed prior to and after 1980, as well as between direct stratospheric measurements from which the cross sections have been inferred. The direct measurements, due to their large uncertainties, do not yet differentiate between the various laboratory determinations (see discussion in *Allen and Delistky* [1991*a*]). However, the latest laboratory results [*Yoshino et al.*, 1988] favor the low values. If this were conclusively confirmed by direct atmospheric measurements, then another source of odd oxygen, with a latitude and altitude behavior similar to that of enhanced Herzberg continuum cross sections, might need to be identified to solve the model observation discrepancy.

Clearly, more studies are required before we can accept any of the above solutions (or their combination) as satisfactory. A remeasurement of the currently recommended values for the kinetic rate coefficients involved in the O_x and HO_x cycles, more accurate atmospheric measurements of the oxygen cross sections in the Herzberg continuum, and direct atmospheric measurements of atomic oxygen abundances, would certainly be most helpful. In addition, any other new source of odd oxygen with the same quantitative latitude- and pressure-varying contribution as that resulting from the increased Herzberg continuum absorption, would equally well help to eliminate the ozone deficit in the pressure range studied in this paper. One possibility we have discussed is the photodissociation of vibrationally excited oxygen, but with the collisional quenching increased by a factor of 4 relative to the estimates presented by *Slanger et al.* [1988]. Laboratory measurements of the various physical parameters involved in this mechanism, in particular the quenching rates and the vibrational distribution of the $O_2^{\ddagger}$ molecules produced in the photolysis of ozone at various wavelengths, are essential. Of equal importance is the need for a clarification of the global distribution of ClO. The measurements of [ClO] by the Microwave Limb Sounder onboard the recently launched Upper Atmosphere Research Satellite may prove or disprove the low ClO distribution utilized here. Finally, in view of the correlation between the calculated ozone deficit and the water vapor distribution in the lower mesophere, it is important to establish the validity of the adopted HO_x chemistry. In particular, our results indicate that the mesopheric ozone deficit might be eliminated without invoking any other model modifications if the calculated abundances of HO_2 were reduced by a factor of 2 (such a

reduction is very hard to achieve within the framework of the currently adopted chemistry). A useful laboratory experiment in this regard would be one in which oxygen with a trace amount of H_2O was photolysed and the resulting HO_2 concentrations checked against theoretical predictions.

Acknowledgments. We thank Y. L. Yung for useful discussions, E. E. Remsberg for information regarding the LIMS mesospheric H_2O distribution, H. Yang and K. K. Tung for making the ClO distribution available to us, and R. Tuomi for providing us with details of their calculations. T. Slanger has kindly shared with us the results of his ongoing experiments prior to publication. D. Crisp and M. Santee are thanked for enabling us to compute the diabatic circulation. This work was supported by NASA grant NAGW 1538. Contribution number 5076 from the Division of Geological and Planetary Sciences, California Institute of Technology, Pasadena.

REFERENCES

Allen, M., and M. L. Delitsky, Stratospheric NO, NO_2, and N_2O_5: A comparison of model results with Spacelab 3 Atmospheric Trace Molecule Spectroscopy (ATMOS) measurements, *J. Geophys. Res., 95,* 14,077-14,082, 1990.

Allen, M., and M. L. Delitsky, A test of odd-oxygen photochemistry using Spacelab 3 atmospheric molecule spectroscopy observations, *J. Geophys. Res., 96,* 12,883-12,891, 1991*a*.

Allen, M., and M. L. Delitsky, Inferring the abundances of ClO and HO_2 from Spacelab 3 atmospheric trace molecule spectroscopy observations, *J. Geophys. Res., 96,* 2913-2919, 1991*b*.

Allen, M., J. I. Lunine, and Y. L. Yung, The vertical distribution of ozone in the mesosphere and lower thermosphere, *J. Geophys. Res., 89,* 4841-4872, 1984.

Brune, W. H., E. M. Weinstock, M. J. Schwab, R. M. Stimpfle, and J. G. Anderson, Stratospheric ClO: In-situ detection with a new approach, *Geophys. Res. Lett., 12,* 441-444, 1985.

Callis, L. B., M. Natarajan, R. E. Bougher, J. M. Russell III, and J. D. Lambeth, Stratospheric photochemical studies using NIMBUS 7 data, 2. Development of inferred trace specie distributions, *J. Geophys. Res., 91,* 1167-1197, 1986.

Clancy, R. T., D. W. Rusch, R. J. Thomas, M. Allen, and R. S. Eckman, Model ozone photochemistry on the basis of Solar Mesosphere Explorer mesospheric observations, *J. Geophys. Res., 92,* 3067-3080, 1987.

Crisp, D., Radiative forcing of the Venus mesosphere. I. Solar fluxes and heating rates, *Icarus, 67,* 484-514, 1986.

Crisp, D., Infrared radiative transfer in the dust-free martian atmosphere, *J. Geophys. Res., 95,* 14,577-14,588, 1990.

Crutzen, P. J., and U. Schmailzl, Chemical budgets of the stratosphere, *Planet. Space Sci., 31,* 1009-1032, 1983.

DeMore, W. B., S. P. Sander, D. M. Golden, M. J. Molina, R. F. Hampson, M. J. Kurylo, C. J. Howard, A. R. Ravishankara, Chemical Kinetics and Photochemical Data for Use in Stratospheric Modeling, *JPL Publ., JPL 90-1,* 1990.

Froidevaux, L., M. Allen, and Y. L. Yung, A critical analysis of ClO and O_3 in the mid-latitude stratosphere, *J. Geophys. Res., 90,* 12,999-13,029, 1985.

Froidevaux, L., M. Allen, S. Berman, and A. Daughton, The mean ozone profile and its temperature sensitivity in the upper stratosphere and lower mesosphere: An analysis of LIMS observations, *J. Geophys. Res., 94,* 6389-6417, 1989.

Garcia, R. R., and S. Solomon, The effect of breaking gravity waves on the dynamics and chemical composition of the mesosphere and lower thermosphere, *J. Geophys. Res., 90,* 3850-3868, 1985.

Gardiner, W. C., *Rates and Mechanisms of Chemical Reactions,* W. A. Benjamin, Menlo Park, Calif., 1972.

Gille, J. C., and J. M. Russell III, The Limb Infrared Monitor of the Stratosphere: Experiment description, performance, and results, *J. Geophys. Res., 89,* 5125-5140, 1984.

Hirschfelder, J. O., C. F. Curtiss, and R. B. Bird, *Molecular Theory of Gases and Liquids,* John Wiley & Sons, New York, 1965.

Jackman, C. H., R. S. Stolarski, and J. A. Kaye, Two-dimensional monthly average ozone balance from Limb Infrared Monitor of the Stratosphere and Stratospheric and Mesospheric Sounder data, *J. Geophys. Res., 91,* 1103-1116, 1986.

Kerridge, B. J., and E. E. Remsberg, Evidence from the Limb Infrared Monitor of the Stratosphere for nonlocal thermodynamic equilibrium in the ν_2 mode of mesospheric water vapour and the ν_3 mode of stratospheric nitrogen dioxide, *J. Geophys. Res., 94,* 16,323-16,342, 1989.

Kinugawa, T., T. Sato, T. Arikawa, Y. Matsumi, and M. Kawasaki, Formation of $O(^3P_j)$ photofragments from the Hartley band photodissociation of ozone at 226 nm, *J. Chem. Phys., 93,* 3289-3294, 1990.

Labitzke, K., J. J. Barnett, and B. Edwards (Eds.), *Atmospheric Structure and its Variation in the Region 20 to 120 km: Draft of a New Reference Middle Atmosphere,* Handbook for MAP, vol. 16,

International Council of Scientific Unions Scientific Committee on Solar-Terrestrial Physics, Paris, 1985.

Madronich, S., Photodissociation in the atmosphere, 1, Actinic flux and the effects of close-up ground reflections and clouds, *J. Geophys. Res., 92,* 9740-9752, 1987.

McElroy, M. B., and R. J. Salawitch, Changing composition of the global stratosphere, *Science, 243,* 763-770, 1989*a*.

McElroy, M. B., and R. J. Salawitch, Stratospheric ozone: impact of human activity, *Planet. Space. Sci., 37,* 1653-1672, 1989*b*.

Michelangeli, D. V., M. Allen, Y. L. Yung, R.-L. Shia, D. Crisp, and J. Eluszkiewicz, Enhancement of atmospheric radiation by an aerosol layer, *J. Geophys. Res., 97,* 865-874, 1992.

Natarajan, M., and L. B. Callis, Examination of stratospheric ozone photochemistry in light of recent data, *Geophys. Res. Lett., 16,* 473-476, 1989.

Natarajan, M., and L. B. Callis, Stratospheric photochemical studies with Atmospheric Trace Molecule Spectroscopy (ATMOS) measurements, *J. Geophys. Res., 96,* 9361-9370, 1991.

Natarajan, M., L. B. Callis, R. E. Bougher, J. M. Russell III, and J. D. Lambeth, Stratospheric photochemical studies using Nimbus 7 data, 1, Ozone photochemistry, *J. Geophys. Res., 91,* 1153-1166, 1986.

Park, H., and T. G. Slanger, $O_2(X)$ vibrational distribution from 248 nm photodissociation of O_3, *EOS, Trans. AGU, 72,* 99, 1991.

Raper, O. F., C. B. Farmer, R. Zander, and J. H. Park, Infrared spectroscopic measurements of halogenated sink and reservoir gases in the stratosphere with the ATMOS instrument, *J. Geophys. Res., 92,* 9851-9858, 1987.

Rapp, D., Interchange of vibrational energy between molecules in collisions, *J. Chem. Phys., 43,* 316-317, 1965.

Rapp, D., and P. Englander-Golden, Resonant and near-resonant vibrational-vibrational energy transfer between molecules in collisions, *J. Chem. Phys., 40,* 573-575, 1964 (erratum see: *J. Chem. Phys., 40,* 3120-3121, 1964).

Remsberg, E. E., J. M. Russell III, J. C. Gille, L. L. Gordley, P. L. Bailey, W. G. Planet, and J. E. Harries, The validation of NIMBUS 7 LIMS measurements of ozone, *J. Geophys. Res., 89,* 5161-5178, 1984.

Rosenfield, J. E., M. R. Schoberl, and M. A. Geller, A computation of the stratospheric diabatic circulation using an accurate radiative transfer model, *J. Atmos. Sci., 44,* 859-876, 1987.

Rusch, D. W., and R. S. Eckman, Implications of the comparison of ozone abundances measured by the solar mesosphere explorer to model calculations, *J. Geophys. Res., 90,* 12,991-12,998, 1985.

Russell, J. M., III, J. C. Gille, E. E. Remsberg. L. L. Gordley, P. L. Bailey, S. R. Drayson, H. Fisher, A. Girard, J. E. Harries, and W. F. J. Evans, Validation of nitrogen dioxide results measured by the Limb Infrared Monitor of the Stratosphere (LIMS) experiment on NIMBUS 7, *J. Geophys. Res., 89,* 5099-5107, 1984.

Russell, J. M., III, C. B. Farmer, C. P. Rinsland, R. Zander, L. Froidevaux, G. C. Toon, B. Gao, J. Shaw, and M. Gunson, Measurements of odd nitrogen compounds in the stratosphere by the ATMOS experiment on Spacelab 3, *J. Geophys. Res., 93,* 1718-1736, 1988.

Santee, M. L., The thermal structure, dust loading, and meridional transport in the martian atmosphere during late southern summer, Ph. D. thesis, California Institute of Technology, Pasadena, 1993.

Slanger, T. G., L. E. Jusinski, G. Black, and G. E. Gadd, A new laboratory source of ozone and its potential atmospheric implications, *Science, 241,* 945-950, 1988.

Solomon, S., and R. R. Garcia, On the distributions of long-lived tracers and chlorine species in the middle atmosphere, *J. Geophys. Res., 89,* 11,633-11,644, 1984.

Solomon, S., J. T. Kiehl, B. J. Kerridge, E. E. Remsberg, and J. M. Russell III, Evidence for nonlocal thermodynamic equilibrium in the ν_3 mode of mesospheric ozone, *J. Geophys. Res., 91,* 9865-9876, 1986.

Tuomi, R., J. A. Pyle, C. R. Webster, and R. D. May, Theoretical interpretation of N_2O_5 measurements, *Geophys. Res. Lett., 18,* 1213-1216, 1991*a*.

Tuomi, R., B. J. Kerridge, and J. A. Pyle, Highly vibrationally excited oxygen as a potential source of ozone in the upper stratosphere and mesosphere, *Nature, 351,* 217-219, 1991*b*.

Waters, J. W., R. A. Stachnik, J. C. Hardy, and R. F. Jarnot, ClO and O_3 stratospheric profiles: Balloon microwave measurements, *Geophys. Res. Lett., 15,* 780-783, 1988.

Webster, C. R., R. D. May, R. Toumi, and J. A. Pyle, Active nitrogen partitioning and the nighttime formation of N_2O_5 in the stratosphere: Simultaneous in situ measurements of NO, NO_2, HNO_3, O_3, and N_2O using the BLISS diode laser spectrometer, *J. Geophys. Res., 95,* 13,851-13,866, 1990.

Weisenstein, D. K., M. K. W. Ko, and N.-D. Sze, The chlorine budget of the present-day atmosphere, *J. Geophys. Res., 97,* 2547-2559, 1992.

World Meteorological Organization, Atmospheric Ozone 1985, *WMO Rep. 16,* Global Ozone Res. and Monit. Proj., Geneva, Switzerland, 1986.

Yang, H., E. Olaguer, and K. K. Tung, Simulation of the present-day atmospheric ozone, odd nitrogen, chlorine and other species using a coupled 2-D model in isentropic coordinates, *J. Atmos. Sci., 48,* 442-471, 1991.

Yoshino, K., A. S.-C. Cheung, J. R. Esmond, W. H. Parkinson, D. E. Freeman, S. L. Guberman, A. Jenouvrier, B. Coquart, and M. F. Merienne, Improved absorption cross-sections of oxygen in the wavelength region 205-240 nm of the Herzberg continuum, *Planet. Space Sci., 36,* 1469-1475, 1988.

PAPER III

The Diabatic Circulation in the Stratosphere as Diagnosed from Microwave Limb Sounder Data

Janusz Eluszkiewicz

Division of Geological and Planetary Sciences,

California Institute of Technology, Pasadena, CA 91125

ABSTRACT

Results for the diabatic circulation in the stratosphere and lower mesosphere between November 1991 and November 1992 are reported. This circulation is diagnosed from the measurements of temperature and ozone acquired by the Microwave Limb Sounder onboard the Upper Atmosphere Research Satellite (UARS). An accurate but fast radiative transfer code and a streamfunction code that avoids the problem of global imbalance in the net diabatic heating rates, are used in the calculations. The computed vertical velocities undergo a semiannual oscillation (SAO) around the tropical stratopause, with the region of downward velocities reaching maximum spatial extent ~1 month before the equinox. This behavior is related to the semiannual oscillation in temperature and ozone and mimics that obtained by *Hitchman and Leovy* [1986] in their analysis of the October 1978 - May 1979 period. An analysis of wave forcing per unit mass, calculated as the residual in the zonal momentum equation, suggests that during the solstices, the tropical SAO is forced by meridional advection of easterly angular momentum, driven by extratropical Rossby wave absorption, whereas in-situ wave absorption prevails at other seasons. The expected lifetime of UARS should permit an extension of the present analysis to several SAO cycles.

1. INTRODUCTION

The transport circulation in the middle atmosphere determines the distribution of long-lived chemical constituents, such as odd oxygen, methane, and nitrous oxide. Since the three-dimensional velocity field cannot be measured directly, one has to rely on theoretical calculations to obtain an estimate of the circulation. The so-called diabatic circulation provides a first approximation to the transport circulation under most stratospheric conditions [*Tung*, 1982; *Plumb and Mahlman*, 1987]. *Garcia and Solomon* [1983] were the first to use the diabatic circulation in a chemical model. In a two-dimensional, zonally averaged approach, the meridional and vertical components of the diabatic circulation can be found by solving the thermodynamic and continuity equations [see e.g., *Shine*, 1989]. This is most conveniently done using the so-called Transformed Eulerian Mean (TEM) equations [*Andrews et al.*, 1987, p. 127]. A major advantage of the TEM formalism is the fact that the eddy heating term in the thermodynamic equation can be neglected under quasi-geostrophic conditions. Moreover, the TEM velocity components are good approximations to the Lagrangian mean circulation which is the relevant quantity for transport. A crucial quantity entering the calculation of the diabatic circulation is the net diabatic heating rate, which is equal to the sum of diabatic heating and diabatic cooling. The two components of the circulation give rise to meridional advection and adiabatic cooling (heating) which balances the net diabatic heating (cooling). In the middle atmosphere, the main source of diabatic heating is the absorption of solar radiation by ozone, whereas cooling is mainly due to the emission of infrared radiation by carbon dioxide, water vapor, and ozone. In addition, a number of other gases (nitrogen dioxide, nitrous oxide, methane) provide minor contributions to heating and cooling. These contributions are important in the lower and middle stratosphere, but will be neglected in the present study, which focuses on the upper stratosphere and lower mesosphere.

The diabatic heating rates and associated diabatic circulation have been calculated by a number of researchers, starting with *Murgatroyd and Singleton* [1961]. The past studies relied either on climatological fields of temperature and ozone [*Rosenfield et al.*, 1987; *Callis et al.*, 1987; *Shine*, 1989; *Marks*, 1989] or

on the seven month period of data obtained by the Limb Infrared Monitor of the Stratosphere (LIMS) instrument between October 1978 and May 1979 [*Solomon et al.*, 1986; *Gille et al.*, 1987]. These studies have contributed greatly to our understanding of the circulation. In particular, they have confirmed the existence of the so-called Brewer-Dobson circulation, with raising motions in the tropics and descending motions over the poles. However, there is still a great need to improve the knowledge of the diabatic circulation. In particular, the climatological studies, while providing estimates of the circulation over a full seasonal cycle, are characterized by rather coarse vertical resolution (~20 km) in and above the upper stratosphere. On the other hand, the LIMS-based studies, which are characterized by much better vertical resolution (~8 km), are incapable of investigating a full seasonal cycle (they are restricted to the 7-month operational period of LIMS).

The advent of the Upper Atmosphere Research Satellite (UARS) offers an unprecedented opportunity to alleviate both of the above limitations. The measurements of temperature and constituent concentrations by the UARS instruments are characterized by high vertical resolution (usually on the order of 5 km or less), while the expected lifetime of UARS should permit the investigation of several seasonal cycles. At this time, UARS has been operational for more than one year, more than doubling the operational period of LIMS. In this study, the diabatic circulation in the stratosphere and lower mesosphere is diagnosed using measurements acquired by the Microwave Limb Sounder (MLS) instrument onboard UARS. This instrument has been built at the Jet Propulsion Laboratory, with J. Waters as the Principal Investigator. In future studies, our results can be compared to those obtained using temperature and constituent data from other UARS instruments, thus further enhancing the confidence one can place on the calculated diabatic circulation.

The organization of this paper is as follows. In section 2, the input fields and the radiative transfer code used in the calculations of diabatic heating rates are briefly described. In section 3, the results for the first year of UARS are presented. The paper concludes in section 4 with a summary and a road map for future investigations.

2. Diabatic Heating Rates

The fields of temperature and ozone used in this paper for the calculation of the diabatic heating rates correspond to the Version 331 and 400 of the MLS inversion algorithm for the times before and after June, 1992, respectively. These data must be considered preliminary, since their validation by comparison with other UARS instruments and other spacecraft, airborne, and ground-based measurements is continuing. In addition, it is expected that future versions of the retrieval algorithms will lead to improved results, especially at high altitudes. In order to account for the asynchronous nature of the UARS data (i.e., the incomplete spatial and temporal sampling) and the 57° inclination of the UARS orbit, these fields have been asynoptically mapped and their zonal averages are used in the calculations. The mapping has been accomplished by means of the Fast Fourier algorithm described by *Salby* [1982] and *Lait and Stanford* [1988] and implemented by L. Elson (manuscript in preparation). The inclination of the orbit also restricts the latitudinal coverage of MLS and other UARS measurements. Since the MLS instrument looks at the atmosphere in a direction perpendicular to the orbit track, the latitudinal coverage at any time extends to about 80° latitude in one hemisphere, but to only ~34° in the other hemisphere. Approximately once a month, the spacecraft is rotated (in the so-called yaw maneuver) by 180° in its track, at which point the latitudinal coverage is reversed between the two hemispheres. In order to obtain global fields necessary for a proper introduction of the boundary conditions, bi-weekly (or nearly so) averages corresponding to periods centered around the yaw times are selected for the calculations. The fields poleward of 79°S and 79°N are obtained by extrapolation. In the period November 1991 - November 1992, ten yaw maneuvers have been performed. However, two of the yaw periods (in May and June) could not be investigated as a result of poor data quality and data gaps, respectively, and thus only eight periods of data, given in the captions to Figures 1-8, are used in the calculations. The heating calculations extend from the ground to 0.1 mbar. They are performed on a grid with 35 points equally spaced in log(pressure) between 0.1 and 650 mbar, 8 points equally spaced in pressure between 650 mbar and the ground, and two additional points at 825 and 875 mbar.

2.1 Solar Heating

The principal source of diabatic heating is the absorption of solar ultraviolet and visible radiation by ozone, with a minor contribution from the absorption by molecular oxygen. In addition, the absorption of near-infrared radiation by carbon dioxide and water vapor and of infrared radiation by ozone also contribute to heating. The infrared contributions are described in section 2.2.

The MLS instrument measures ozone concentrations using microwave emission at 205 GHz. The radiance measurements are inverted by means of a sequential estimation algorithm developed by the MLS team (L. Froidevaux, personal communication) and yield ozone abundances at pressures less than 100 mbar. Between 100 and 464 mbar, the ozone abundances are constrained to values obtained from the two-dimensional model of Lawrence Livermore National Laboratory. At lower altitudes, ozone concentrations have been set to the 464-mbar value. This seems to be a reasonable procedure, for three reasons: (1) the main focus of the present study is on the upper stratosphere and lower mesosphere, (2) lower tropospheric ozone abundances are more than one order of magnitude lower than peak stratospheric concentrations, and (3) global measurements of tropospheric ozone are not available. A test calculation for January 1992 (analogous to that presented in Figure 2 below), in which ozone abundances at pressures greater than 464 mbar were set to zero, produced less than 5% changes in the computed diabatic velocities (except in some regions of near-zero velocities, particularly in the lower stratosphere).

The solar heating rates are computed by means of a delta-Eddington/adding code developed by *Crisp* [1986]. A Lambertian surface with albedo 0.3 is assumed. Despite enhanced aerosol concentrations in the stratosphere caused by the eruption of Mt. Pinatubo, the presence of aerosols is ignored (they could, however, be included in future studies using the Crisp code). There exists theoretical evidence that the effect of Mt. Pinatubo aerosols on the stratospheric circulation is small, due to a cancellation effect [*Kinne et al.*, 1992]. The essence of this argument is that the main effect of increased aerosol abundances is to enhance the absorption of upwelling infrared radiation from the troposphere. This causes more vigorous vertical advection, which brings in ozone-poor air into the middle stratosphere, thus causing a decrease in the solar heating which balances the increase in the infrared heating. The neglect of aerosols in the present

study has been prompted by the desire to obtain a database of heating rates for future reference and the difficulty in obtaining global estimates of aerosol properties and abundances. As aerosol measurements from other UARS instruments become available, they could be included in the calculations. A sample calculation, in which climatological cloud abundances were assumed in the troposphere, showed a negligible effect on the heating rates at pressures less than ~10 mbar. I expect that the same will be true when aerosols in the lower stratosphere are included.

2.2 Infrared Cooling

The principal mechanism of radiative cooling is the transfer of radiation in the 15-μm band of carbon dioxide, for which a mixing ratio of 330 parts per million by volume (ppmv) is assumed. In addition, minor contributions are provided by ozone. Water vapor is neglected in the present study, but preliminary results using MLS water vapor measurements show that this omission has a very small effect on the circulation at pressures less than ~10 mbar. The infrared radiative transfer is strongly dependent on temperature, of course. Based on preliminary validation studies, it is presently believed that temperature retrievals are reliable at pressures greater than 0.4 and 0.2 mbar for Versions 331 and 400, respectively (E. Fishbein, personal communication). At pressures greater than 46 mbar, temperatures provided by the National Meteorological Center (NMC) are utilized, since the O_2 line used for pressure and temperature retrievals becomes saturated.

A quasi-random code developed by *Crisp* [1990] is used in the infrared calculations. This code utilizes the Voigt line profile and line parameters obtained from the HITRAN database [*Rothman et al.*, 1987]. By treating line positions as statistically independent within narrow (5 cm^{-1} wide) spectral intervals, the code accounts for the spectral overlap between different lines. Its high accuracy has been demonstrated by comparison with line-by-line calculations [*Crisp*, 1989 and manuscript in preparation]. The principal limitation of the code is its inability to handle simultaneous multiple scattering and non-grey absorption, which may be important in the presence of stratospheric aerosols. This limitation is not important for the present study, where clear-sky conditions are assumed.

3. Diabatic Circulation

The net diabatic heating rates are obtained as the sum of solar heating and infrared cooling rates, calculated in the manner described in section 2. Given the net heating rates, the vertical and meridional components of the diabatic circulation are computed from the TEM thermodynamic and continuity equations (with the temperature tendency and the eddy heating terms in the thermodynamic equation neglected). These equations are solved by means of a numerical approach proposed by R.-L. Shia (as coded by *Santee* [1993]), in which they are combined into one streamfunction equation and the latter is differentiated with respect to latitude, thereby introducing boundary conditions at both poles naturally. In doing so, the scheme avoids numerical instabilities associated with integrating the undifferentiated streamfunction equation from pole to pole. In addition, a major advantage of this approach is that it avoids the problem of any global imbalance between heating and cooling rates. This problem has been shown to have serious consequences for the resulting diabatic circulation [*Shine*, 1989]. It must be noted, however, that the problem of any errors in the meridional gradients of the net heating rates is not alleviated by the present approach. The calculations are performed on a grid spaced 5° in latitude and 2 km in log-pressure altitude. No-flow boundary conditions are applied at 0.1 mbar, at the ground, and at the poles. Since the computed circulation is very small at 100 mbar, applying the rigid lid there instead of at the ground, would have a negligible effect on the results. The results are only shown for the region between 100 and 0.4-0.2 mbar, with the upper boundary being determined by the quality of temperature data (see section 2.2).

In addition to the diabatic circulation, the zonally averaged zonal velocity at latitudes higher than 5° is computed using the gradient wind relationship and the geopotential fields computed from MLS temperatures and the 100-mbar reference level obtained from the National Meteorological Center. The zonal wind at the equator is obtained by interpolation (as was done by *Hitchman and Leovy* [1986]). Given the three TEM velocity components, it is possible to calculate the forcing of the circulation as a residual in the zonal momentum equation [*Hartmann*, 1976; *Shine*, 1989]. This forcing is the sum of contributions from planetary and small scale waves. It is thought that the former dominate in the stratosphere, but their

contribution (the divergence of the Eliasen-Palm flux) cannot be separately determined in a zonally-averaged approach.

Figures 1 through 8 show the computed distributions of zonally averaged gradient wind, meridional and vertical components of the diabatic circulation, and wave forcing per unit mass. The time derivative of gradient wind (approximated as a finite difference) and thus the forcing is only computed between 30°S and 30°N, which is the region of overlap between the south- and north-looking yaw states. Future studies may explore alternative ways of computing this derivative (e.g., directly from the Fourier components obtained via Elson's asynoptic FFT mapping) and thus extend the latitudinal coverage of the forcing. The present approach permits examination of the 30°S - 30°N region.

Several features are evident in Figures 1-8. The northern hemisphere westerlies are weak in January, a manifestation of a minor stratospheric warming. The final warming in the southern hemisphere is well underway by the end of October. The Brewer-Dobson circulation (upwelling in low- to mid-latitudes, downwelling at high latitudes) is present in the stratosphere. As noted by previous investigators, the region of downwelling extends to greater heights in the winter hemisphere and is probably connected to a mesospheric cross-equatorial cell [*Leovy*, 1964]. At mid-latitudes, the vertical velocity is upward at most seasons throughout the altitude range studied in the present work. However, in the tropics, a region of downwelling exists in the upper stratosphere and lower mesosphere. From December through February, this region expands downward from a level in the lower mesosphere. This behavior mimics that obtained by *Hitchman and Leovy* [1986], who computed the diabatic circulation using LIMS data. A region of downwelling around the tropical stratopause was also computed by *Solomon et al.* [1986] and *Gille et al.* [1987], again based on LIMS data. On the other hand, it was not obtained in the studies based on climatological data, since the poor vertical resolution of the climatological temperature fields, as well as the monthly averaging used to obtain those fields, tend to reduce the amplitude of vertical temperature contrasts [*Hitchman,* 1985]. This illustrates one of the UARS advantages mentioned in section 1. As discussed by Hitchman and Leovy, the presence of a region of downwelling around the tropical stratopause is related to the high-temperature phase of the semiannual oscillation (SAO). The time of maximum temperatures at

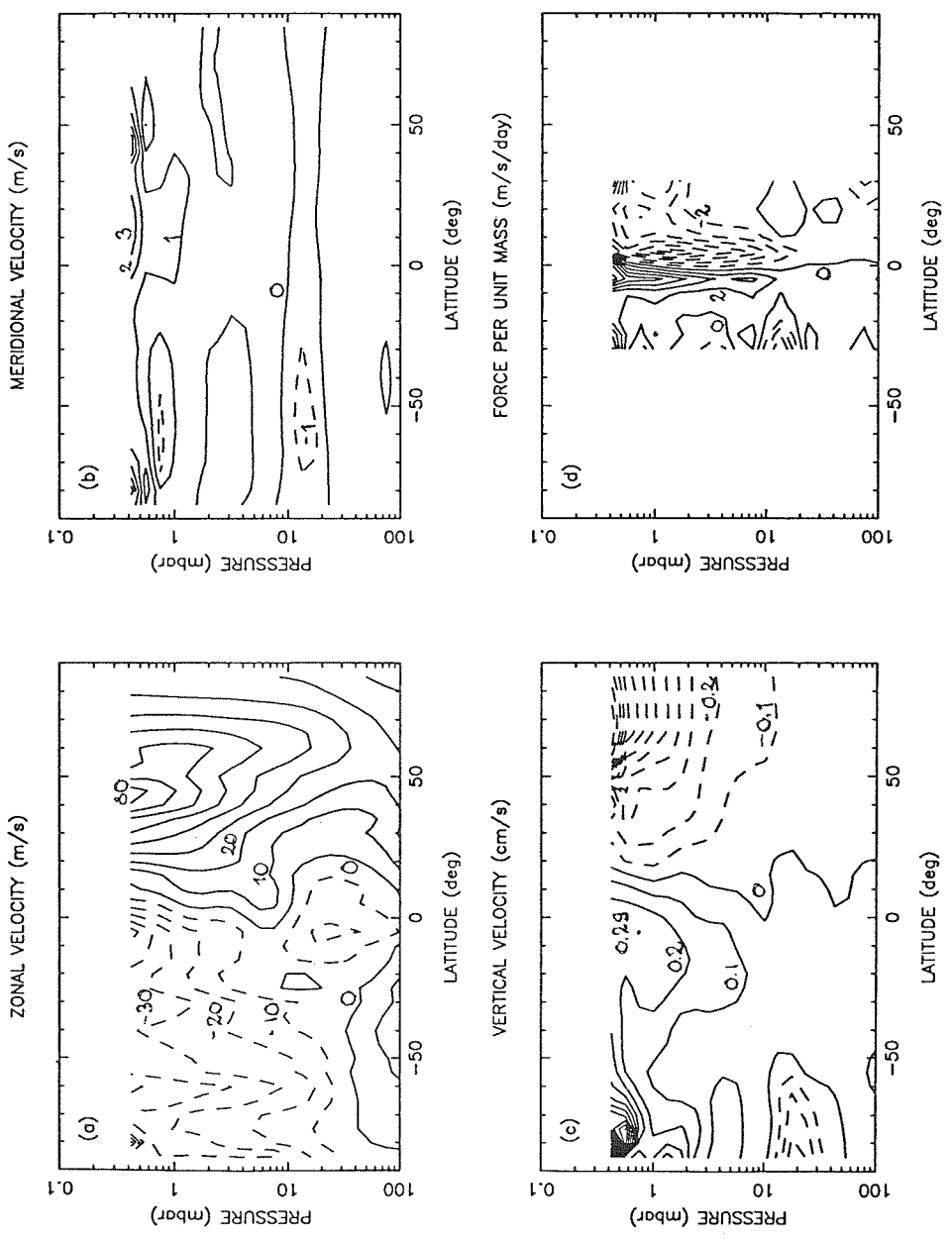

Fig. 1. *(a)* Zonal wind (m s^{-1}) calculated from the gradient wind relationship. *(b)* Meridional component of the diabatic circulation (m s^{-1}). *(c)* Vertical component of the diabatic circulation (cm s^{-1}). *(d)* Momentum residual in the zonal momentum equation (m s^{-1} day^{-1}). All fields are zonal and time averages for the period November 27 - December 3 and December 5 - 12, 1991. Data Version 331 were used in the calculations.

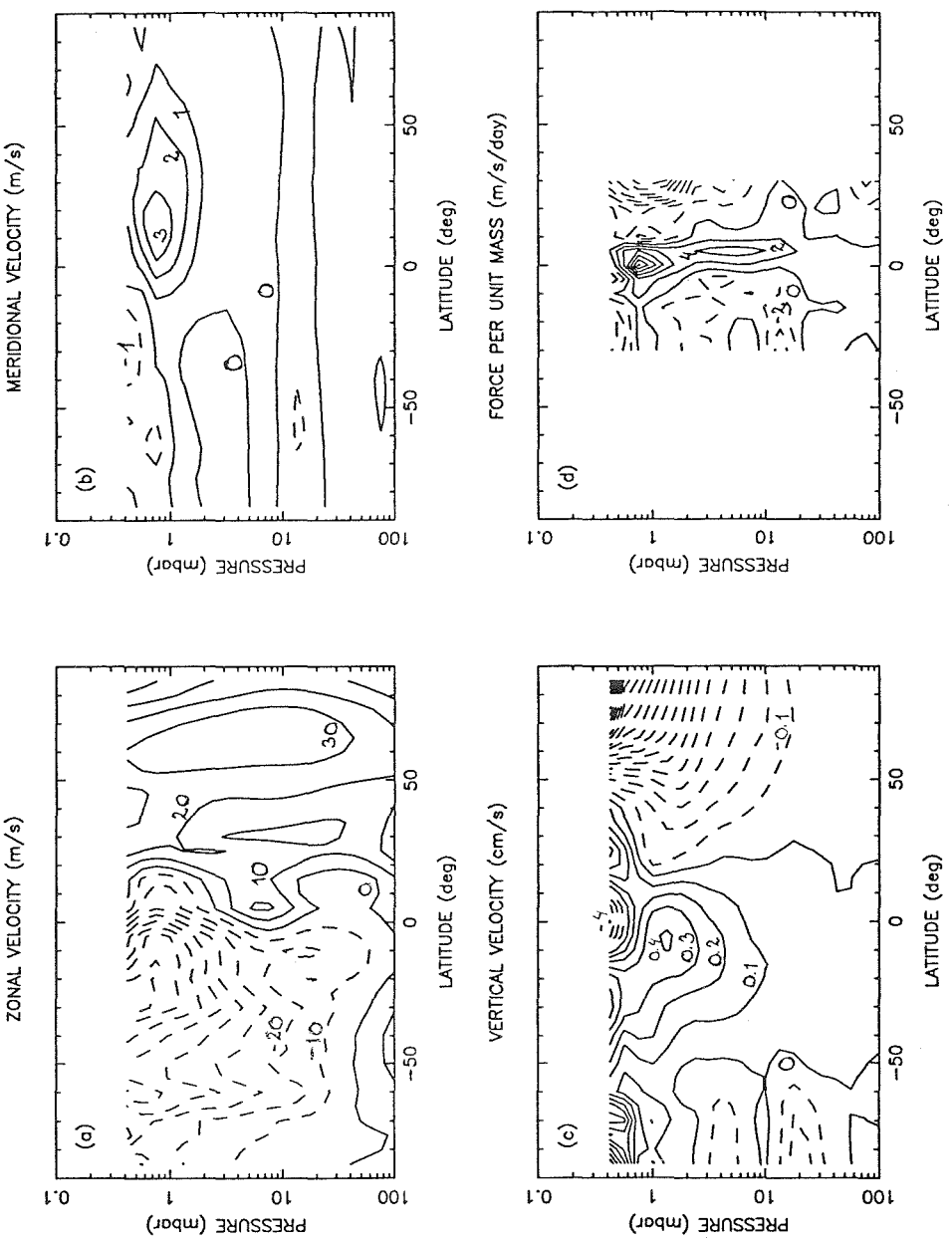

Fig. 2. Same as Figure 1, but for the period January 5 - 12 and January 15 - 22, 1992. Data Version 331.

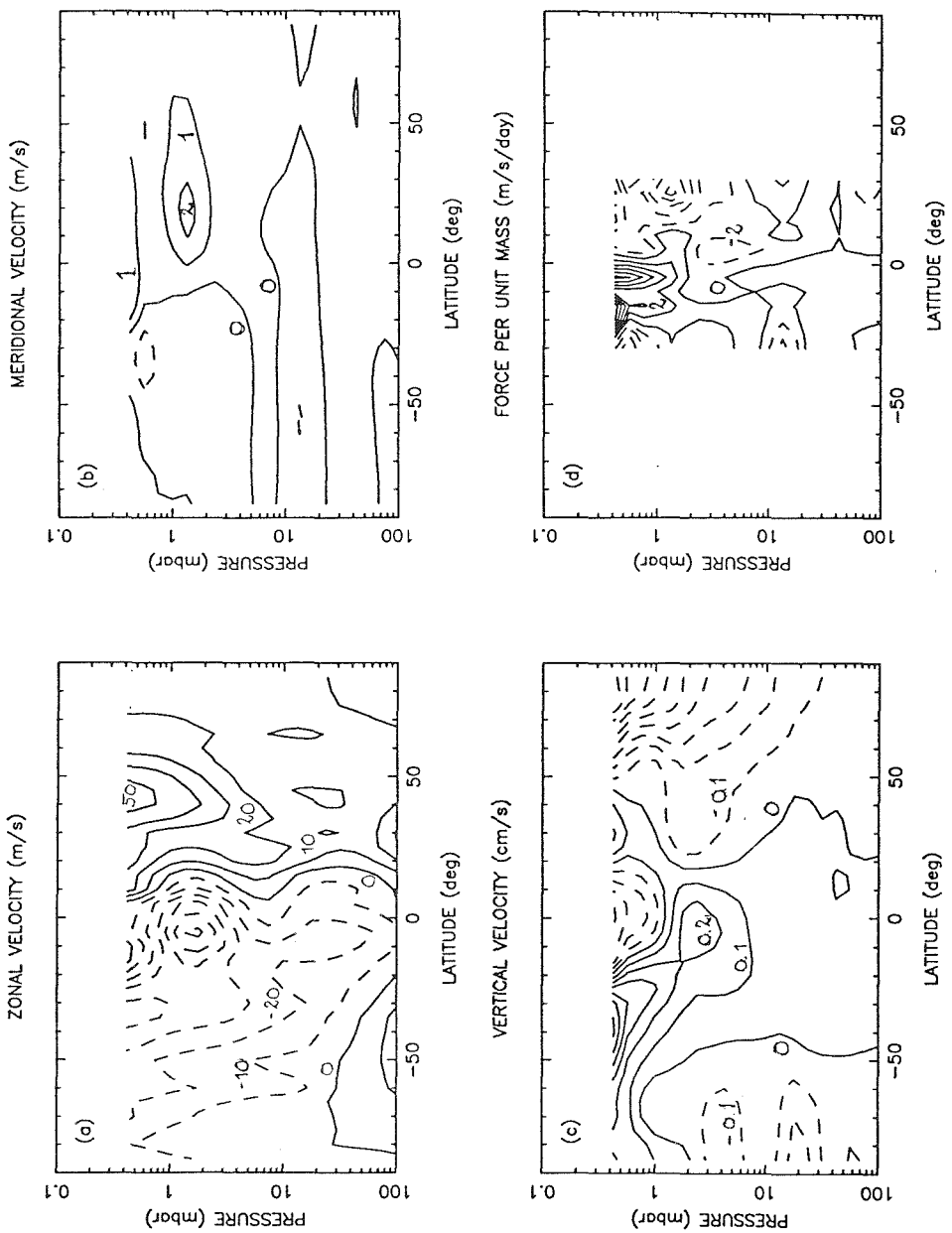

Fig. 3. Same as Figure 1, but for the period February 6 - 13 and February 15 - 22, 1992. Data Version 331.

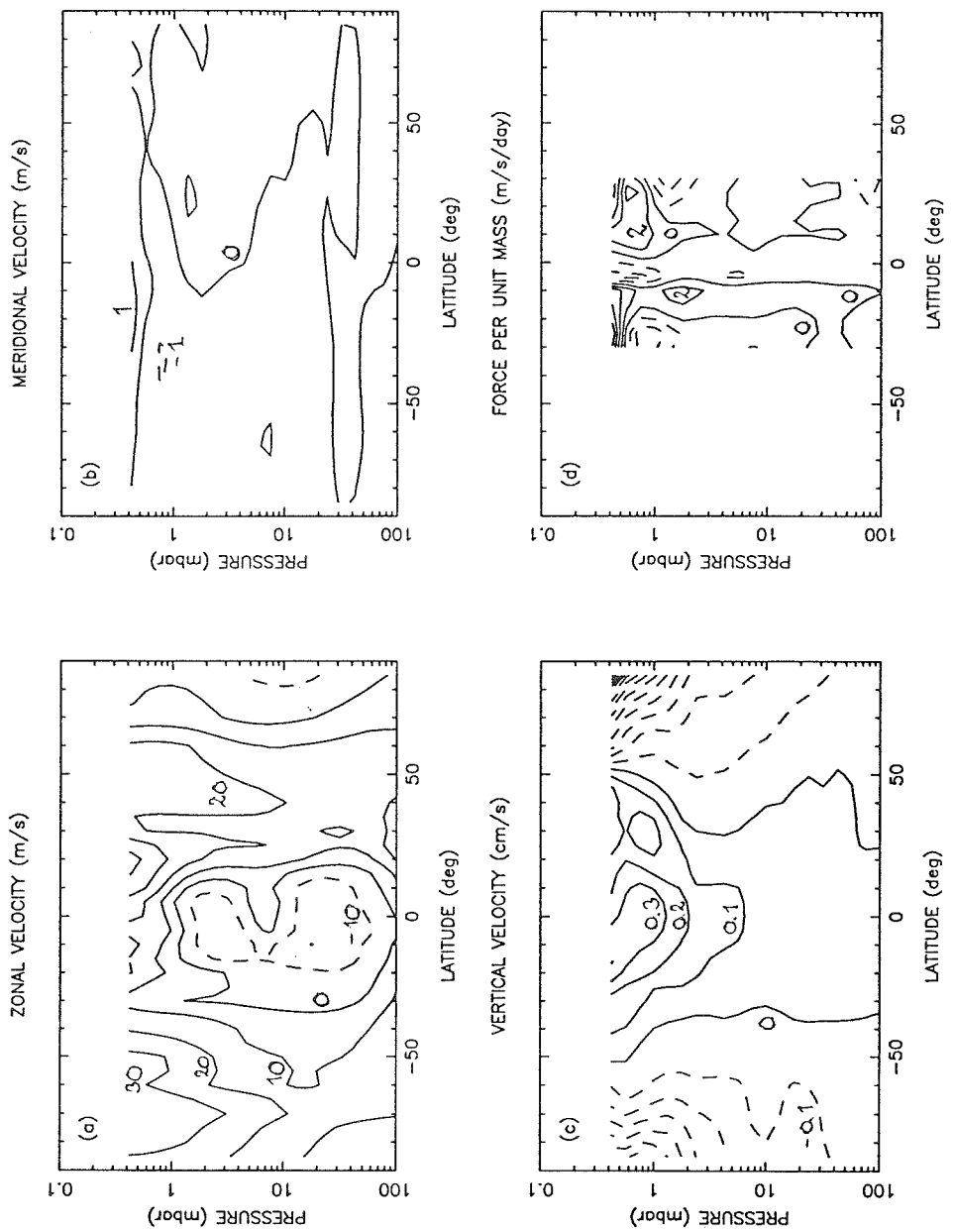

Fig. 4. Same as Figure 1, but for the period March 18 - 22 and March 27 - April 2, 1992. Data Version 331.

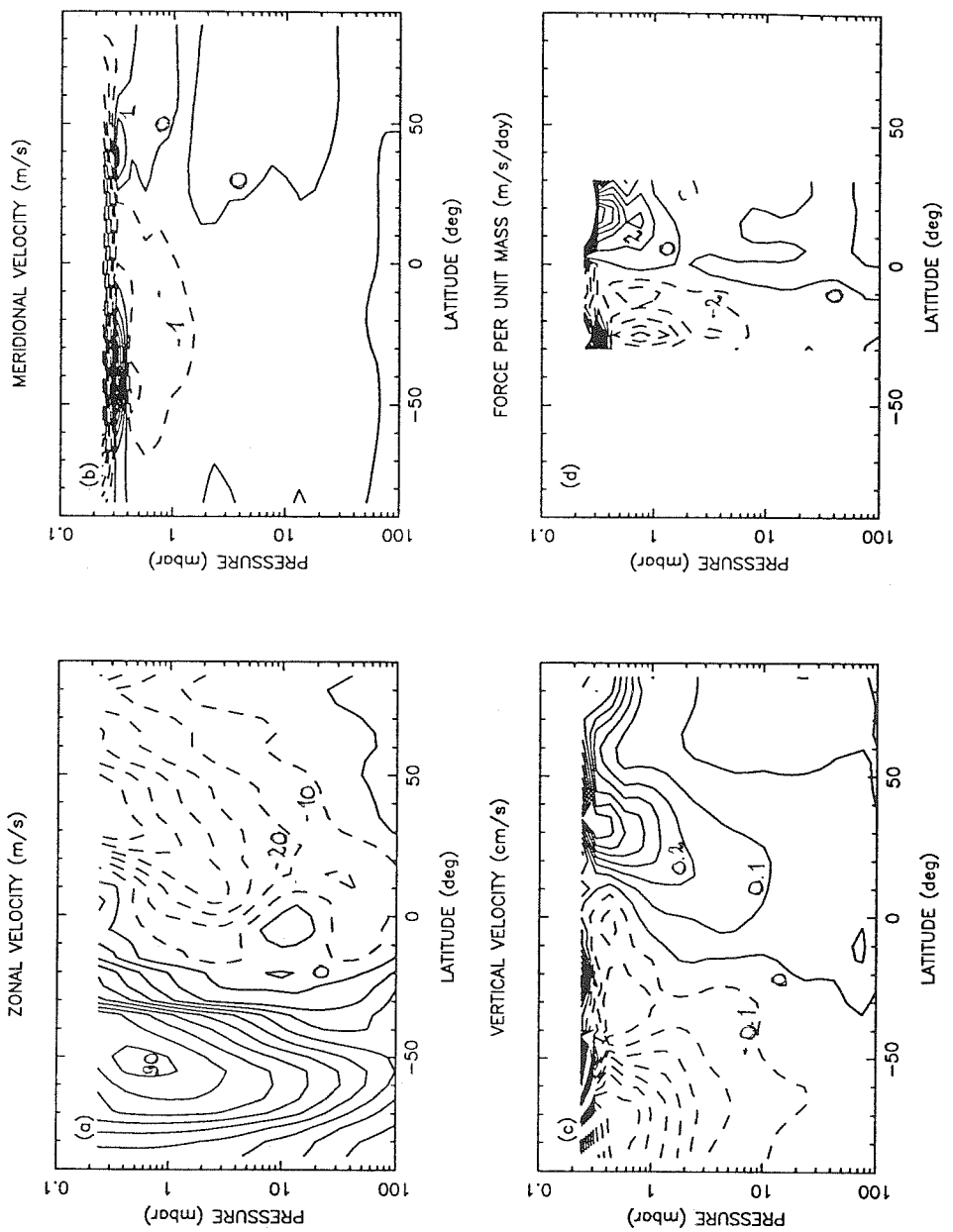

Fig. 5. Same as Figure 1, but for the period June 28 - July 5 and July 19 - 25, 1992. Data Version 400.

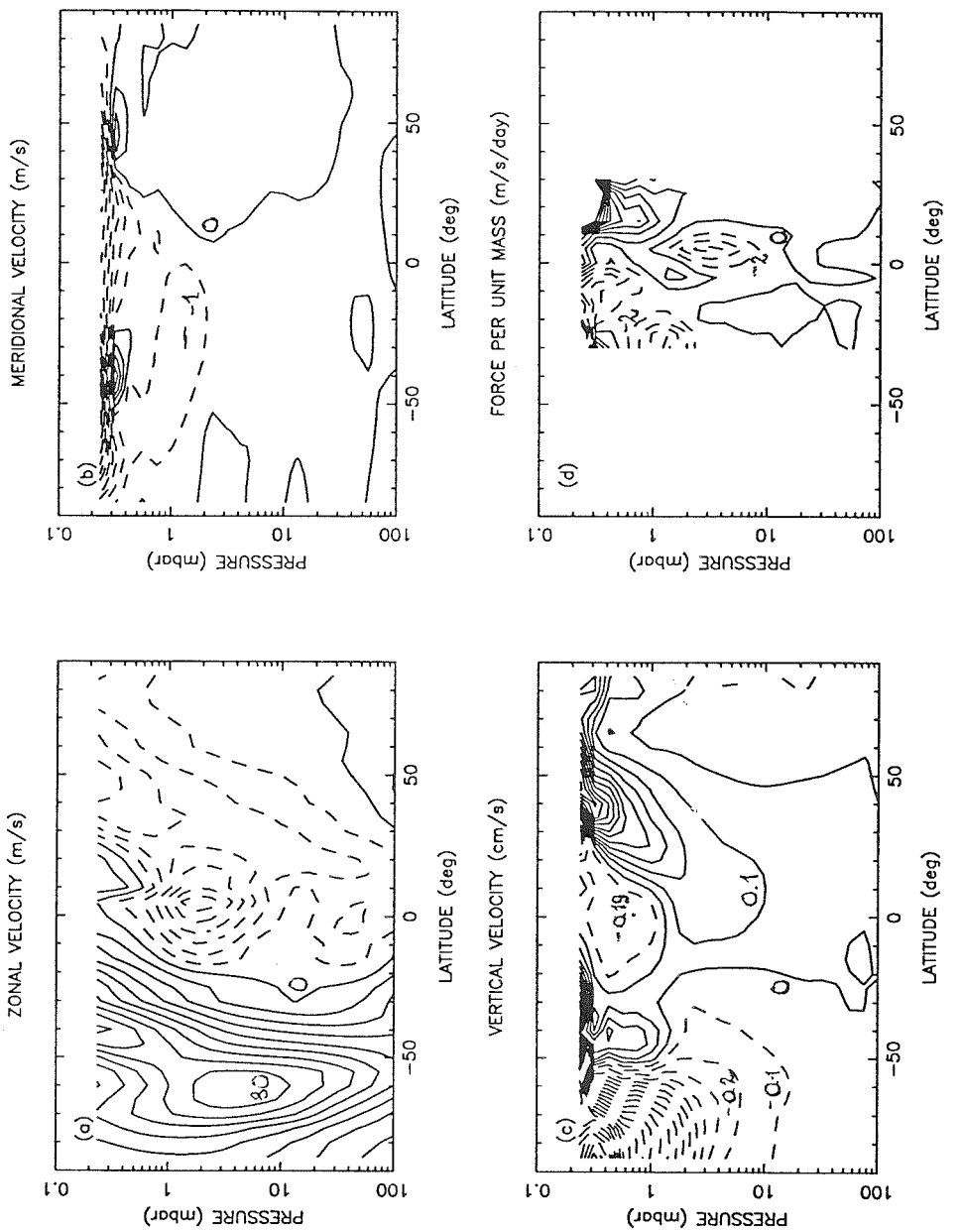

Fig. 6. Same as Figure 1, but for the period August 5 - 12 and August 14 - 21, 1992. Data Version 400.

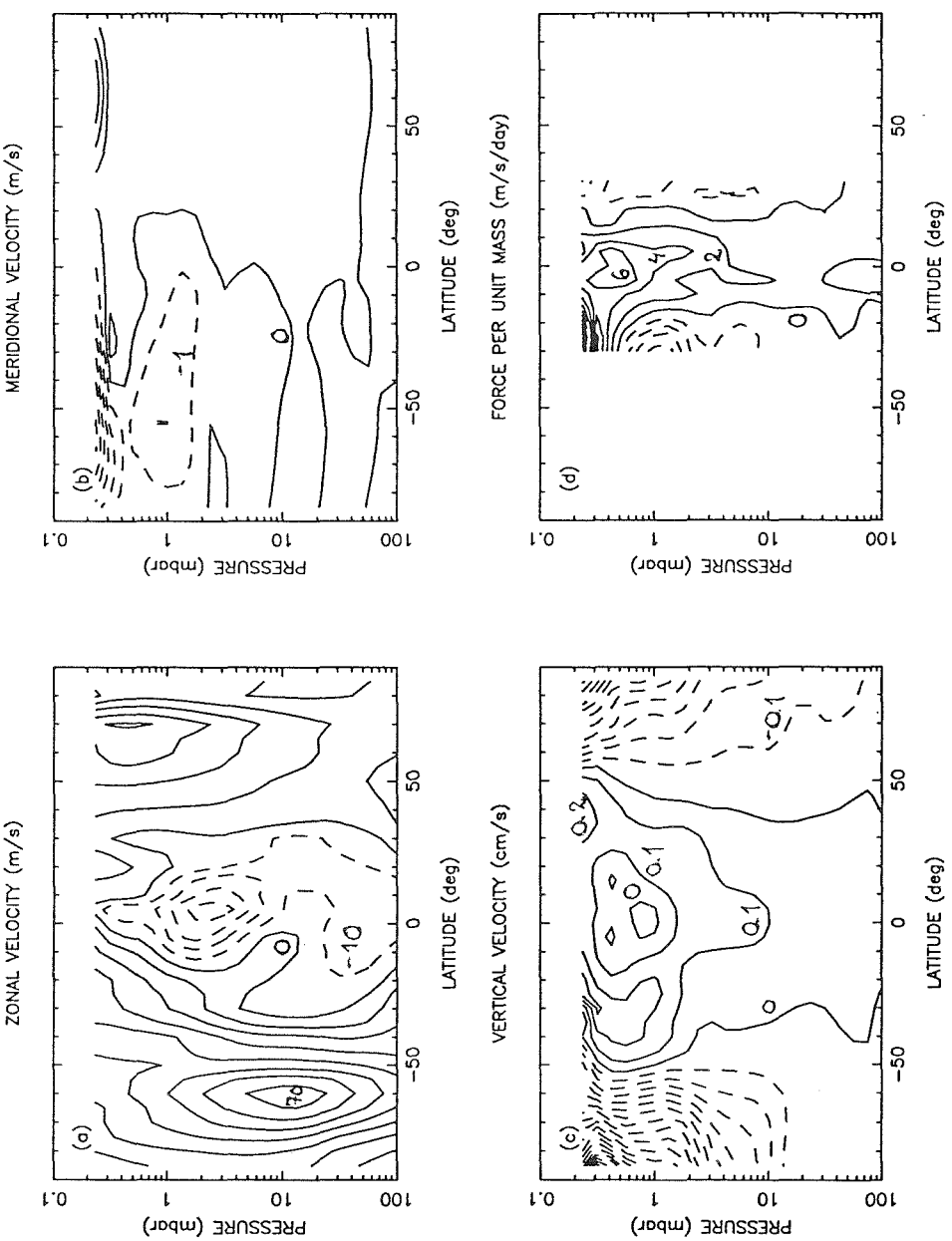

Fig. 7. Same as Figure 1, but for the period September 13 - 20 and September 22 - 29, 1992. Data Version 400.

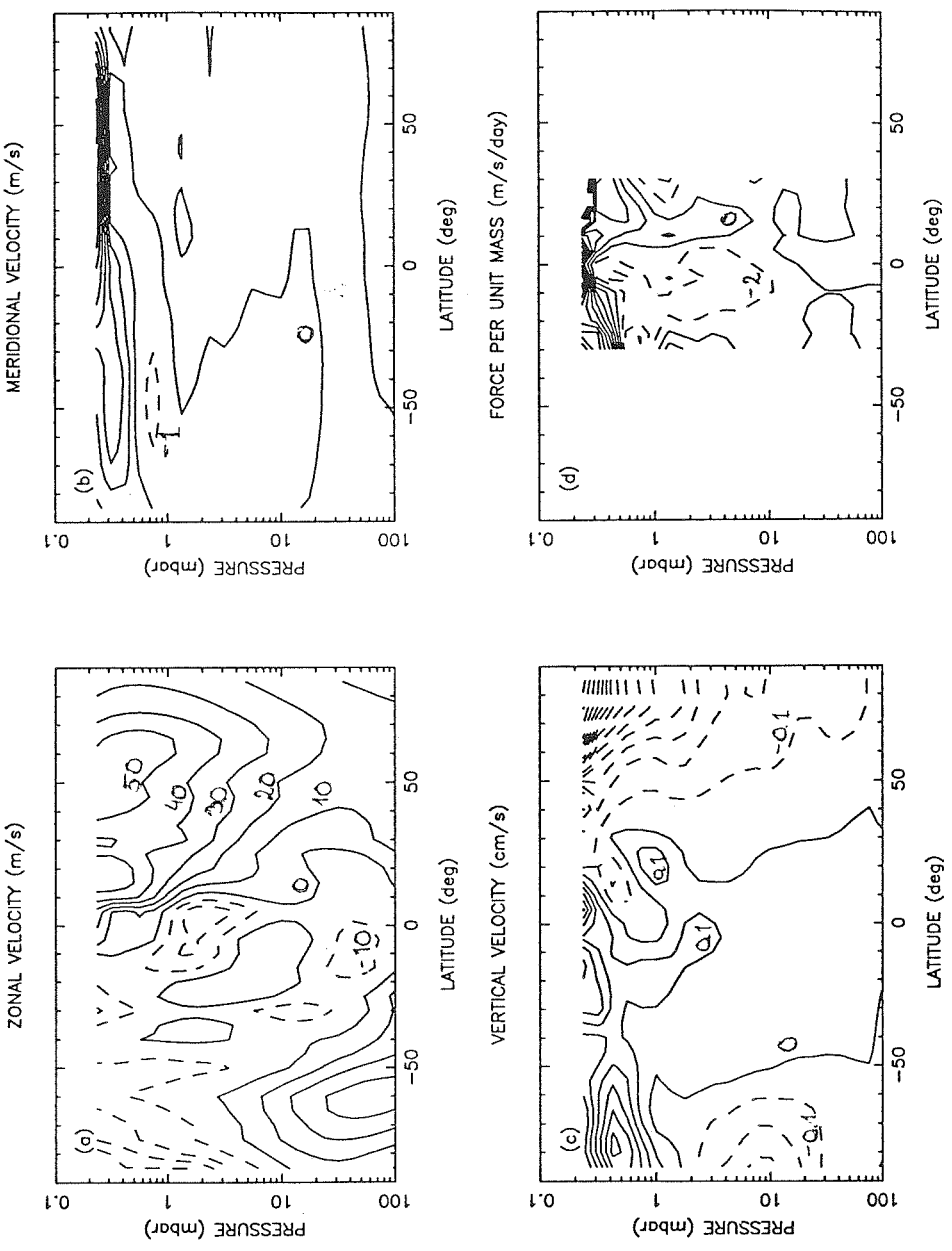

Fig. 8. Same as Figure 1, but for the period October 21 - 28 and October 30 - November 6, 1992. Data Version 400.

the tropical stratopause corresponds to a time of maximum diabatic cooling (since at those levels cooling is dominated by the cooling-to-space mechanism), as well as to a time of minimum solar heating (since temperature and ozone are anti-correlated). These two effects combine to cause a maximum in the net diabatic cooling and thus a maximum in the downward vertical velocities about one month before the equinox (see Figures 3 and 7). Unfortunately, because of data gaps, it is not possible to demonstrate the downward propagation of the region of downwelling at the tropical stratopause in the months preceding the fall equinox of 1992. It is hoped that this will be done in 1993. The implications of the tropical SAO forthe distribution of chemical tracers have been studied by *Solomon et al.* [1986] and *Gray and Pyle* [1986]. In particular, those investigators noted the role played by the region of downwelling in producing the "double-peak" structure in the distributions of nitrous oxide, methane, and water vapor. The inability of climatological studies to reproduce the observed methane distribution [*Yang et al.,* 1991] may contribute, via its effect on the resulting ClO distribution, to the long-standing "ozone deficit" problem (see discussion in section 3.4 of Paper II). These results illustrate the importance of obtaining an accurate estimate of the diabatic circulation for application in chemical models. Such estimates must go beyond the present study in treating the circulation in the lower stratosphere, where a number of important factors (clouds, water vapor) can significantly alter the circulation.

The forcing of the SAO can only tentatively be determined at present. It is commonly believed that the westerly phase of the tropical SAO is caused by momentum deposition due to the dissipation of Kelvin waves, but their contribution cannot be quantified in a zonally averaged approach. The excursions of easterlies from the summer into the winter hemisphere suggest that both meridional advection of easterlies and Rossby wave absorption near the zero-wind line may be responsible for the easterly phase of the SAO. The greatest contribution to the zonal momentum residual in January is from the northward advection by residual circulation, which in particular accounts for the peak at the equatorial stratopause in Figure 2*d*. This is illustrated in Figure 9, which shows the distributions of the three terms in the zonal momentum equation (time derivative of the gradient wind, meridional advection of zonal momentum, and vertical advection of zonal momentum; see e. g., the left-hand side of equation (1) in *Shine* [1989]), as well

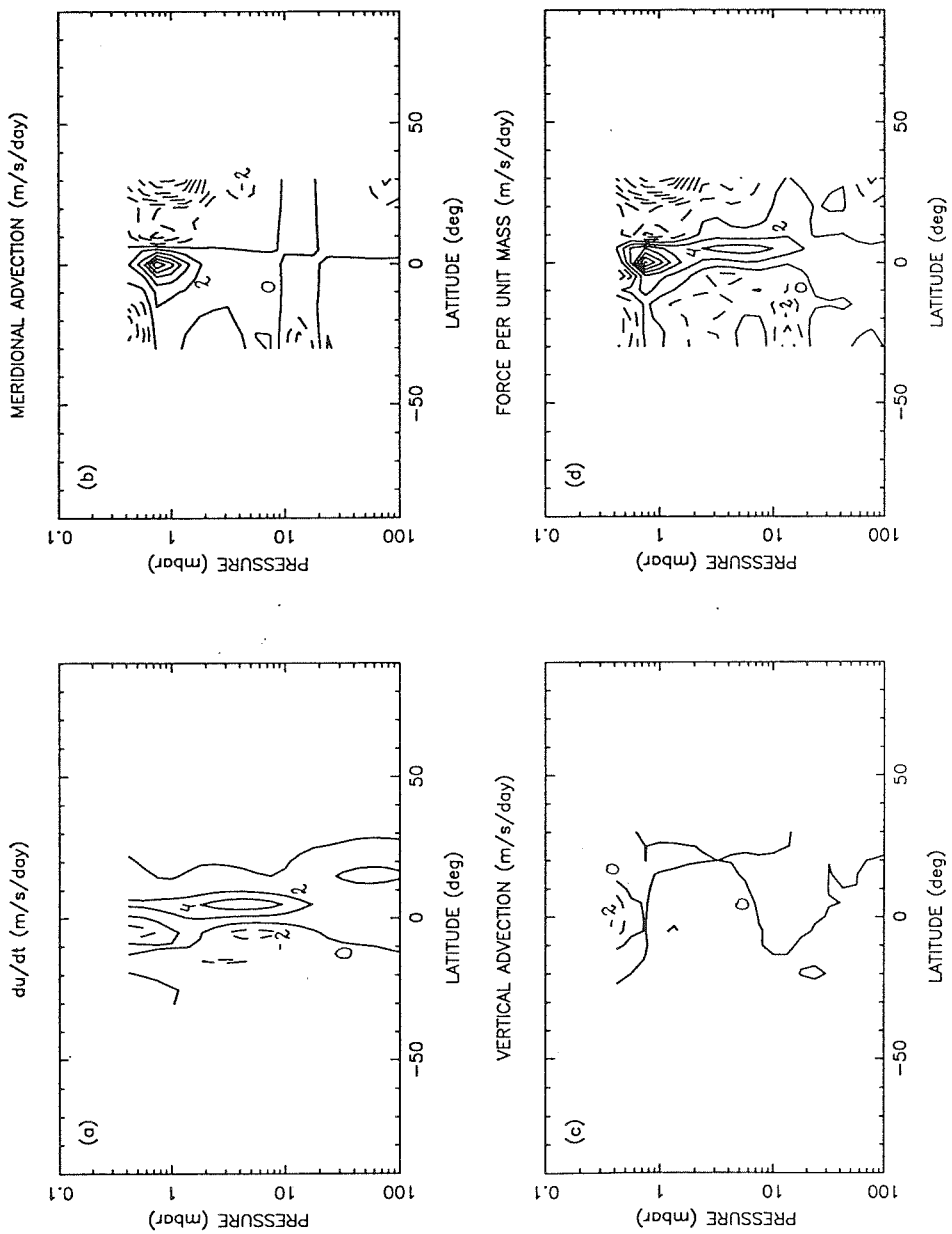

Fig. 9. The contribution to the zonal momentum residual from *(a)* the gradient wind time derivative, *(b)* meridional advection of zonal momentum, and *(c)* vertical advection of zonal momentum (cf. the left-hand side of equation (1) in *Shine* [1989]). Panel *(d)* shows the distribution of the sum of the three terms shown in panels *(a)*-*(c)*. This figure is for the period January 5 - 12 and January 15 - 22, 1992.

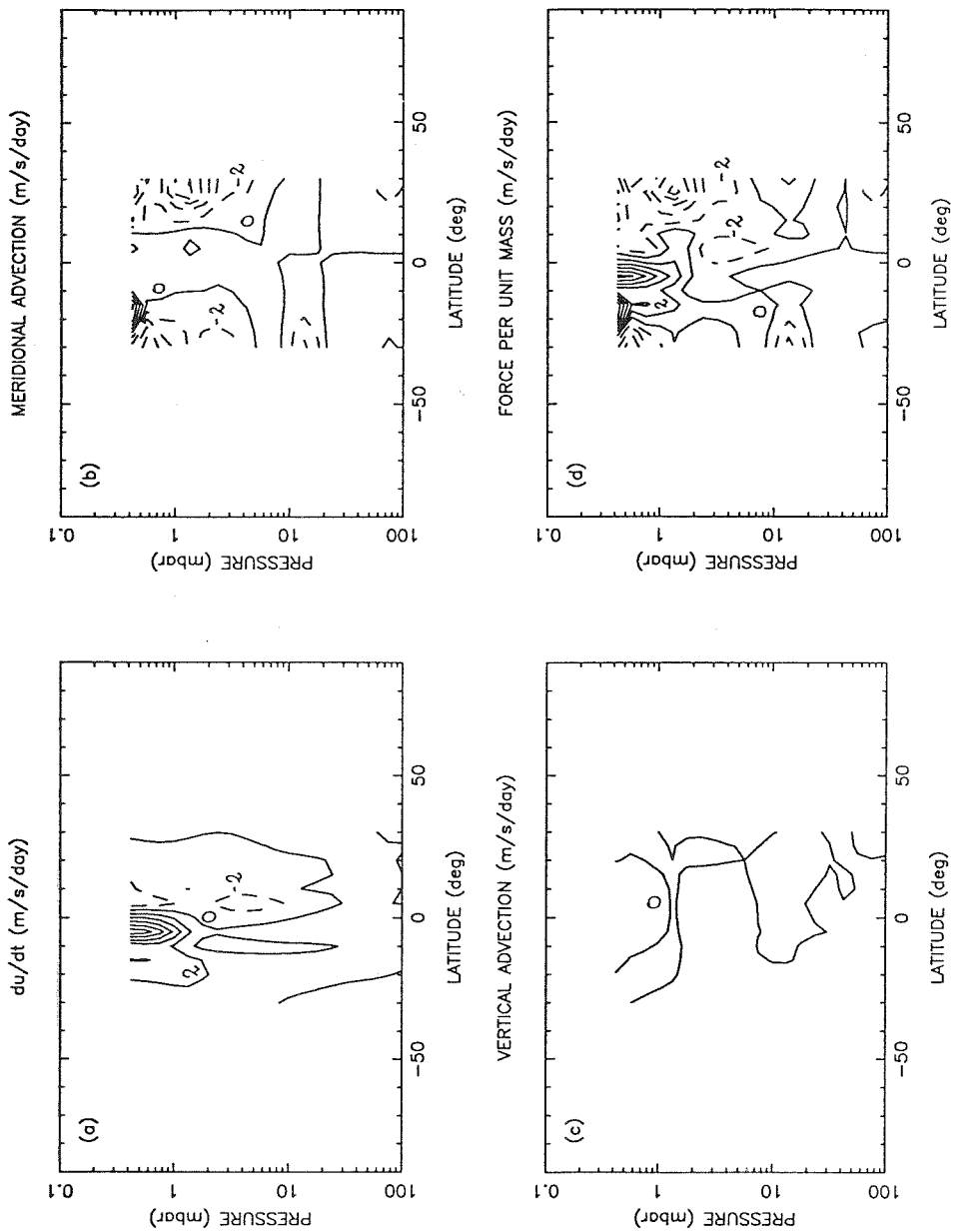

Fig. 10. Same as Figure 10, but for the period February 6 - 13 and February 15 - 22, 1992.

as their sum (the momentum residual). It is unlikely that the dominance of meridional advection is an artifact of the way the zonal wind is calculated at the equator, since the linear interpolation I adopted provides a conservative estimate of the meridional gradient in the zonal wind. Meridional advection also dominates in June-July and to a lesser extent in August, whereas in the remaining months the momentum residual at the equator mainly stems from the time derivative of the zonal wind (as shown in Figure 10 for February), thus implying a greater contribution from in-situ wave absorption. It should be noted that the dominance of the advection term also implies a role for Rossby wave absorption, since the latter is the likely drive for the residual circulation. However, in this case absorption would take place in the extratropics. This picture is consistent with the greater intensity of wave activity during the solstices at winter high latitudes.

4. SUMMARY AND CONCLUSIONS

In this paper, the zonally averaged diabatic circulation has been computed for the period November 1991 - November 1992, based on temperature and ozone data acquired by the Microwave Limb Sounder (MLS) onboard the Upper Atmosphere Research Satellite (UARS). In the tropical upper stratosphere and lower mesosphere, a semiannual oscillation (SAO) in the vertical component of the circulation is diagnosed, with the region of downwelling reaching maximum spatial extent one month before equinox. This SAO is related to the tropical SAO in temperature and ozone and has been documented previously by *Hitchman and Leovy* [1986], who used LIMS data for the period October 1978 - May 1979. The present study extends their analysis to a full annual cycle, albeit for a different year. An analysis of wave forcing, calculated as the residual in the zonal momentum equation, indicates that during the solstices, the SAO is forced by meridional advection of easterly angular momentum driven by extratropical Rossby wave absorption, whereas in-situ wave absorption prevails at other seasons.

The expected lifetime of MLS should allow the present analysis to be extended to several SAO cycles. In addition, the altitude range might be extended above the current upper boundary of 0.4-0.2 mbar

with the advent of improved inversion algorithms, particularly for temperature. It may also be possible to compute the forcing due to planetary-scale waves directly (as the divergence of the Eliasen-Palm flux). For this to be achieved, accurate estimates of the three-dimensional horizontal velocity field are needed. Work in this area is in progress by various UARS investigators (G. Manney, personal communication).

Acknowledgments. This work has been made possible thanks to the foresight of and support I received from R. Zurek, who is a Theoretical Principal Investigator on the UARS Science Team, and D. Crisp, who developed the radiative transfer code. The many years of great effort by other members of the UARS team, in particular J. Waters, L. Froidevaux, E. Fishbein, and L. Elson, are also gratefully acknowledged. Part of this work was conducted at the Jet Propulsion Laboratory, California Institute of Technology, under contract with NASA.

REFERENCES

Andrews, D. G., J. R. Holton, and C. B. Leovy, Middle Atmosphere Dynamics, Academic Press, 1987.

Callis, L. B., R. E. Boughner, and J. D. Lambeth, The stratosphere: Climatologies of the radiative heating and cooling rates and the diabatically diagnosed net circulation fields, *J. Geophys. Res., 92,* 5585-5607, 1987.

Crisp, D., Radiative forcing of the Venus mesosphere. I. Solar fluxes and heating rates, *Icarus, 67,* 484-514, 1986.

Crisp, D., in *Two-dimensional intercomparison of stratospheric models,* Nasa Conf. Publ. 3042, p. 89, 1989.

Crisp, D., Infrared radiative transfer in the dust-free martian atmosphere, *J. Geophys. Res., 95,* 14,577-14,588, 1990.

Garcia, R. R. and S. Solomon, A numerical model of the zonally averaged dynamical and chemical structure of the middle atmosphere, *J. Geophys. Res., 88,* 1379-1400, 1983.

Gille, J. C., L. V. Lyjak, and A. K. Smith, The global residual mean circulation in the middle atmosphere for the northern winter period, *J. Atmos. Sci., 44,* 1437-1452, 1987.

Gray, L. J. and J. A. Pyle, The semi-annual oscillation and equatorial tracer distributions, *Quart. J. Roy. Meteorol. Soc., 112,* 387-407, 1986.

Hartmann, D. L., The dynamical climatology of the stratosphere in the southern hemisphere during late winter 1973, *J. Atmos. Sci., 33,* 1789-1802, 1976.

Hitchman, M. H., An observational study of wave-mean flow interaction in the equatorial middle atmosphere, Ph. D. thesis, University of Washington, Seattle, 1985.

Hitchman, M. H. and C. B. Leovy, Evolution of the zonal mean state in the equatorial middle atmosphere during October 1978 - May 1979, *J. Atmos. Sci., 43,* 3159-3176, 1986.

Kinne, S., O. B. Toon, and M. J. Prather, Buffering of stratospheric circulation by changing amounts of tropical ozone: A Pinatubo case study, *Geophys. Res. Lett., 19,* 1927-1930, 1992.

Lait, L. R. and J. L. Stanford, Applications of asynoptic space-time Fourier transform methods to scanning

satellite measurements, *J. Atmos. Sci., 45,* 3784-3809, 1988.

Leovy, C. B., Simple model of thermally driven mesospheric circulation, *J. Atmos. Sci., 21,* 327-341, 1964.

Marks, C. J., Some features of the climatology of the middle atmosphere revealed by Nimbus 5 and 6, *J. Atmos. Sci., 46,* 2485-2508, 1989.

Murgatroyd, R. J. and F. Singleton, Possible meridional circulations in the stratosphere and mesosphere, *Quart. J. Roy. Meteorol. Soc., 87,* 125-135, 1961.

Plumb, R. A. and J. D. Mahlman, The zonally averaged transport characteristics of the GFDL general circulation/transport model, *J. Atmos. Sci., 44,* 298-327, 1987.

Rosenfield, J. E., M. R. Schoeberl, and M. A. Geller, A computation of the stratospheric diabatic circulation using an accurate radiative transfer model, *J. Atmos. Sci., 44,* 859-876, 1987.

Rothman, L. S., R. R. Gamache, A. Goldman, L. R. Brown, R. A. Toth, H. M. Pickett, R. L. Poynter, J.-M. Flaud, C. Camy-Peyret, A. Barbe, N. Husson, and M. A. H. Smith, The HITRAN database: 1986 edition, *Applied Optics, 26,* 4058-4097, 1987.

Salby, M. L., Sampling theory for asynoptic satellite observations. Part I: Space-time spectra, resolution, and aliasing, *J. Atmos. Sci., 39,* 2577-2600, 1982.

Santee, M. L., The thermal structure, dust loading, and meridional transport in the martian atmosphere during late southern summer, Ph. D. thesis, California Institute of Technology, Pasadena, 1993.

Solomon, S., J. T. Kiehl, R. R. Garcia, and W. Grose, Tracer transport by the diabatic circulation deduced from satellite observations, *J. Atmos. Sci., 43,* 1603-1617, 1986.

Shine, K., Sources and sinks of zonal momentum in the middle atmosphere diagnosed using the diabatic circulation, *Quart. J. Roy. Meteorol. Soc., 115,* 265-292, 1989.

Tung, K. K., On the two-dimensional transport of stratospheric trace gases in isentropic coordinates, *J. Atmos. Sci., 39,* 2330-2355, 1982.

Yang, H., E. Olaguer, and K. K. Tung, Simulation of the present-day atmospheric ozone, odd nitrogen, chlorine and other species using a coupled 2-D model in isentropic coordinates, *J. Atmos. Sci., 48,* 442-471, 1991.